MODELLING AND *IN VIVO* MONITORING OF THE TIME DEPENDENT MECHANICAL PROPERTIES OF TISSUE ENGINEERING SCAFFOLDS

A Thesis Submitted to the College of

Graduate Studies and Research

In Partial Fulfillment of the Requirements

For the Degree of Doctor of Philosophy

In the Department of Mechanical Engineering

University of Saskatchewan

Saskatoon, Saskatchewan, Canada

By

Nahshon K. Bawolin

PERMISSION TO USE

In presenting this thesis in partial fulfillment of the requirements for a Postgraduate degree from the University of Saskatchewan, I agree that the Libraries of this University may make it freely available for inspection. I further agree that permission for copying of this thesis in any manner, in whole or in part, for scholarly purposes may be granted by the professor or professors who supervised my thesis work or, in their absence, by the Head of the Department or the Dean of the College in which my thesis work was done. It is understood that any copying or publication or use of this thesis or parts thereof for financial gain shall not be allowed without my written permission. It is also understood that due recognition shall be given to me and to the University of Saskatchewan in any scholarly use which may be made of any materials of my thesis.

Requests for permission to copy or make use of material in this thesis in whole or in part should be addressed to:

Head of the Department of Mechanical Engineering
3B48 Engineering Building
57 Campus Drive, Saskatoon, SK
Saskatoon, Saskatchewan, S7N 5A9

ABSTRACT

When organs and tissue fail either due to pre-existing disease progression or by accidental damage, current state of the art treatment involves the replacement of the damaged or diseased tissue with new donor derived organs/tissue. The limitations of these current approaches include a limited supply of tissue for treatments and the immune response of the patient's own body against the new implanted tissue/organs. To solve these issues, tissue engineering aims to develop artificial analogs derived from a patient's own cells instead of donor tissue/organs for treatment. To this end, a promising approach, known as scaffold-based tissue engineering, is to seed engineered constructs or scaffolds with cells to form artificial analogs, which then develop with time into new tissue/organs for implantation. The mechanical properties of the scaffold play a critical role in the success of scaffold-based treatments, as the scaffold is expected to provide a temporary support for the generation of new tissue/organs without causing failure at any time during the treatment process. It is noted that due to the degradation of scaffold in the treatment process, the mechanical properties of the scaffold are not constant but change with time dynamically. This raises two scientific issues; one is the representation of the time-dependent mechanical properties and the other one is the monitoring of these properties, especially in the *in vivo* environments (i.e., upon the implantation of scaffolds into animal/patient bodies). To address these issues, this research is aimed at performing a novel study on the modelling and *in vivo* monitoring of the time dependent mechanical properties of tissue engineering scaffolds.

To represent the time-dependent mechanical properties of a scaffold, a novel model based on the concept of finite element model updating is developed. The model development involves three steps: (1) development of a finite element model for the effective mechanical properties of the scaffold, (2) parametrizing the finite element model by selecting parameters associated with the scaffold microstructure and/or material properties, which vary with scaffold degradation, and (3) identifying selected parameters as functions of time based on measurements from the tests on the scaffold mechanical properties as they degrade. To validate the developed model, scaffolds were made from the biocompatible polymer polycaprolactone (PCL) mixed with hydroxyapatite (HA) nanoparticles and their mechanical properties were examined in terms of the Young modulus. Based on the bulk degradation exhibited by the PCL/HA scaffold, the molecular weight was selected for model updating. With the identified molecular weight, the finite element model

developed was effective for predicting the time-dependent mechanical properties of PCL/HA scaffolds during degradation.

To monitor and characterize scaffold mechanical properties *in vivo*, novel methods based on synchrotron-based phase contrast imaging and finite element modeling were developed. The first method is to represent the scaffold mechanical properties from the measured deflection. In this method, the phase contrast imaging is used to characterize the scaffold deflection caused by ultrasound radiation forces; and the finite element modelling is used to represent the ultrasonic loading on the scaffold, thus predicting the mechanical properties from the measured deflection. The second method is to characterize the scaffold degradation due to surface erosion, which involves the remote sensing of the time dependent morphology of tissue scaffolds by phase contrast imaging and the estimation of time dependent mass loss of the scaffolds from the sensed morphology. The last method is to relate the elastic mechanical property and nonlinear stress-strain behavior to the scaffold geometry, both changing with time during surface erosion. To validate the above methods, scaffolds was made from varying biomaterials (PLGA and PCL) and their mechanical properties (degradation, mass loss, and elastic modulus) were examined experimentally. The results obtained illustrate the methods developed in this research are effective to monitor and characterize scaffold mechanical properties.

The significance of this research is that the model developed for the scaffold mechanical properties can be used in the design of scaffolds with the desired mechanical properties, instead of the trial and error methods typical in current scaffold design; and that these novel monitoring methods based on synchrotron imaging can be used to characterize the scaffold time-dependent mechanical properties in the *in vivo* environments, representing an important advance in tissue engineering.

ACKNOWLEDGEMENTS

I wish to sincerely thank all of the individuals who committed their time and expertise to this research project. In particular, I would like to thank my academic supervisors Dr. Daniel Chen and Dr. Chris Zhang for their constant guidance and advice throughout my time as a Graduate student and research assistant. I also wish to thank Dr. Allan Dolovich, whose advice regarding inverse problems and solid mechanics was invaluable to this research, and to thank Dr. James Johnston for his advice on computational simulation, numerical methods, and high performance computing. In addition I would like to extend my gratitude and thanks to all the members of my advisory committee. Their careful criticism and examination of my work ensured the quality of this research. I also wish to acknowledge the contribution of Dr. Minggan Li, whose help with the dispensing process and scaffold fabrication was invaluable, and the help of Dr. Ning Zhu whose knowledge of biology and medicine were greatly appreciated. I also had the pleasure and honor of working with Mr. Doug Bitner, whose technical advice and practical help related to the dispensing process contributed greatly to the success of this work.

Finally I wish to express gratitude to both the Saskatchewan Health Research Foundation and the University of Saskatchewan, for providing the financial support for this study.

TABLE OF CONTENTS

CO-AUTHORSHIP

The manuscripts included in this thesis are co-authored; however it is the mutual understanding of all authors that Nahshon Bawolin, as the first author, is the primary investigator of the research work. The contributions of other authors are greatly appreciated and acknowledged in this thesis.

LIST OF FIGURES

CHAPTER 1

INTRODUCTION

1.1: Background

One of the unaddressed challenges in medicine is the treatment of tissue/organ damage from disease or injury. In the ideal case, disease mechanisms would be interrupted and or reversed long before the need for the replacement of tissue and or organs, but in the case where the damage is caused by accident or injury there is no logical way to avoid tissue/organ replacement, and the current state of the art understanding of many disease processes is insufficient to arrest or control their progression. Current treatment methods rely on the replacement of damaged or diseased tissue with donor supplied replacements, which suffer from patient immune system rejection, necessitating the use of immunosuppressive drugs and/or other treatments that leave the patient vulnerable to infection.

Possible future treatments to the problem of replacement organs/tissue can be broadly defined as either 1) dependent on artificial implantable devices that perform the function of the unviable tissues/organs, or 2) biological in nature. With regards to the first approach, many mechanical devices such as artificial hearts and implantable heart-lung machines have been proposed and designed, with some having reached a rather advanced state of development. For example, damage to the nervous system both peripheral and central has encouraged the invention of electrodes and electrode arrays designed to bridge gaps in the nervous system or even stimulate nerves or the brain itself in an attempt to allow man-made devices the ability to replace the functionality of living systems in the body.

The biological approaches to this issue can be further subdivided into two categories. The first possibility is to use xenographic methodologies so as to provide an inexhaustible supply of genetically modified rejection free organs from animals or possibly even fully human organs grown directly in genetically modified organisms. The second possibility is classical tissue engineering that involve either cells alone, scaffolds alone, or their combination. Cell alone treatments provide cells with the environmental signalling necessary to command them to

reorganize and expand into desired tissue and organs. This field is closely aligned with embryology, since what is being attempted is the control over a process that already occurs during natural human development. The ultimate goal would be a type of bioreactor that could incubate a patient's own genetically compatible cells in something akin to an artificial womb and coax them into becoming the desired tissue or organs necessary for patient treatment. These methods require a deeper understanding of the fundamental inner workings of cells and biology in general and therefore may take considerable time to reach fruition.

Simpler near term possible approaches have also been proposed. The method known as scaffold alone tissue engineering supplies a substrate or prosthetic extracellular matrix that simulates the behavior of the existing extracellular environment within which cells are naturally embedded. Once this prosthetic is implanted into the wound area, cell populations within the scaffold eventually exist due to cell migration from the surroundings. While such methods have shown some success in treating injury and disease, there is a limit to how thick such scaffolds can be while still offering a realistic chance that cells will be able to migrate into the new extracellular matrix substitute. Cell and scaffold approaches provide readymade populations of cells already pre-seeded into the scaffold, which eliminates the need for migrating cell populations. Scaffold-cell tissue engineering has already been successfully applied to simple tubular structures and hollow organs like bladders and kidneys, but very complex three dimensional organs have yet to be regenerated using this method. Nevertheless, this approach to the replacement of tissue/organs holds great promise. This process involves the construction of an artificial extracellular matrix, often referred to as a tissue scaffold, which is then seeded with patient derived cells. The cells are expected to organize and proliferate inside the porous structure of the scaffold, until they form new functioning tissue/organs. Simultaneously, the scaffold itself is expected to gradually degrade with time and eventually be completely absorbed by the body. In this report, reference to the tissue scaffold or just scaffold will refer to the unseeded construct itself, while tissue engineering construct or construct will refer to the seeded scaffold.

The mechanical properties of the construct are critical to its proper function. In some treatment plans, the scaffold will be implanted into the body after seeding, and will be expected to temporarily fulfill the mechanical function of the tissue it replaces. In situations where the

scaffold is initially incubated *in vitro*, the seeded cells may require mechanical stimulation, which the scaffold must successfully bear. If the scaffold displays permanent deformation under the loading it experiences in its operating environment, then it has experienced failure. Likewise, a scaffold that displays an unacceptable magnitude of deformation or fracture/breakage during the treatment period must be redesigned to eliminate this unacceptable behavior. It is also known that the mechanical stimulation given by a cells' surroundings influences the behavior of those cells, so the mechanical properties of a scaffold will have a critical influence on the local mechanical environment experienced by the cells, which will influence their metabolic and differentiation behavior. All of the above issues highlight the necessity to design scaffolds with controllable and known mechanical properties.

The tissue scaffold at all points in time during the treatment process will display a certain deflection response when it is subjected to loading. Various features of this response can be quantified as specific mechanical properties of the scaffold. For instance, the deflection of a scaffold given a certain magnitude of load is known as the stiffness of the scaffold. Whether the scaffold is incubated by itself in a bioreactor and subjected to artificial loads to control seeded cell behavior, or is implanted directly in the body and expected to temporarily fulfill the mechanical function of the tissue it is replacing, the scaffold mechanical behavior is very important. The ideal scaffold design would not be physically damaged by loading or deform permanently at any time during the treatment period. In order to realize this ideal design, realistic models that capture the relevant features of the scaffold must be developed.

One fundamental issue present is the difference in behavior of the scaffold *in vitro* and *in vivo*. In order to quantify this difference, one may explore all of the fundamental mechanisms that are contributing to this difference in behavior, or alternatively, a black box phenomenological approach may be taken where experimentation *in vivo* provides the information required for scaffold modelling. In this latter approach, scaffolds implanted within the body would need to be monitored with time to evaluate their degradation. Since explantation of the scaffold at certain intervals of time for evaluation may corrupt or alter the scaffolds, and only provides global measurements of scaffold qualities without difficult procedures like physical histological slicing, an *in vivo* imaging based method of scaffold evaluation holds promise as an improvement over

the current state of the art. This thesis therefore considers signals generated by the scaffold in the living body that may be measured externally to quantify various scaffold design parameters as functions of time in a biological environment that is difficult to replicate artificially in the laboratory.

1.2: Research Issues

Two fundamental issues exist in scaffold based tissue engineering, which are addressed by the research presented in this thesis. The two broad issues are 1) the selection or development of an appropriate model for the specific scaffold behavior that is of interest, and 2) the development of experiments and methods to acquire information about scaffold behavior. The first issue is defined as the modelling of the behavior of tissue scaffolds and the regenerating tissue within them. The second issue is the experimental identification of the parameters in an appropriate model so that it has the ability to represent the true *in vivo* behavior of the scaffold.

Designing a system as complex as a tissue scaffold through experiments alone would be challenging, as it would require an unrealistic number of experiments necessary to blindly identify the ideal design for a tissue scaffold, considering the significant number of parameters that influence scaffold behavior. A more realistic approach is to gain an understanding of scaffold behavior and properties from limited experiments, and then to employ this information to assemble a mathematical representation of scaffold behavior. This simplified, scope specific, mathematical representation can then be utilized to design scaffolds with the desired behavior and properties through optimization, and this final optimized design can then be validated experimentally.

In tissue engineering, the use of composite materials is becoming more common, which results in a need for models that consider the composite nature of the scaffold. Composites combine the traits of many different constituents to give an effective material that acquires some of the qualities of its individual phase materials. For example, in bone tissue engineering, the exceptional resistance to fracture of bone is replicated somewhat by bone tissue scaffold material by combining a hard brittle ceramic phase such as Hydroxyapatite with a soft compliant phase

like Polycaprolactone. In this manner the scaffold is attempting to emulate natural bone, where soft collagen is reinforced by Hydroxyapatite ceramic. In addition, artificial analogs to the internal loading schemes found in living tissue to stop crack propagation are beginning to be considered for tissue scaffold applications. This raises a need for the development of tissue scaffold degradation models which include multiple structural levels, and the influence of composite material microstructure on degradation.

The realm of experimental design for scaffolds is further complicated by the fact that the *in vivo* environment does not behave exactly like the simplified *in vitro* table top models that are often used to quantify the behavior of new scaffold designs. For example, various enzymes may be present in the living environment that may not be taken into account in simplified degradation studies in buffered saline. In addition, mild inflammation or other responses of the body to the existence of the scaffold may change its chemical environment and accelerate degradation. The cells within the scaffold also produce metabolic waste products which would normally be handled by the body's natural acid base control systems. Since the natural pH balancing mechanisms of the body take a certain amount of time to neutralize the metabolic waste products, these substances have a window of opportunity to influence scaffold degradation. The solution to these increased complexities to the degradation modelling of the scaffold is to ultimately run degradation experiments on select scaffold designs *in vivo* through animal testing. This raises the issue of how to ideally monitor the scaffold inside the living environment, which would be preferable to the difficulties associated with scaffold removal before characterization.

Once a realistic mathematical model of scaffold degradation and mechanical performance has been obtained, the next step in the development of a model is to estimate its parameters with experimental evidence collected from the true *in vivo* behavior of the scaffold during the treatment process. Methods for the *in vivo* monitoring of tissue scaffolds are needed to collect the data required to allow tissue scaffold degradation models the ability to predict scaffold behavior in the body. One promising method to monitor the elastic property of the scaffold, which is related to other interesting properties such as crystallinity and molecular weight, is to remotely palpitate the scaffold with an ultrasonic radiation force, and use some imaging technique to measure the deflection of the scaffold while it is being loaded by the ultrasound beam. Since

safety concerns limit the ultrasound intensity allowed within the body, the magnitude of the stiffness that is measurable by this method depends on the resolution of the deflection detecting method. The attenuation of high frequency sound waves in the body limits the use of high resolution ultrasound to characterize deflections below a certain size. Even the use of x-rays to visualize the deflection caused by the relatively small ultrasound force on a significantly stiff target scaffold may fail in observing any noticeable movement. There is therefore a need to discover a way to detect the faint movements generated by this method of palpitation.

In addition to the elastic property of the scaffold, the full stress-strain behavior of the scaffold is of interest. There is however no way in which an ultrasound beam of allowable power can deform a scaffold into the plastic region and conduct a full stress-strain test on the scaffold *in vivo*. There is therefore a need for some other signal which is observable from a distance outside of the body to carry enough information to reconstruct the nonlinear stress-strain behavior of the scaffold. This is an ongoing area of research; to identify ways in which to determine the elasticity, yield point, and elongation at failure inside the body from some remotely observable parameter.

Finally, another very important quality of scaffolds undergoing degradation is their mass. Current methods of mass characterization during degradation involve marking the scaffold material with some type of identifying substance as a tracer or the full removal of the scaffold so that it can be studied outside of the body. Neither of these approaches are ideal. It would be very useful if a signal related to mass loss that can be detected outside of the body could be found. Further to this goal, a search for such a signal is conducted.

1.3: Research Objectives

The time dependency of the mechanical properties of tissue scaffolds complicates the design of these devices. In addition, the operating environment of the scaffold makes experimental monitoring of the scaffold without its physical removal challenging. These two issues lead to the following research objectives: 1) develop a model that predicts the time dependent Young

modulus of a tissue scaffold, and 2) develop experimental methods to monitor the scaffold remotely.

The first objective of this research is vital because it will allow the design of scaffolds to meet specific time dependent mechanical property requirements with a more practical computer model based scaffold development process instead of an experimental less guided approach to scaffold design. This objective will be accomplished in a four step process: 1) model development, 2) model parameterization, 3) model updating, and 4) model validation. In model development a model based on finite element homogenization and finite element rate-diffusion is developed to represent the time dependent modulus of the scaffold. Geometric and/or chemical parameters in the model are then chosen for updating in the parameterization step. Tissue scaffolds are then fabricated and degraded, and their mechanical properties with time are characterized by load-displacement testing. The parameterized model is then updated at each considered time step, and the updating parameter is represented as a time dependent function. The finite element model with the ability to represent the time dependent Young modulus is then validated with experimental data from the degradation of a scaffold with different geometry, but made from an identical material and degraded under the same conditions.

The second objective is significant because there is a need to be able to remotely monitor a scaffold's properties in situations where it is not practical to remove the scaffold for testing or directly place instruments on the scaffold to characterize its properties with time. There are three time dependent characteristics of the scaffold that are of interest: 1) the change in Young modulus from the degradation of the bulk scaffold material, 2) the change in Young modulus of the scaffold from surface erosion, and 3) the mass loss of the scaffold with time. The first characteristic of the scaffold will be determined by deflecting a scaffold with an ultrasonic radiation force and estimating its effective Young modulus from the measured deflection. The second and third objective will be accomplished by experimentally determining the morphology of the scaffold with time by synchrotron radiation phase contrast imaging. The changes in the volume of space occupied by the tissue scaffold material with time can be determined through imaging and be related to mass loss and changes in Young modulus due to a reduction in the amount of scaffold material present.

1.4: Organization of Thesis

The first chapter of this thesis is a general introduction to the concept of tissue engineering and the research issues addressed by this work. The second chapter is to review the current state of the art in both time dependent and time independent scaffold modelling. In particular, various analytical and numerical approaches to scaffold mechanical property modelling are introduced. A review of common approaches for modelling scaffold degradation is also presented. Finally, current state of the art in *in vivo* monitoring was presented and discussed. The current state of the art in *in vivo* monitoring involves the tagging of the scaffold material with tracer material that is then tracked via some means in the body, or by the full explant of the scaffold and the characterization of the scaffold degradation outside of the body.

The third chapter examines the modelling of the time independent and time dependent mechanical properties of a semi-crystalline polymeric ceramic composite scaffold for bone tissue engineering applications. A detailed model is developed by considering all of the structural levels of the scaffold. Measurements of scaffold elastic property with time were then employed to estimate the parameters of the model instead of tabletop experiments for identifying individual parameters separately. This model with the so identified parameters was then validated for different but similar geometric configurations.

The use of ultrasound for remote measurement of the scaffold stiffness and issues associated with the uniqueness, stability, and existence of a solution to this inverse problem are considered in the fourth chapter. The use of the Fourier transform of a spacially periodic optical signal for deflection characterization is also presented.

Estimating the stiffness and mass changes with time from geometry when scaffolds degrade via the surface degradation pathway is considered in the fifth and sixth chapters. They introduce the possibility of utilizing surface degrading materials in the construction of the mechanical support skeletons of hybrid scaffolds for cartilage tissue engineering, which could then be characterized *in vivo* through phase contrast geometry monitoring. Particularly in the fifth chapter, morphology monitoring of the scaffold *in situ* is employed to measure the mass loss of a scaffold with time

from imaging data. The mass loss measured from imaging data was then validated by comparing its predictions for mass loss from the direct measurement of mass loss by weighing. The parameters of a time dependent model for scaffold surface degradation were then estimated from the mass loss with time as inferred from the imaging data.

In the sixth chapter, this morphology measurement technique is extended and employed to estimate the decline in the scaffold's stiffness. By visually examining the scaffold with time it was possible to relate the time dependent geometry of the scaffold to its effective stiffness. In addition, the nonlinear stress-strain curve was also reconstructed with some success from geometry data obtained through imaging.

The seventh chapter of the thesis is a general discussion to unite all of the separate studies together and describe how they mutually complement each other and achieve the previously established research objectives. The eighth chapter presents the conclusions drawn from this work and some future avenues of research.

CHAPTER 2

A BRIEF REVIEW OF THE MODELING OF THE TIME DEPENDENT MECHANICAL PROPERTIES OF TISSUE ENGINEERING SCAFFOLDS*

*****This chapter has been published as "Bawolin, N. K., Zhang, W. J., Chen, X. B., 2010, A Brief Review of The Modeling of the Time Dependent Mechanical Properties of Tissue Engineering Scaffolds, Journal of Biomimetics, Biomaterials, and Tissue Engineering. vol. 6, p. 19-33." According to the Copyright Agreement, "the authors retain the right to include the journal article, in full or in part, in a thesis or dissertation".

2.1: Summary

Many methodologies have been proposed and executed to model both time independent and time dependent tissue scaffold behavior. In this paper these methods are reviewed and their applicability to the research in this thesis are considered. In essence this paper was a search for an appropriate modelling approach that could then be applied in the research presented in the following chapter. It was of interest to see if any existing models could be adopted from the literature to model the particular system of a Hydroxyapatite reinforced Polycaprolactone matrix composite scaffold ideal for bone tissue engineering.

Of all of the models reviewed, the diffusion based models that consider the diffusion of hydrolysis causing mediums into the scaffold held the most promise of having predictive power; i.e., the ability to predict scaffold degradation for different scaffold geometry, once the model parameters have been estimated from experiment. The concept of Finite Element model updating was also proposed as a method to consider the time dependent behavior of the scaffold. In classical vibration based Finite Element Model Updating, the modes of vibration are characterized and related to scaffold properties, which are updated with time to match the changing modal data of the scaffold. The primary strength of this method is that it theoretically has a signal that can be characterized *in vivo* (the modes of vibration). It also tests the whole scaffold, and derives model parameters from this experimental data. This allows every effect on

scaffold properties to be included in the estimation of parameters, some of which may be overlooked if the model parameters are just estimated from individual independent experiments related to specific phenomena.

An ideal approach to model the elastic property of the scaffold at every moment in time has been identified. Finite element based homogenization with periodic boundary conditions is not only significantly more computationally efficient that fully detailed finite element modelling, it is also executable with well-established commercial software like ANSYS. In addition, the time dependent model based on detailed simulation of mass transfer within the scaffold allows models to be predictive and capable of replicating the behavior of the actual scaffold even when geometry is changed, so long as the scaffold material and the biological environment remain the same. Finally, full scale testing of the scaffold is proposed as a way to estimate the models in the time dependent and time independent models of scaffold elasticity, so as to include the effects of scaffold manufacturing on the estimated parameters.

2.2: Introduction

One of the most promising approaches to the development of artificial tissue substitutes relies upon the utilization of an artificial prosthetic of the extra-cellular matrix, known as the tissue scaffold. This construct provides support for the attachment of cells, which are then expected to proliferate, differentiate, and organize eventually into new tissue. Two primary approaches to the regeneration process may be pursued after scaffold fabrication, cell seeding, and the inclusion of other factors; 1) transplantation into the *in vivo* environment immediately or after a brief period of incubation, and 2) long term incubation *in vitro* followed by implantation after substantial or total tissue growth and scaffold dissolution. In the former, the implanted scaffold is expected to perform tissue functions temporarily and gradually allocate functionality to the tissue during its degradation. If the tissue function is structural support, the mechanical properties displayed by the scaffold become critical design aspects, and should ideally match those of the surrounding tissue throughout the treatment period.

The tissue scaffold is a classic multiphase system, consisting of a scaffold occupied volume, and a porous region either occupied by tissue, fluid, empty space, or some combination thereof. The effective mechanical properties of the entire construct are a function of the properties of the constituent phases and their respective volume fractions, all of which may be functions of time.

Two primary processes are at work in the scaffold during treatment; scaffold degradation and resorption, and the gradual growth of tissue in the pores of the scaffold. While the former drives a mechanical property decline in the scaffold occupied regions of the construct, the latter tends to increase the mechanical properties of the porous region. If these two competing trends are not carefully balanced by the scaffold design, the effective properties of the construct will vary with time, leading to a suboptimum outcome. The ideal would be for the behavior of the regenerating tissue in the pores and the scaffold backbone to result in a relatively constant value for the effective properties, and that this be equal to those of the surroundings. The design for such a device could be ascertained by an *ad hoc* experimental method, costly in both time and resources, or theoretical methods, employed to model the behavior of the scaffold during tissue regeneration and scaffold degradation, could guide the design process.

There are three general types of degradation behavior that have been observed experimentally for tissue scaffolds composed of polymeric materials. These three degradation pathways are 1) surface erosion, 2) bulk degradation, and 3) internal degradation. These behaviors are illustrated in Fig. 2-1.

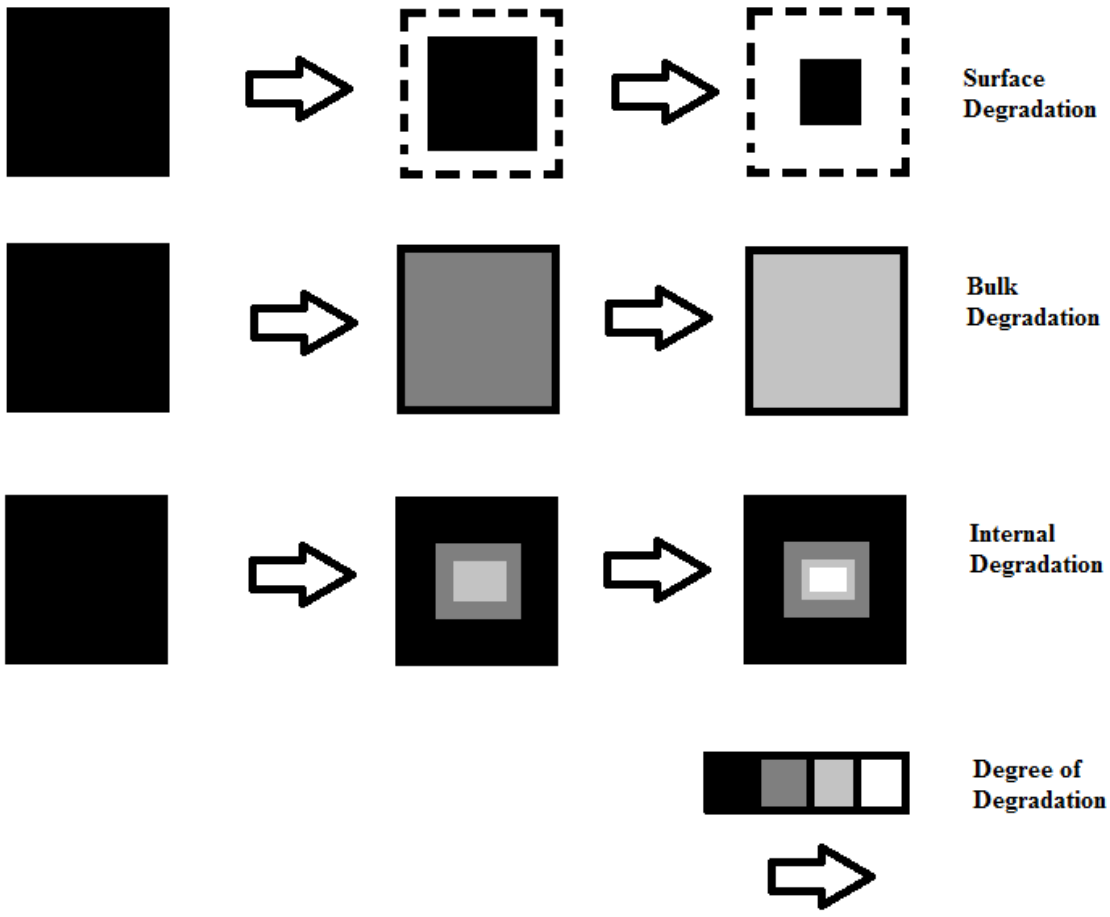

Figure 2-1: Scaffold degradation behaviors

The possible scope of scaffold models can be divided into six broad categories: 1) the construct's effective mechanical properties at a particular time, given the known properties of its constituents and the geometry of its microstructure; 2) the bulk degradation of the scaffold component of the construct; 3) surface degradation of the scaffold component of the construct; 4) changes to the crystallinity of the construct with time; 5) the regeneration of tissue within the scaffold's pores; and 6) both the tissue regeneration and scaffold dissolution and the dependence of both on each other. Previous work by the author and collaborators [1] has successfully demonstrated objectives 1) and 2).

2.3: Models of the Mechanical Properties of Tissue Scaffolds

Models of tissue scaffolds take in as input the various chemical, material, and geometric parameters of the tissue scaffold, such as pore geometry, crystallinity, molecular weight, and the mechanical properties of the scaffold material, and give as output the effective mechanical properties of the tissue scaffold. Since the tissue scaffold can be considered as a traditional multiphase material, and additionally a material with a periodic microstructure, the various methods in the literature that have been developed to consider composites may be used to predict the properties of tissue scaffolds. These composite methods may be divided into two broad categories; 1) analytical approaches, and 2) numerical approaches.

2.3.1: Analytical Models

The simplest model of a composite material is known as the rule of mixtures. In this model, the property of interest for each of the constituents of the composite is multiplied by its volume fraction, and the sum is the predicted property of the mixture [2].

$$P_c = P_f v_f + P_m v_m \tag{2.1}$$

where P_c is the property of the composite P_f that of the filler, and P_m that of the matrix. v_f and v_m are the volume fractions of the filler and matrix respectively. This average is known as the Voit average, and is valid for isostrain conditions of loading. For isostress conditions of loading, the effective property of the composite is given by the Reuss average modulus,

$$P_c = \frac{P_f P_m}{P_m v_f + P_f v_m} \tag{2.2}$$

An extension of these models is the Takayanagi model for dispersed phases. This model considers the composite as a series of springs which are arranged in a series-parallel or parallel-series arrangement, as shown in Fig. 2-2. For the series-parallel model, the effective property is given by

$$\frac{1}{P} = \frac{\varphi}{\lambda P_A + (1-\lambda)P_B} + \frac{1-\varphi}{P_B} \tag{2.3}$$

and for the parallel-series model, the expression is

$$P = \lambda\left(\frac{\varphi}{P_A} + \frac{1-\varphi}{P_B}\right)^{-1} + (1-\lambda)P_B \tag{2.4}$$

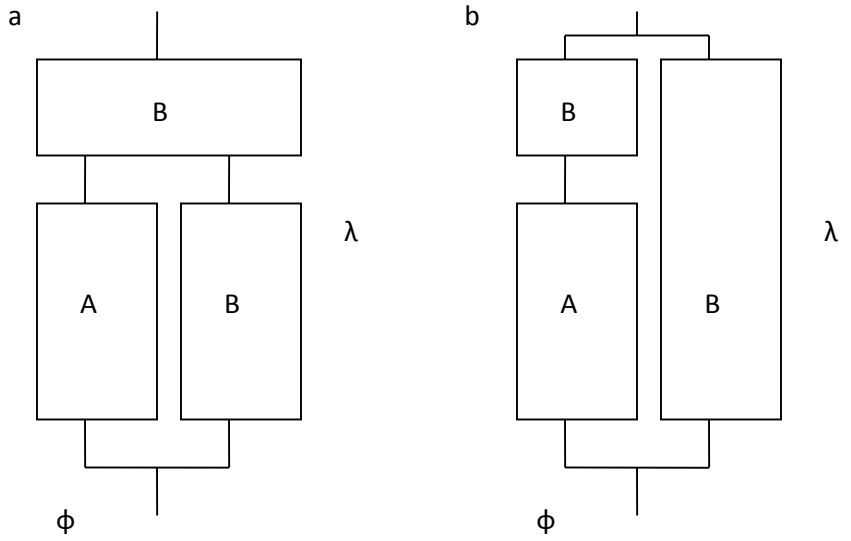

Figure 2-2: Takayanagi Models a) Series-Parallel, and b) Parallel-Series

Homogenization methods all attempt to replace a heterogeneous material where the material properties are location dependent with an equivalent homogeneous material that displays approximately identical behavior to that of the heterogeneous material. The properties of this equivalent material can be predicted from the volume averaged stresses and strains in the composite's constituents [3].

$$\bar{\sigma} = \sum_{r=1}^{n} v_r \bar{\sigma}_r \tag{2.5}$$

where $\bar{\sigma}$ is the average stress in the equivalent homogenized material, v_r is the volume fraction of constituent *r* and the overbar indicates a volume average. $\bar{\sigma}_r$ is therefore the volume averaged stress in each of the composite's material phases. In a similar manner strain in the equivalent homogenized material is expressed as,

$$\bar{\varepsilon} = \sum_{r=1}^{n} v_r \bar{\varepsilon}_r \tag{2.6}$$

For each phase in the composite, a constitutive relationship exists between the strain and stress in the material phase.

$$\sigma_r = C_r \varepsilon_r \tag{2.7}$$

where C_r is the stiffness tensor for the constituent. For the effective composite material, the stiffness is related to the average stress and strain fields in the composite,

$$\bar{\sigma} = C\bar{\varepsilon} \tag{2.8}$$

From this expression it is apparent that an effective stiffness matrix for the composite can be determined if the volume average strain and stress in the composite is known or can be

computed. The volume average strain inside each constituent may be related to the average strain in the composite through,

$$\bar{\varepsilon}_r = A_r \bar{\varepsilon} \tag{2.9}$$

where A_r is the concentration tensor for phase *r*. The sum of the concentration tensors for each constituent multiplied by the constituent's volume fraction gives the identity matrix *I*.

$$\sum_{r=1}^{n} v_r A_r = I \tag{2.10}$$

Equations (2.5-2.10) may be combined to give the effective stiffness matrix of the composite as a function of the stiffness matricies of the composite's constituents.

$$C = C_1 + \sum_{r=2}^{n} v_r (C_r - C_1) A_r \tag{2.11}$$

From (2.11) it is apparent that the effective stiffness matrix of the composite can be determined from the constituent stiffness matricies if A_r is known, and equation (2-9) provides a way for its calculation. Various methods for the calculation of A_r lead to different methods for homogenizing. These methods are introduced and reviewed in [4]. While it is possible to calculate A_r for simple geometries, numerical solutions must be employed for irregularly shaped inclusions.

Another analytical method for the calculation of effective properties is known as the Halpin Tsai method [5]. The analytical solutions for effective properties of composites reinforced with inclusions with simple geometries were rearranged into a general form,

$$\frac{p}{p_m} = \frac{1+\xi\eta\phi}{1-\eta\phi}\ ,\ \eta = \frac{\frac{p_f}{p_m}-1}{\frac{p_f}{p_m}+\xi} \qquad (2.12)$$

where ξ is a shape factor that takes into account the geometry of the filler and ϕ is the filler volume fraction. With fillers of irregular geometry, it is challenging to find analytical expressions for A_r. In these cases it is usually necessary to turn to numerical methods for homogenization.

2.3.2: Full Body Finite Element Analysis

In this approach to the problem, the finite element method is employed to evaluate computationally, the behavior of the tissue scaffold. A finite element model of the entire scaffold is assembled, which includes every structural detail of the scaffold, from the geometry of the pores, to the inclusion of various microstructure details in the scaffold material itself, such as the inclusion of small particles or various material phases. Once such a model is established, deflection boundary conditions may be applied to the model to represent the effect of a material property test, such as a load deflection or beam bending. An example of this method is found in the work of Milan, Planell, and Lacroix [6] where a virtual load displacement test on a cylindrical scaffold is conducted to predict the mechanical properties of the scaffold and the internal mechanical environment within the pores during scaffold loading.

This method, while intuitive and accurate, requires considerable computational resources in order to encompass all of the structural details of the scaffold. In order to reduce the computational burden, a representative section of each structural level in the scaffold may be separately analyzed to give its effective mechanical properties, allowing each structural level to be replaced by an equivalent continuous phase. This procedure is known as homogenization.

2.3.3: Standard Mechanics Homogenization

The standard mechanics approach to homogenization takes a representative piece of microstructure and subjects it to a compressive or tensile test, calculating the average stress after each small increment of displacement experienced by the body. This yields a complete stress-strain curve which is taken as the effective behavior of the microstructure [7]. An isolated section of the whole however does not behave identically *in situ*. This is demonstrated in [8] by increasing the size of the chosen representative volume. The mechanical properties estimated from the study of each representative volume gradually reach an asymptote as the size of the chosen RV increases, as illustrated in Fig. 2-3.

2.3.4: Representative Volume FE Model with Periodic Displacements

The ideal homogenization method will give an accurate prediction for the in situ behavior of the microstructure by the analysis of the smallest possible unit cell. Ideally, the unit cell should be one periodic component of the microstructure. In order to analyze only one periodic cell and still achieve an accurate prediction for the behavior of the cell when it is surrounded by its neighbors, the boundary conditions chosen for the analysis must be similar to the actual boundary conditions experienced by the cell.

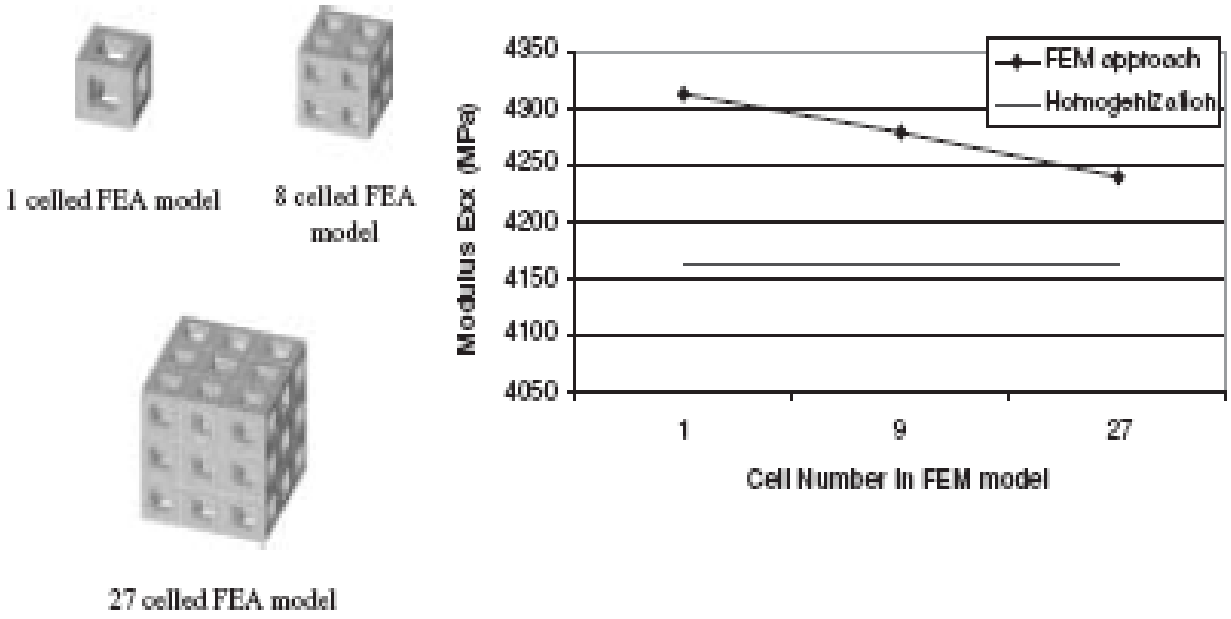

Figure 2-3: Effective modulus by the FE standard mechanics method, and the asymptotic homogenization method, as a function of RV size [8].

Periodic boundary conditions allow the cells to be tiled together to create the global body without gaps or overlapping, which is a good average representation of the behavior of all of the unit cells within the global body during global body elongation or compression. In [9] a square unit cell is subjected to the following displacement boundary conditions,

$$u_i^{K-} - u_i^{K+} = \bar{S}_{ij}(x_j^{K-} - x_j^{K+}) \qquad (2.13)$$

where $i, j = 1, 2, 3$, $\bar{S}_{ij}$ is the average RV strain, u_i is the displacement of the point under consideration in the x_i direction, x_j are the Cartesian coordinates of the point on the RV boundary, and $K+$ and $K-$ indicate whether the point under consideration is in the positive or negative x_j direction. The average stress and strain are then determined from the FEM model by,

$$\bar{S}_{ij} = \frac{1}{V_{RV}} \int_{V_{RV}} S_{ij} dV_{RV} \tag{2.14}$$

$$\bar{T}_{ij} = \frac{1}{V_{RV}} \int_{V_{RV}} T_{ij} dV_{RV} \tag{2.15}$$

where $\bar{S}_{ij}$ and S_{ij} are the average and local strains respectively, $\bar{T}_{ij}$ is the average stress, and T_{ij} is the local stress. By calculating the average stress in the body while consecutively applying six separate average global strains $\bar{S}_{ij}$, by applying the appropriate deflection boundary conditions as given by (2.13), the effective stiffness matrix of the scaffold may be determined.

$$\begin{Bmatrix} \bar{T}_{11} \\ \bar{T}_{22} \\ \bar{T}_{33} \\ \bar{T}_{23} \\ \bar{T}_{31} \\ \bar{T}_{12} \end{Bmatrix} = \begin{bmatrix} \bar{C}_{11} & \bar{C}_{12} & \bar{C}_{13} & \bar{C}_{14} & \bar{C}_{15} & \bar{C}_{16} \\ & \bar{C}_{22} & \bar{C}_{23} & \bar{C}_{24} & \bar{C}_{25} & \bar{C}_{26} \\ & & \bar{C}_{33} & \bar{C}_{34} & \bar{C}_{35} & \bar{C}_{36} \\ & & & \bar{C}_{44} & \bar{C}_{45} & \bar{C}_{46} \\ & Symm & & & \bar{C}_{55} & \bar{C}_{56} \\ & & & & & \bar{C}_{66} \end{bmatrix} \begin{Bmatrix} \bar{S}_{11} \\ \bar{S}_{22} \\ \bar{S}_{33} \\ \bar{S}_{23} \\ \bar{S}_{31} \\ \bar{S}_{12} \end{Bmatrix} \tag{2.16}$$

Once the stiffness matrix is known, the effective compliance matrix may be calculated from its inverse. The effective mechanical properties of the scaffold such as its Young modulus and Poisson ratio in various directions are then determined from the compliance matrix [10].

2.3.5: Asymptotic Homogenization

Asymptotic homogenization replaces the strain in a body with an asymptotic series, which represents the strain in the global composite body as a average strain at the highest structural level plus rapidly varying strains caused by the microstructure levels of the composite.

$$u^{\varepsilon} = u^{\theta} + \varepsilon^1 u^1 + \varepsilon^2 u^2 + \varepsilon^3 u^3 + ... \tag{2.17}$$

where u^{ε} is the total displacement, u^{θ} is the displacement on the most macroscopic level, u^{i}, i = 1,2,… is the displacement at increasingly more microscopic levels, and ε is the scale size between adjacent structure levels

Inserting this representation of the strain into the differential equations describing the behavior of a deforming solid and solving the resulting equations with a numerical method, such as the finite element method, allows the effective behavior of the global body to be estimated from the known mechanical properties of the constituent phases [11]. This method also assumes that the deflections on the boundary of the unit cell are periodic, leading to estimates for effective properties superior to those given by the standard mechanics approach to homogenization.

2.4: Time Dependent Models of Tissue and Tissue Scaffolds

Time dependent models of tissue scaffolds can be thought of as time independent models for which the parameters change with time. These time dependent parameters in turn are also functions of various geometric variables and material properties, and the qualities of the degradation environment.

2.4.1: Models of Scaffold Degradation and Declining Mechanical Properties

The degradation of the scaffold framework of the tissue engineering is often a less complex process than the response of tissue, therefore initial approaches to the computer simulation of tissue scaffold behavior with time have neglected the tissue response and have focused only on the degrading scaffold.

The approach taken by Wilson , Bossnar, and Kholes [12] rests upon the assumption that scaffold degradation, characterized by mass loss, is independent of cell growth and tissue behavior, and may be represented as an empirical exponential expression of the form,

$$M(t) = SCM + [GAG]_{ss}\left(1 - e^{-t/\tau_{GAG}}\right) + [Collagen]_{ss}\left(1 - e^{-t/\tau_{Collagen}}\right) + [Scaffold]_{ss} e^{-t/\tau_{Scaffold}} \quad (2.18)$$

where $M(t)$ is the time dependent mass of the tissue construct, SCM is seeded cell mass, $[GAG]_{ss}$ is the steady state concentration of extracellular matrix glycosaminoglycans, $[Collagen]_{ss}$ is the steady state concentration of collagen, $[Scaffold]_{ss}$ is the steady state concentration of the scaffold material, and τ_{GAG}, $\tau_{Collagen}$, and $\tau_{Scaffold}$ are time constants for the accumulation of extracellular matrix components and the scaffold mass loss. These time constants were estimated in this study from the experimental measurement of mass loss and accumulation for both seeded and unseeded scaffolds. Briefly, at appropriate time intervals, seeded scaffolds were removed from incubation, digested, and subject to biochemical analysis to ascertain the mass of the accumulating collagen and glycosaminoglycans. The unseeded scaffolds were characterized for mass loss by simple dry and wet weight measurements.

While this model does not give estimates for the mechanical properties of the tissue scaffold with time, it is apparent that an experimental approach could possibly relate the mass loss of the scaffold due to degradation and the mass accumulation in the pores of the scaffold to the effective mechanical properties of the tissue construct.

The primary limitations of this model are that the time constants for extracellular matrix accumulation and scaffold mass loss are complex functions of geometry and material properties. A model such as this lacks predictive power due to its reliance on the estimation of parameters from experimental evidence. Such parameters, once identified are not guaranteed to be relevant if the geometry of the scaffold changes. In addition, this model's focus on mass loss neglects the possibility of bulk degradation, where the decline in mechanical properties of the scaffold may proceed with little to no mass loss or changes in geometry. The limitations of simple empirical models has led to the development of mechanistic or phenomological models for scaffold degradation.

In the work of Mohammadi and Jabbari [13], a Monte Carlo based algorithm is used to simulate the hydrolytic breaking of polymer chains, yielding predictions for the average molecular weight and molecular weight distribution in the scaffold construct with time. This algorithm seeds the individual elements within a partitioned porous scaffold volume with polymer chains, where polymer chain length is randomly selected from the Schultz–Flory distribution. Once polymer chain seeding is accomplished, a randomly selected polymer chain is sundered after a given time interval, resulting in the formation of two new chains and a degradation byproduct.

By representing the time between chain scissions in each element as a function of byproduct concentration, the catalyzing effect of degradation byproducts on the degradation process was included in this model. Furthermore, once the chain length of the polymer reaches a certain minimum length, it is assumed free to diffuse out of the scaffold body, leading to estimations for mass loss with time.

While this model gives a time history of the molecular weight of the scaffold, it does not translate the molecular weight decline into predictions for the mechanical properties of the scaffold. This particular model's use of bulk elements for interior regions of the scaffold, where byproducts are assumed to accumulate, and surface elements where catalyzing byproducts are released from the scaffold neglects the mass transport of degradation byproducts through the scaffold, and the effect this mass transport may have on degradation. In addition, this model does not include the effect of crystallinity on the degradation process even though the authors argue that this may be included by adjusting the probability of chain scission in the elements to account for the impermeable inert nature of the polymer crystalline phase.

In the work of Wang, Pan, Han, Sinka, and Ding, [14] a model for scaffold degradation is formulated which takes into account the transport of degradation byproducts and their influence on the degradation process. Briefly, the model consists of a phenomological representation of the hydrolysis degradation process,

$$\frac{dR}{dt} = \frac{dC_e}{dt} = k_1 C_e C_w + k_2 C_e C_w C_m{}^n \tag{2.19}$$

where k_1 and k_2 are the non catalyzed and catalyzed rate constants respectively, C_e is the ester bond concentration in the polymer phase of the scaffold, C_w is the water concentration in the polymer, C_m is the monomer end group concentration in the polymer, and n is the monomer disassociation term which is related to the moles of hydrogen ions released per mole of degradation byproduct dissolved in water. The molecular weight at any given point of time is related to the ester bond concentration by

$$\frac{C_e}{C_{e_0}} = \frac{M_W}{M_{W_0}} \tag{2.20}$$

where C_{e_0} and M_{W_0} are the initial ester bond concentration and the initial molecular weight.

The primary shortcomings of this model are that it does not move from molecular weight predictions to predictions of mechanical properties. Furthermore, the model neglects the important process of crystallization and the time dependency of the transport properties of the scaffold.

An extension of the above model may be found in the work of Han and Pan [15]. In this modification, an additional feature is added to include the time dependent crystallinity of the scaffold, and the effect of this process on the transport properties of the scaffold. Utilizing the fundamental equations of Avrami, the modification calculates the production of new nucleation sites in the scaffold and assumes that new spherulites of crystal growth begin at these new sites. The increase in nucleation site concentration within the scaffold, created by the scission of polymer chains, is determined by,

$$dN = -\zeta N - \frac{N}{1 - X_c} dX_c + \frac{N_0}{C_{e_0}} dR \tag{2.21}$$

where N is the concentration of nuclei in the scaffold (moles/ m^3), ζ is the probability, assumed to be unity, that at any given time nuclei will initiate new crystal growth, X_c is the crystallinity, whose increase is engulfing nuclei in the body, N_0 is the initial concentration of nuclei in the body, which is assumed to be zero at $t = 0$, and dR is the increase in the concentration of the monomer byproducts of degradation. Once the increase in nucleation sites is calculated, a spherulite is assumed to begin its gradual growth at most of the new nucleation points, where the number of nucleation sites that result in new crystal growth are calculated from the probability of growth initiation at new sites. The volume of the spherulites are then allowed to expand until a radius limit is reached. The extended volume of crystal, or the volume of crystal if no impingement occurs, is then determined [15].

$$X_{ext} = \int_0^t V_{\text{sin}\,gle}(t - \tau) N_n d\tau \tag{2.22}$$

where $V_{Single}(t - \tau)$ is the total crystal volume, at time t, of all of the spherulites nucleated at time τ and N_n is the number of nuclei at t. Assuming a spherical shape for the growing crystals, the achievable radius r is constrained by the molecular weight of the polymer. The following is used as an approximation of the radius of each spherulite with time,

$$r = r_{\max}\left(1 - e^{-\frac{G}{r_{\max}}(t-\tau)}\right) \tag{2.23}$$

where $r_{\max}$ is the maximum possible radius for each spherulite, and G is the crystal growth rate for the polymer at the operating temperature of the scaffold. The extended volume is therefore,

$$X_{ext} = \int_0^t \frac{4}{3}\pi \left(r_{\max} \left(1 - e^{-\frac{G}{r_{\max}}(t-\tau)} \right) \right)^3 N_n(\tau) d\tau \qquad (2.24)$$

The extended volume of the crystal may then be related to the change in crystallinity of the scaffold. Avrami's theory of crystallization yields the actual transformed volume fraction with impingement X_c from the transformed volume fraction with no blockage or impingement from surrounding growth X_{ext}.

$$\frac{dX_c}{dX_{ext}} = (1 - X_c)^{\lambda} \qquad (2.25)$$

where the impingement factor λ is a fitting parameter for situations where the nucleation points are not randomly distributed, or the crystal growth factor G is not equal in all directions [16].

The transport properties are determined in this model by a separate finite element analysis of a cubical representative volume. The addition of a new phase into the representative volume changes the effective diffusion coefficient of the FEM model, whose predictions are ultimately fitted to an empirical surface, which is used to estimate the effective diffusion coefficient of a two phase material.

$$D_{eff} = D_{slow} + \left(1.3V_{fast}{}^2 - 0.3V_{fast}{}^3\right)\left(D_{fast} - D_{slow}\right) \qquad (2.26)$$

where D_{eff} is the effective diffusion coefficient of the two phase composite, D_{slow} is the diffusion coefficient of the more impenetrable phase of the material and D_{fast} is the diffusion coefficient of the more pervious phase.

The primary weakness of this model is again the lack of a prediction of mechanical properties from the estimated molecular weight. The inclusion of the crystal phase adds another dimension to the modeling of the mechanical properties, since the properties displayed by both the crystal and amorphous phases of the polymer must also be considered. This model also assumes isotropic transport properties, and neglects the influence of inclusion shape on the effective diffusion coefficient of the scaffold material. The use of a simple empirical expression to give the effective transport properties leaves much possible improvement. The use of random walking algorithms or empirical approaches such as the Maxwell Garnett approximation may yield better modeling of the transport properties of the scaffold [17]. This particular model also neglects the diffusion of water in the scaffold, with the possibility of a water concentration gradient, or the absorption of water by a hydrophilic phase of the scaffold, which may be important parameters influencing the degradation.

The authors Wang et al. [18] developed a model based on their previous work which proposes an entropy spring model for the scaffold material. This model, assuming that the scaffold polymeric material is completely amorphous, represents the Young Modulus of the scaffold material as an entropy spring, where the increase in entropy from strand length reduction leads to a decline in the stiffness of the polymer with molecular weight. This publication also considers the use of simple experimentally derived relationship between average molecular weight and Young Modulus. Their previously devised degradation model [14] is then utilized to predict the molecular weight distribution inside the device, as well as the distribution of Young Modulus with time. In the work of Arosio et al., a degradation model for a drug delivery device is considered where the authors have linearly related the decline in molecular weight of the device to its expected Young Modulus and bending strength [19]. No attempt however is made to relate the yield strength, elongation at yield, or other interesting mechanical properties to the molecular weight.

In [20] a probabilistic model is employed to model the hydrolysis reaction and decide at what time intervals to scission the polymer chains in each small volume element in the model. The autocatalysis due to monomer migration is represented with a rate-diffusion model that modifies

the probability of chain scissioning in each element based on its time dependent monomer concentration.

In all of the above time dependent degradation modeling approaches, a dynamic model is developed which yields the molecular weight of the degrading polymer with time. With the exception of a small number of the models reviewed, [18,19] these molecular weights are not translated into mechanical property predictions for the scaffold or the scaffold material. The possible addition of other material phases to the scaffold material leads to the need for modifications to the existing theories to consider the simultaneous degradation of multiple polymeric phases in the scaffold device, and the use of multiscale homogenization techniques to find the effective mechanical properties of these multiphase materials at each time point.

2.4.2: Models of Tissue Regeneration and Behavior

Ultimately, models of scaffold degradation should be coupled with models of tissue growth on the scaffold. A vast number of cell behavior models may be found in the literature, the problem being relevant to fields as diverse as tumor treatment to agriculture. The following is a small sampling of the state of the art of cell and tissue behavior modeling.

The first issue that must be considered is simply the distribution of cell concentration within the scaffold as a function of time. The number of cells present in a tissue engineering scaffold is not just a function of the proliferation and death of seeded cells on the scaffold, but must also include the migration of cells from the scaffold surroundings *in vivo*. In the work of Anderson and Chaplain [21], the problem of the migration of endothelial cells from the surroundings was considered, with an emphasis on the modeling of tumor induced angiogenesis. In this model, the number of cells increases or decreases at a specific location at a rate established by chemical signals. The cell migration is assumed to be the sum of a random walk, a motion induced by the concentration gradient of tumor angiogenesis factor (TAF), and motion induced by the chemical gradient of cellular fibronectin. Their model gives the concentration of endothelial cells n at a specific point as a function of TAF concentration c, and fibronectine concentration f.

$$\frac{dn}{dt} = D_n \nabla^2 n - \nabla\left(\frac{\chi_0 k_1}{k_1 + c} n \nabla c \right) - \nabla(\rho_0 n \nabla f) \tag{2.27}$$

$$\frac{df}{dt} = \omega n - \mu n f \tag{2.28}$$

$$\frac{dc}{dt} = -\lambda n c \tag{2.29}$$

where D_n is a diffusion coefficient representing the random movement of cells caused by no particular stimuli, χ_0 is a chemotaxis parameter representing the cell behavior in response to TAF, k_1 is a parameter representing the decline in cell TAF sensitivity as TAF concentration increases, and ρ_0 represents the sensitivity of cells to fibronectine. The concentration of fibronectine with time is a function of the fibronectine production rate per cell ω and the amount of fibronectine consumed by each cell, which is represented by the parameter μ. The concentration of TAF is assumed to decline with time due to cell consumption represented by the parameter λ. This model represents a clear method for determining the movement of cells from the external surroundings into the scaffold as a function of chemical stimulation, and may also accurately model the migration of cells within a scaffold.This approach, however, does not consider cell proliferation or death, or the possibility of non-chemical or mechanical stimulations for cell migration. In the work of Kelly and Prendergast [22], the concentration of cells is represented as,

$$\frac{dn^i}{dt} = D^i \nabla^2 n^i + P^i(S) n^i - K^i(S) n^i \tag{2.30}$$

where *n* is cell concentration, *i* represents cell type, D represents the migration of cells as a quasi-diffusion process, *P* is the proliferation rate which is a function of chemical and mechanical stimulation *S*, and *K* is the cell death and differentiation rate. In this model, the

stimulation S is chosen to be the strain γ experienced by the cells, and the fluid velocity v in the tissue.

$$S = \frac{S_0}{l} + \frac{v}{m} \tag{2.31}$$

where l and m are experimental parameters determined from mesenchymal stem cell (MSC) differentiation experiments. When S achieves a certain value, MSCs are assumed to differentiate into bone, cartilage, or connective tissue. A quadratic relationship is assumed to hold between cell population growth or decline and the strain experienced by the cells.

$$P^i(S)n^i - K^i(S)n^i = a^i + b^i S_0 + c^i {S_0}^2 \tag{2.32}$$

where a, b, and c, are experimentally determined parameters for each cell type in the scaffold. While this model does consider the proliferation, differentiation and migration of cells, it does make simplifying assumptions such as ignoring the effect of chemical signaling in cell migration. The approach taken here has the potential to be expanded by inclusion with the previous approach to yield cell concentration within a scaffold as a function of both chemical and mechanical stimulation.

In the work of Checa and Prendergast [23], a cubic volume is filled with a lattice, where each lattice point is considered to be a possible cell location. Each point is surrounded by 6 neighbor points which are considered possible locations for new cells generated by mitosis. After mitosis, two lattice points are selected at random and filled with new cells. If no new lattice points exist, then mitosis/proliferation is prohibited. In order to model cell migration, cells are randomly assigned a new lattice position from the six possible neighboring positions after a fixed time interval related to the cell type, and if all lattice positions are occupied, cell migration is prohibited. In order to determine cell differentiation, the mechanical stimulation found in [22] is employed with an addition. A model similar to that in [21] is used to consider the infiltration of blood vessels into the cubic tissue volume, and the concentration of blood vessels is used as an

additional parameter to control the differentiation of the cells in the cubic volume. The capillaries are assumed to follow the path pioneered by the infiltrating endothelial cells. The steps in the developed algorithm are illustrated in Fig. 2-4.

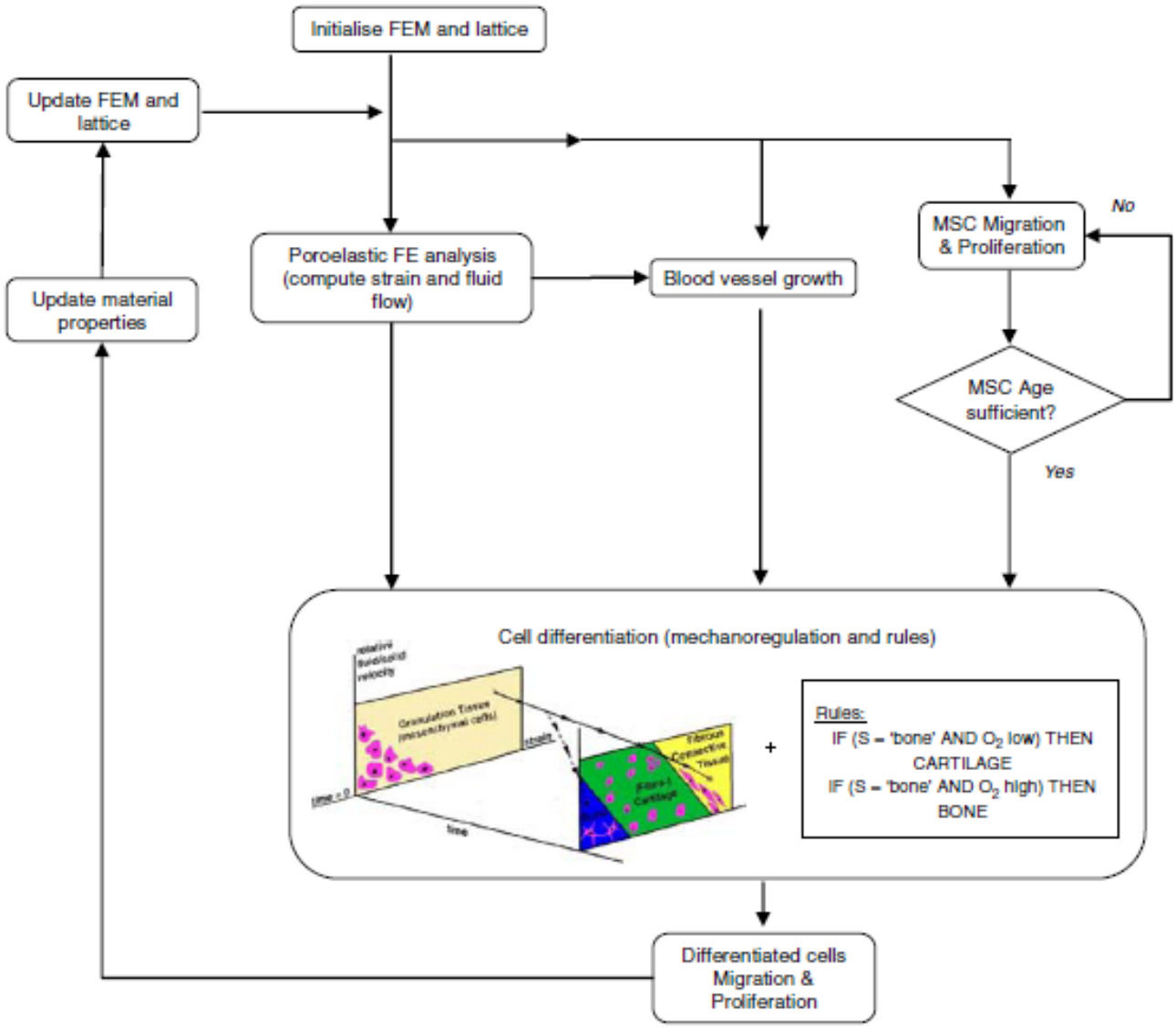

Figure 2-4: Modeling of Cell differentiation proliferation and death within a cubic tissue volume [22]

The drawbacks of this modeling approach are that it neglects the possibility of mechanical or chemical stimulation to the migration, proliferation, and death of the cells. The model also comprises a large number of parameters which are collected from a variety of experiments carried out under a variety of conditions on different animals. This may be an area where a unique contribution may be made from the field of structural dynamics. If the modes of vibration or other mechanical properties of a scaffold could be measured with time and related to the various parameters, it should be possible to estimate a best unique set from the domain encompassing all possible parameter values from a single experiment, ensuring that all parameter estimates are for the same experimental conditions.

2.4.3: Models of Simultaneous Scaffold Degradation and Tissue Regeneration

In the work of Adachi, Osako, Tanaka, Hojo, and Hollister [24], a model of both scaffold degradation and tissue regeneration is proposed for bone tissue engineering. In their model, the hydrolysis of a polymer scaffold is driven by the concentration of water at each point within the scaffold, and a linear relationship between molecular weight and polymer stiffness is utilized to give the spatial distribution of Young Modulus in the scaffold. In this model the volume occupied by tissue, scaffold and fluid are discretized, and the driving force for scaffold dissolution, water concentration, is calculated within the scaffold with time. The molecular weight distribution within the scaffold is then determined at each time step and related linearly to the Young modulus of the scaffold material at each spatial point within the scaffold. The external loading of the scaffold results in a strain distribution within the scaffold pores that becomes the impetus for new tissue regeneration. When molecular weight is reduced to a certain level, that specific portion of the scaffold is assumed to be able to diffuse out of the scaffold body leading to mass loss. The primary limitations of this model are that it does not consider the influence of cell diffusion into the scaffold, and its influence on tissue growth.

In the work of Sanz-Herrera, Garcıia-Aznar and Doblare [25], a tissue engineering scaffold's degradation, and the regeneration of bone tissue in the scaffold pores is modeled. The movement of MSC, osteoblasts, and endothelial cells into the scaffold is represented as a simple diffusion process driven by only the concentration gradients of the various cells into the scaffold. The

degradation of the scaffold is considered to be a simple hydrolysis process where only water concentration controls the degradation rate. In this model, the concentration of cells in the scaffold as well as mechanical stimulation control the rate of tissue regeneration. In both of these works, the developed models must be further validated experimentally both *in vivo* and *in vitro*.

The tissue regeneration and scaffold degradation are mutually dependent on one another. The mechanical stimulation of tissue on its scaffold substrate is known to affect the behavior of the regenerating tissue, and concurrently, the regenerating tissue is known to generate metabolic waste products which increase the acidity of the surroundings, leading to enhanced hydrolysis in the scaffold. Future research must clarify the metabolic production rate of cells as a function of loading, and the effect of metabolic waste products on the degradation of the scaffold.

2.5: Unresolved Issues in Modeling of Time Dependent Mechanical Properties of Tissue Scaffolds

Of the models reviewed, only three considered the scaffold tissue regeneration and scaffold degradation simultaneously [12, 24, 25]. Of the three only two utilized a mechanistic approach with predictive ability [24, 25]. These predictive models are limited by the neglect of the influence of cell metabolic byproducts on scaffold degradation. The hydrolysis of the scaffold in these models is considered to be a function of the concentration of water within the scaffold alone.

The issue of model parameter identification has also been made in the literature [22]. In many cases, computational models entail the identification of a host of parameters from the literature or from other experimental models, where the resulting parameters have been measured or inferred at a variety of experimental conditions.

Many of the current manufacturing methods employed for scaffold fabrication require first the construction of the scaffold and then cell seeding, because the scaffold manufacturing method is not biocompatible. The cells are then expected to be drawn into the pre-wetted scaffold by capillary action, which often results in unsatisfactory cell distribution [26]. Since the initial cell

distribution will have an effect on tissue development [27], it is a critical parameter influencing the mechanical property history of the scaffold. One possible resolution to this issue would be to have the scaffold supply cues to the cells, resulting in their migration to specific parts of the scaffold [28]. An alternative to this is a biocompatible manufacturing method which would allow the cells to be either distributed evenly in the scaffold or positioned at specific locations within the scaffold during fabrication.

In many of the models, the use of homogenization and the averaging of potential is employed to determine the effective diffusion coefficients for cell migration and mass transfer within the scaffold. This process of averaging results in an approximation to the effective diffusion coefficients of a multiphase material. It is likely that random walk simulations may give better predictions for the mass transport properties of the scaffold [29]. Ultimately, validation of diffusion models will likely need to employ the ability of nuclear magnetic resonance spectroscopy to observe the internal motion of the various diffusing species within the scaffold [30].

With the increasing use of complex multiphase scaffold materials composed of many separate polymeric and ceramic constituents, there exists a need for the simultaneous simulation of the hydrolysis degradation of multiple polymeric phase materials, where each phase may display different degradation behavior.

Most of the existing models for scaffold degradation that do predict the mechanical properties of the scaffold with time are limited to the consideration of linear mechanical properties alone, and do not allow for the influence of strain rate on the properties or the prediction of the entire stress-strain curve of the scaffold.

Since the ultimate objective is to have mathematical models that can predict scaffold behavior in the human *in vivo* environment, any model that is eventually adopted will have its parameters estimated to match experimental evidence from the *in vivo* behavior of scaffolds left to degrade and regenerate tissue in this specific environment. One must consider how the behavior of the scaffold can be experimentally evaluated inside such surroundings. Explanting the scaffold will

not be acceptable in this case, so there is therefore a need for methods which can evaluate the scaffold behavior externally without scaffold removal. In addition, there is a need to be able to monitor a scaffold's performance with time once it has been implanted in the body. If it was somehow possible to perfectly replicate the living environment in an artificial bioreactor, directly measuring the tissue scaffold mechanical properties with time would be possible. The problem is that the mechanical properties of incubated tissue increase with time in the bioreactor, but then stop at a stage far below the performance native tissue displays inside the body. The perfect replication of the living environment artificially is exceedingly difficult. There are therefore advantages currently to implanting a scaffold into the living body and allowing the natural environment to influence the regeneration of tissue in the scaffold directly. There have even been proposals to incubate tissue scaffolds in an *in vivo* bioreactor. In this proposal a bioreactor is directly implanted into the living environment to take advantage of the totality of the body's cell differentiation signals and environmental details [31,32,33]. Even in this case, the ability to remotely infer the scaffold properties with time would be useful.

2.6: Future Research Directions

A possible experiment to determine the influence of metabolic cell by-products on degradation would involve monitoring the pH change of bioreactor growth medium with time and correlating this change with hydrogen ion production of the cells. By performing such tests at various loading conditions, the influence of strain rate and straining frequency on cell proliferation and metabolic waste production rate could be elicited. The production of metabolic waste would also be inferred from these experiments as a function of cell number. By measuring the initial and final cell numbers and pH of the growth medium, a relationship between tenocyte or chondrocyte number and hydrogen ion production may be established. Cell experiments must also identify the sensitivity of the proliferation rate to the concentration of growth factor which may be included in the scaffold. Finally, the extracellular matrix (ECM) excretion rate per cell must be ascertained as a function of strain and growth factor concentration. Once these phenomenological models are assembled with estimated parameters, the accumulation of the developing ECM layer on the inner surface of the scaffold pores can be estimated.

In the field of structural mechanics, the concept of FEM model updating is employed to estimate the various parameters in FEM models of a particular system by forcing agreement between experimental evidence and model predictions [34]. In classical FEM model updating, the model output that is related to the model parameters are the frequencies and amplitudes of the modes of vibration, but the general concept should be applicable for a variety of different model outputs. In this approach, a variety of seeded scaffold properties would be characterized with time during scaffold degradation and tissue regeneration, and the various parameters of the FEM model updated with time to force agreement between model and experiment. In order to ensure a unique solution, the parameter change during each time step would be forced to be a minimum, or the number of simultaneously monitored mechanical properties of the scaffold would be selected to match or exceed the number of parameters for updating. By estimating all of the various parameters in the scaffold degradation and tissue regeneration models simultaneously with the same experiment, the parameters so estimated are all determined under the same experimental conditions. If this method of inferring scaffold parameters from the observed modes of vibration via FEM model updating is combined with Ultrasound or Magnetic Resonance imaging of the scaffold modes of vibration under ultrasonic stimulation, this process may allow another way for *in vivo* monitoring of the tissue scaffold.

Using Polylactic Glycolic Acid (PLGA) dissolved in a Dimethyl Sulfoxide/Water solution, a more biocompatible solvent/polymer solution for tissue engineering, the scaffolds manufactured using PLGA and Iron Oxide (IO) will employ simultaneous scaffold manufacture and cell seeding. Briefly, the dissolved polymer mixed with IO nanoparticles is dispensed into a 3-d structure, layer by layer via pneumatic pressure extruded direct printing. The strands may be loaded with dissolved growth factor protein by dissolving said material into the DMSO with the PLGA before scaffold layer construction. The individual layers may also be incubated in laminin solution to adjust the scaffold surface properties.

After each layer is fabricated, gamma radiation sterilized, and possibly freeze dried to give a porous nanoscale microstructure, cell solution containing Tenocytes or Chondrocytes will be dripped onto the manufactured scaffold layers, and these individual layers will be incubated to promote cell attachment. Once seeding is accomplished with sophisticated control over growth

factor concentration and distribution, the individual layers will be positioned layer by layer and fused together by Cyanoacrylate adhesive or by PLGA/DMSO mixed with iron oxide.

The technology for manipulating and actuating plate like surfaces has already been pioneered for the manufacture of electronics. Using a vacuum or magnet based gripping mechanism, a manipulator may seize each layer and precisely position it for fusion with the previously positioned and fused layers.

Once the scaffold is manufactured and seeded, the entire construct is immersed in growth medium and subjected to a sinusoidal time dependent load, utilizing a Bose Biodynamic mechanical testing instrument. At appropriate intervals, the construct will be characterized for stiffness and yield, and then unloaded. It is also proposed that the scaffold be removed from the medium and the wet weight of the scaffold be measured. The wet weight can then be a measure of mass accumulation from cell growth and ECM excretion. Parameters which cannot be estimated by separate experimentation can be estimated using the FEM model updating approach.

2.7: Conclusions

The mathematical modeling of tissue scaffold time dependent properties is gradually becoming a useful tool for the development of tissue constructs. The problem of model parameter value selection and the consideration of the effect of cell metabolic products on scaffold dissolution are two critical issues that have not yet been addressed.

A method from the field of structural dynamics may prove to be a useful tool in the evaluation of scaffold degradation and tissue regeneration by allowing the various parameters in scaffold degradation and tissue growth models to be simultaneously inferred from experimental observations of a degrading scaffold.

The influence of pH change from cell metabolic activity and colony number has not previously been considered in the modeling of tissue scaffold degradation, yet it is a critically important

parameter that must be quantified if computer models of simultaneous scaffold degradation and tissue regeneration are to become useful tools for the design of clinically viable tissue engineering scaffolds.

Acknowledgements

The authors wish to thank the financial support provided by the Saskatchewan Health Research Foundation (SHRF) and the Natural Science and Engineering Research Council (NSERC) of Canada.

References

[1] Bawolin, N. K., Li, M. G., Chen, X. B., Zhang, W. J., "Modeling Material-Degradation-Induced Elastic Property of Tissue Engineering Scaffolds," Journal of Biomechanical Engineering, vol. 132, pp. 111001-1-111001-7, 2010.

[2] Ward, I. M., Sweeney, J., "*The Mechanical Properties of Solid Polymers*," John Wiley & Sons, Ltd., 2004.

[3] Valavala, P.K., Odegard, G.M., "Modelling Techniques for Determination of Mechanical Properties of Polymer Nanocomposites," *Rev. Adv. Mater. Sci*., vol. 9, p. 34-44, 2005.

[4] Qu, J., Cherkaoui, M., *Micromechanics of Solids*, John Wiley and Sons Inc., 2006.

[5] Halpin, J. C., Kardos, J. L., "The Halpin-Tsai Equations: A Review," *Polymer Engineering and Science*, vol. 16, no. 5, p. 344-352, 1976.

[6] Milan, J., Planell, J., Lacroix, D., Computational modelling of the mechanical environment of osteogenesis within a polylactic acid–calcium phosphate glass scaffold, *Biomaterials* vol. 30, p. 4219-4226, 2009.

[7] Fang, Z., Yan, C., Sun, W., Shokoufandeh, A., Regli, W., Homogenization of heterogeneous tissue scaffold, *ABBI*, vol. 2 no. 1, p. 17-, 2005.

[8] Fang, Z., Starly, B., Sun, W., Computer-aided characterization for effective mechanical properties of porous tissue scaffolds, *Computer-Aided Design*, vol. 37, p. 65-72, 2005.

[9] Berger, H., Kari, S., Gabbert, U., Rodriguez-Ramos, R., Bravo-Castillero, J., Guinovart-Diaz, R., A comprehensive numerical homogenisation technique for calculating effective coefficients of uniaxial piezoelectric fibre composites, *Materials Science and Engineering A*, vol. 412, p. 53-60, 2005.

[10] Nasser, S., Hori, M., *Micromechanics: Overall properties of heterogeneous materials*, (Elsevier, North-Holland, 1999).

[11] Fang, Z., Yan, C., Sun, W., Shokoufandeh, A., and Regli, W., Homogenization of heterogeneous tissue scaffold: A comparison of mechanics, asymptotic homogenization, and finite element approach, *ABBI 2005*, vol. 2, no. 1, p. 17–29, 2004.

[12] Wilson, C., Bonassar, L., Kohles, S., Modeling the dynamic composition of engineered cartilage, *Archives of Biochemistry and Biophysics*, vol. 408, p. 246-254, 2002.

[13] Mohammadi, Y., Jabbari, E., Monte Carlo Simulation of Degradation of Porous Poly(lactide) Scaffolds, *Macromol. Theory Simul.*, vol. 15, p. 643-653, 2006.

[14] Wang, Y., Pan, J., Han, X., Sinka, C., Ding, L., A phenomenological model for the degradation of biodegradable polymers, *Biomaterials*, vol. 29 p. 3393-3401, 2008.

[15] Han, X., Pan, J., A model for simultaneous degradation and crystallisation in biodegradable polymers, *Biomaterials*, vol. 30, p. 423-430, 2009.

[16] Starink, M., On the meaning of the impingement parameter in kinetic equations for nucleation and growth reactions, *Journal of Materials Science*, vol. 36, p. 4433-4441, 2001.

[17] Kalnin, J., Kotomin, E., Maier, J., Generalised Maxwell-Garnett equation: Application to electrical and chemical transport, *Phys.Chem.Chem.Phys.*, vol. 8, p. 1310–1314, 2006.

[18] Wang, Y., Han, X., Pan, J., Sinka, C., An entropy spring model for Young's modulus change of biodegradable polymers during biodegradation, *Journal of the Mechanical Behavior of Biomedical Materials*, vol. 3, p. 14-21, 2010.

[19] Arosio, P., Busini, V., Perale, G., Moscatelli, D., Masi, M., A new model of resorbable device degradation and drug release, *Polymer International*, vol. 57, p. 912-920, 2009.

[20] Chen, Y., Zhou, S., Li, Q., Mathematical modeling of degradation for bulk-erosive polymers: Applications in tissue engineering scaffolds and drug delivery systems, Acta Biomaterialia, vol. 7, p. 1140–1149, 2011.

[21] Anderson, A., Chaplain, M., Continuous and discrete mathematical models of tumor-induced angiogenesis, *Bulletin of Mathematical Biology*, vol. 60, p. 857, 1998.

[22] Kelly, D., Prendergast, P., Mechano-regulation of stem cell differentiation and tissue regeneration in osteochondral defects, *Journal of Biomechanics*, vol. 38, p. 1413-1422, 2005.

[23] Checa, S., Prendergast, P., Chondrogenesis and integration of mesenchymal stem cells within an in vitro cartilage defect repair model, *Annals of Biomedical Engineering*, vol. 37 No. 1, p. 2556-2562, 2009.

[24] Adachi, T., Osako, Y., Tanaka, M., Hojo, M., Hollister, S. J., Framework for optimal design of porous scaffold microstructure by computational simulation of bone regeneration, *Biomaterials*, vol. 27, p. 3964-3972, 2006.

[25] Sanz-Herrera, J. A., Garcia-Aznar, J. M., Doblare, M., Micro-macro numerical modelling of bone regeneration in tissue engineering, *Computational Methods Applied to Mechanical Engineering*, vol. 197, p. 3092-3107, 2008.

[26] Freed, L., Vunjak-Novakovic, G., Culture of organized cell communities, *Advanced Drug Delivery Reviews*, vol. 33, p. 15-30, 1998.

[27] Vunjak-Novakovic, G., Martin, I., Obradovic, B., Treppo, S., Grodzinsky, A. J., Langer, R., and Freed, L. E., Bioreactor cultivation conditions modulate the composition and mechanical

properties of tissue-engineered cartilage, *Journal of Orthopedic Research*, vol. 17, p. 130-138, 1999.

[28] Harley, B., Kim, H., Zaman, M. Yannas, I., Lauffenburger, D., Gibson, L., Microarchitecture of Three-Dimensional Scaffolds Influences Cell Migration Behavior via Junction Interactions, *Biophysical Journal*, vol. 95, p. 4013-4024, 2008.

[29] J. Kalnin, E. Kotomin, J. Maier, Calculations of the effective diffusion coefficient for inhomogeneous media, Journal of Physics and Chemistry of Solids Vol. 63 Issue 3, p. 449-456, 2002.

[30] Thurecht, K., Hill, D., Whittaker, A., NMR Microscopy: A Tool for Measuring Monomer Diffusion in Supercritical CO^2, *Macromol. Chem. Phys.*, vol. 207, p. 1539-1545, 2006.

[31] Stevens, M. M., Marini, R. P., Schaefer, D., Aronson, J., Langer, R., Shastri, V. P., In vivo engineering of organs: The bone bioreactor, PNAS, vol. 102 no. 32, p. 11450-11455, 2005.

[32] Khayyeri, H,. Checa, S., Tagil, M., O'Brien, F. J., Prendergast, P. J., Tissue differentiation in an in vivo bioreactor: in silico investigations of scaffold stiffness, J. Mater Sci: Mater. Med., vol. 21, p. 2331–2336, 2010.

[33] Liu, Y., Möller, B., Wiltfang, J., Warnke P. H., Terheyden, H., Tissue Engineering of a Vascularized Bone Graft of Critical Size with an Osteogenic and Angiogenic Factor-Based In Vivo Bioreactor, Tissue Engineering Part A. vol. 20, No. 23-24, p. 3189-3197, 2014.

[34] Sinha, J., Friswell, M., *Nuclear Engineering and Design*, vol. 223, p. 11, 2003.

CHAPTER 3

MODELING MATERIAL-DEGRADATION-INDUCED ELASTIC PROPERTY OF TISSUE ENGINEERING SCAFFOLDS*

*****This chapter has been published as "Bawolin, N. K., Li, M. G., Chen X. B., Zhang, W. J., 2010, Modeling Material-Degradation-Induced Elastic Property of Tissue Engineering Scaffolds, ASME Journal of Biomechanical Engineering, vol. 132, p. 111001-1 to 111001-7." According to the Copyright Agreement, "the authors retain the right to include the journal article, in full or in part, in a thesis or dissertation".

3.1: Summary

The mechanical properties of tissue scaffolds play a fundamental role in scaffold behavior during treatment. It is therefore critical to understand the mechanical behavior of the scaffold at all times during the treatment period. Further to this aim, a mathematical model was constructed of the linear elastic property of a tissue scaffold for a specific type of material; a composite blend of the soft compliant biodegradable plastic Polycaprolactone matrix, and hard ceramic Hydroxyapatite reinforcing inclusions. This model included all of the structural levels of the scaffold, and considered some novel effects such as solvent plasticization of the scaffold matrix material. The parameters in this model were estimated from experimental evidence and the model was then validated with additional experimental data.

A novel static model of a tissue scaffold elastic property was developed that considered a complex composite material with many separate structural levels. The Maxwell Garnett approach found in electric engineering for the prediction of mixture properties was employed to model the effective diffusion coefficients of the scaffold material. A heat treatment approach to adjusting the initial crystallinty of the scaffold was explored. Finally, a time dependent model of tissue scaffold elasticity degradation was developed and its parameters estimated. This model was then validated for a different scaffold geometry.

In more detail, a Polycaprolactone biomaterial was dissolved in the organic solvent chloroform, mixed with hydroxyapatite bone ash nanoparticles and then dispensed into a three dimensional structure which solidified as the volatile solvent evaporated, leaving behind a solid three dimensional nanoparticle reinforced porous scaffold structure. These scaffolds were compression tested and their measured stiffness employed to estimate the parameters of the static scaffold model of stiffness. The model was then validated in the following manner; 1) transversely isotropic scaffolds were created with specific known geometric parameters and compression tested to determine their Young moduli, and 2) model predictions were compared to the experimental measurements of stiffness.

Tissue scaffolds with a specific strand radius and strand spacing were then degraded at body temperature in phosphate buffered saline. The static model was employed to inversely determine the molecular weight of the scaffold from measurements of the scaffold stiffness at various specific times during the degradation process. This knowledge of how the molecular weight changed with time was then employed to estimate the parameters in a separate time dependent degradation model of the scaffold. Finally, the time dependent model was employed to estimate the time dependent stiffness of a scaffold assembled out of the same polycarolactone/hydroxyapatite biomaterial but with a different strand spacing and radius. This fulfilled the research objective of creating a model that could simulate the degradation of unseeded tissue scaffolds fabricated out of a specific biomaterial when they are immersed in phosphate buffered saline and incubated at body temperature.

It is possible to construct relatively simple models of scaffold degradation that can successfully represent the behavior of the scaffold with time. A calibration set of scaffolds can be degraded and tested at various time points to give data on the degradation behavior of the scaffold material, which allows all of the effects of manufacturing to be included in the collection of experimental data about the material degradation properties. Once this information is available, it can be employed to estimate the parameters in a model, which then becomes geometry independent. As long as the material and the biological medium remain the same, the model is able to predict the behavior of scaffold with different strand diameters and strand spacing.

3.2: Introduction

The limitations of existing treatments for organ and tissue failure have led to the development of tissue engineering, which aims to discover methods to create artificial tissues and organs. One promising method is the use of a tissue engineering scaffold to provide temporary support and guidance for seeded cells, eventually forming new tissue to replace the damaged or diseased ones [1]. In this method, the mechanical properties the scaffold used play a crucial role in the success of the treatment. If the scaffold stiffness is much greater than that of the surrounding tissue, the majority of the load is born by the scaffold, leading to the eventual absorption of the tissue surrounding the scaffold, which will result in implant detachment [1]. Stiffness in excess of the surrounding tissue will also lead to tissue damage and inflammation, due to a foreign body response from the immune system [2]. The foreign body reaction proceeds first with monocyte attachment to the implant surface and their differentiation into macrophages, which then excrete Cytokines for communication to the other cell types involved in the foreign body reaction. Eventually, foreign body giant-cells (FBGCs) surround the implant in fibrotic scar tissue, and the FBGCs begin to release oxygen radicals, enzymes, and acidic products, which chemically attack the implant, leading to its degradation and failure [3]. Macrophages show a demonstrable selective preference for high modulus substrates [4]. Conversely, if the scaffold implant has much greater compliance than the surrounding tissue, the scaffold will experience unacceptable deflection under the loading environment in the implant area. To avoid these undesirable situations, the elastic properties of the scaffold should be near those of the surrounding tissue [2]. Maintaining the stiffness of the scaffold matching with the surroundings is complicated by the dynamic nature of scaffold behavior [2]. The scaffold is simultaneously degraded by the body, and reinforced by new tissue generation. Ideally, these two processes would be balanced so that the increase in stiffness from the regeneration of the tissue would compensate for the reduction in stiffness due to scaffold dissolution, approximately maintaining the effective stiffness of the scaffold constant. For this, knowing the mechanical properties of the scaffold as applied to *in vitro* cell culture or *to in vivo* implantation becomes an important issue.

Existing studies on the time dependent properties of scaffolds tend to consider only the effect of polymer hydrolysis on the molecular weight of the scaffold [5, 6, 7]. A few tried to proceed from molecular weight to the mechanical properties of the scaffold of amorphous polymer [8, 9]. In

these studies, however, the effect of the crystalline phase on the mechanical properties was neglected. Many models with the exception of those in references [5] and [6] do not consider the catalyzing effect of the monomer byproducts of scaffold degradation. No existing present study, to the authors' knowledge, models the degradation of polymer/ceramic composite materials. Current models also combine both the modeling of the scaffold and the time dependent change in scaffold molecular weight, which result in parameter estimation processes that require significant computer resources. Many of the existing models utilize experiments to estimate the various parameters in the models in order to reproduce experimental data. The applications of those parameters to predict the behavior of other devices with different geometry have not been reported yet. Finally, the mass transport parameters from models, such as that in [8], utilize empirical expressions fitted to the output of FEM models. It seems likely that more accurate diffusion models be possible based on the random walk algorithm or the Maxwell Garnett expression. Moreover, the models reviewed in the above cannot currently contend with devices that possess separate physical structural levels and separate material constituents on each level. These issues are addressed in the present study by performing a three step process to model the time-dependent mechanical properties of a tissue engineering scaffold.

The three steps in this study are: 1) construct a time independent finite element (FE) model for the linear elastic properties of a tissue scaffold, 2) parameterize the FE model by selecting parameters associated with the scaffold microstructure and/or material properties, which vary with scaffold degradation; and 3) identify selected parameters as functions of time based on measurements of the tests on the scaffold mechanical properties as they degrade for given biological conditions. Thus, the finite element model developed with the so-identified time-variable parameters will allow for prediction of the mechanical properties of tissue scaffolds for given biological conditions. To validate the resultant model, scaffolds were made from the biocompatible polymer Polycaprolactone (PCL) mixed with Hydroxyapatite (HA) nano-particles; and their mechanical properties were examined in terms of the Young Modulus.

In the present study, the time independent models were adopted from the literature. The novel contribution rests on the integration of existing models with the model updating technique in order to predict the time-dependent elastic property of tissue engineering scaffolds, with its

experimental validation. Notably, while the stress-strain mechanical properties of the tissue scaffold are highly nonlinear with respect to strain and also strain rate dependent, these nonlinear effects were neglected and only the initial linear elastic stress-strain behavior of the scaffold was considered in the present work. Furthermore, while the modeling approach enacted in this study may be later expanded to consider tissue regeneration as well, this approach was initially only applied to the study of scaffold degradation alone.

3.3: Modeling the Time-Dependent Mechanical Properties

3.3.1: Finite Element Modeling of the Effective Mechanical Properties of Scaffolds

Various methods can be employed to mathematically evaluate the effective Young modulus of tissue engineering scaffolds. The most intuitive method is to assemble a FE model of the entire system, which includes all of the details of the microstructure and the overall shape of the global scaffold body [10]. Such a model would then be subjected to boundary conditions that simulate standard experimental procedures such as Tensile, Compressive, or three point bending mechanical tests [10] [11]. However, such an approach requires significant computational power to encompass both the microstructure of the scaffold, and the dimensions of the global scaffold body.

To simplify the analysis, representative volumes (RV) of each heterogeneous structural level can be analyzed individually to determine its effective or averaged properties. Each level is then to be replaced by its equivalent homogeneous material. In this study, the particular case of a scaffold composed of a semi-crystalline polymer reinforced with spherical inclusions is presented. Such a tissue scaffold displays three unique structural levels, which must each be homogenized to predict the scaffold's effective properties. These three structural levels are 1) the semi-crystalline polymer, 2) the ceramic reinforced composite material, and 3) the scaffold pore microstructure. The first two structural levels are homogenized with analytical Halpin Tsai models, and the third is evaluated by a finite element homogenization approach.

Treating the semi-crystalline polymer as a composite material with crystal and amorphous phases, an analytical Halpin Tsai model, with an inclusion shape parameter estimated from experiment, was employed in this study to find the effective modulus (E_{SC}) of the polymer for given molecular weight and crystallinity. The inclusions were assumed to be elliptical, and the transverse and longitudinal elasticity from the Halpin Tsai model were averaged, by using the approach of Fornes and Paul [12], to give an effective modulus for a randomly oriented elliptical reinforcement,

$$E_{SC} = 0.184E_L + 0.816E_T \tag{3.1}$$

where E_L and E_T are the effective longitudinal and transverse young moduli of a unit cell with a longitudinally oriented elliptical inclusion, and E_{SC} is the effective Young modulus of the unit cell if the elliptical inclusions have a random orientation. These moduli are calculated from the Halpin Tsai models,

$$E_L = abM_W\left(\frac{1+5.6\left(\frac{(E_C/(abM_W))-1}{(E_C/(abM_W))+5.6}\right)X_C}{1-\left(\frac{(E_C/(abM_W))-1}{(E_C/(abM_W))+5.6}\right)X_C}\right) \tag{3.2}$$

$$E_T = abM_W\left(\frac{1+2\left(\frac{(E_C/(abM_W))-1}{(E_C/(abM_W))+2}\right)X_C}{1-\left(\frac{(E_C/(abM_W))-1}{(E_C/(abM_W))+2}\right)X_C}\right) \tag{3.3}$$

where E_C is the Young modulus of polymer crystal, X_C is the polymer crystallinity, M_W is the molecular weight of the polymer, a is a solvent plasticization parameter, and b is the linear

relationship between the molecular weight of the polymer and the Young modulus of the amorphous region of the semi-crystalline polymer.

This semi-crystalline polymer is modified by the addition of a reinforcement phase, which is selected to improve the mechanical properties and biocompatibility of the semi-crystalline polymer. This improvement to the mechanical properties is represented by another Halpin Tsai model, where the shape parameter ζ is that for spherical inclusion geometry.

$$E_{CP} = E_{SC}\frac{1+\zeta\eta V_I}{1-\eta V_I}$$
$$\eta = \frac{E_I / E_{SC} - 1}{E_I / E_{SC} + \zeta} \qquad (3.4)$$
$$\zeta = 2 + 40V_I^{10}$$

where E_{CP} is the composite modulus, E_I is the inclusion modulus, and V_I is the inclusion volume fraction.

An RV of a single isolated scaffold pore, shown in Fig. 3-1, was meshed using the commercial finite element software ANSYS (ANSYS Inc., USA). The meshing was accomplished by initially defining cubic volumes within the RV that could be meshed with a mapped hexahedral mesh. The remaining irregular sections of the RV were meshed with tetrahedral elements. This RV could then be subjected to simulated mechanical properties tests by the application of appropriate boundary conditions (BCs). However, the application of these BCs would not account for the effect of the neighboring unit cells, and would not be a good approximation to the actual boundary conditions experienced by each RV *in situ* [13]. Since the scaffold is a periodic array of RVs, to avoid overlap between neighboring RVs and have each RV display the same deformation shape, the BCs on the RV boundary must be periodic [14]. The RVs may then be tiled together to form the macroscopic object with no overlap or gaps, better approximating the behavior of the actual unit cells in the macroscopic body. The following expressions are the periodic BCs for a square RV [14],

$$u_i^{K+} - u_i^{K-} = \bar{S}_{ij}\left(x_j^{K+} - x_j^{K-}\right) \tag{3.5}$$

where u_i is the displacement on the boundary, $\bar{S}_{ij}$ is the average strain in the RV, and the subscripts $K+$ and $K-$ indicate opposite sides of the RV. The average properties of the RV are assumed to be equal to the effective properties of the scaffold,

$$\bar{S}_{ij} = \frac{1}{V}\int_V S_{ij}\,dV \tag{3.6}$$

$$\bar{T}_{ij} = \frac{1}{V}\int_V T_{ij}\,dV \tag{3.7}$$

where $\bar{T}_{ij}$ is the average stress in the RV, and V is the RV volume. If the scaffold obeys Hooke's law, the average stress and strain in the RV are related to the scaffold effective stiffness matrix $\bar{C}$.

$$\begin{Bmatrix} \bar{T}_{11} \\ \bar{T}_{22} \\ \bar{T}_{33} \\ \bar{T}_{23} \\ \bar{T}_{31} \\ \bar{T}_{12} \end{Bmatrix} = \begin{bmatrix} \bar{C}_{11} & \bar{C}_{12} & \bar{C}_{13} & \bar{C}_{14} & \bar{C}_{15} & \bar{C}_{16} \\ & \bar{C}_{22} & \bar{C}_{23} & \bar{C}_{24} & \bar{C}_{25} & \bar{C}_{26} \\ & & \bar{C}_{33} & \bar{C}_{34} & \bar{C}_{35} & \bar{C}_{36} \\ & & & \bar{C}_{44} & \bar{C}_{45} & \bar{C}_{46} \\ & \textit{Symm.} & & & \bar{C}_{55} & \bar{C}_{56} \\ & & & & & \bar{C}_{66} \end{bmatrix} \begin{Bmatrix} \bar{S}_{11} \\ \bar{S}_{22} \\ \bar{S}_{33} \\ \bar{S}_{23} \\ \bar{S}_{31} \\ \bar{S}_{12} \end{Bmatrix} \tag{3.8}$$

If a known average strain is applied to the RV using (3.5), which results in all strains but $\bar{S}_{11}$ in (3.8) becoming equal to zero, the average stress in the body may then be used to calculate the first column of matrix $\bar{C}$. In a similar fashion, all of the columns of $\bar{C}$ may be determined. The pore geometry of the rapid prototyping scaffold is illustrated in Fig. 3-1. Once $\bar{C}$ is known for such a geometry, its inverse, the effective compliance matrix $\bar{D}$, easily yields the transverse and

longitudinal effective Young modulus $\overline{E}_1$ and $\overline{E}_3$, and the effective scaffold Poisson ratios $\overline{\nu}_1$, and $\overline{\nu}_3$ [15].

3.3.2: Parameterizing the Finite Element Model

The FE model parameterization should first identify all of the time dependent parameters in the model associated with the scaffold microstructure and/or material properties, which vary with scaffold degradation.

The tissue scaffolds degraded *in vitro* displayed bulk degradation, which was the focus of this study. In bulk degradation, water and degradation byproducts form a uniform concentration gradient within the scaffold and the scaffold molecular weight is uniformly diminished by hydrolysis, causing a gradual reduction in the mechanical properties of the scaffold material [1]. After a length of time, the polymer strands are sufficiently scissioned that their reduced length permits them to diffuse out of the scaffold body, resulting in mass loss. Prior to this time, the length of the polymer chains is large enough to prevent mass transport out of the scaffold.

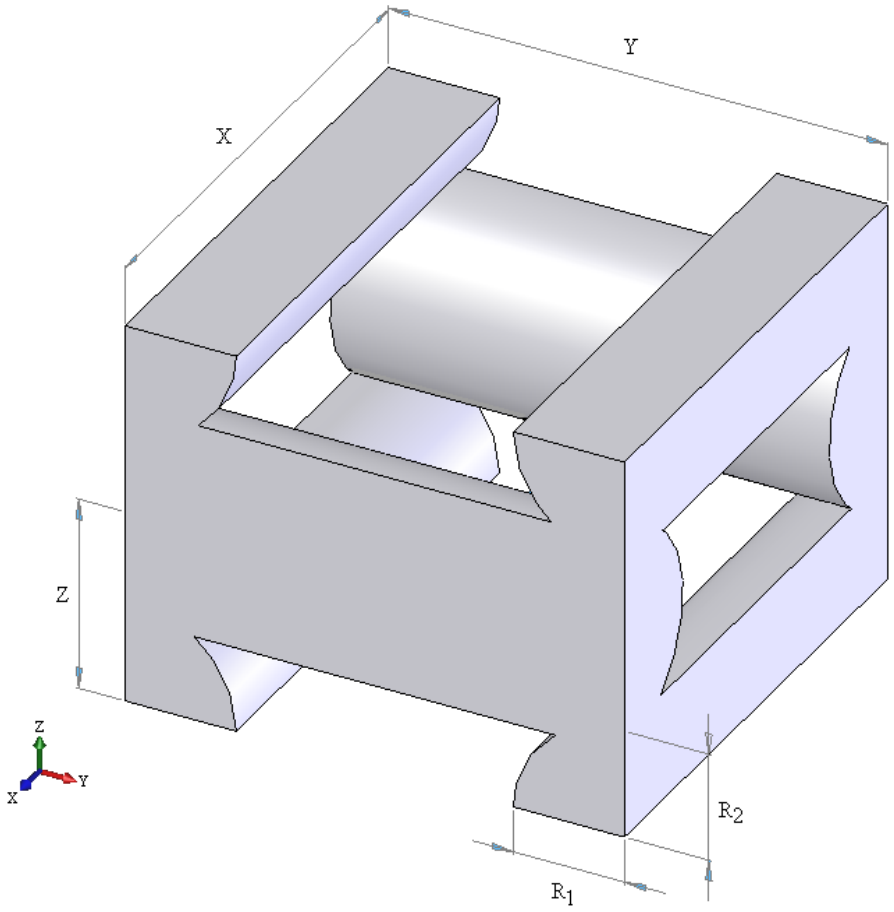

Figure 3-1: Representative volume of a scaffold

3.3.3: Model Parameter Identification and Updating

In the field of structural design, analysis, and dynamics, FE models used to model the system often give only a poor approximation to actual system behavior due to less accurately estimated model parameters. These model parameters are therefore updated with experimental data so that the model better represents the actual behavior of the system [16]. In model updating, the system is represented as two sets of coordinates in two spaces; 1) the model parameter space, and 2) the model output space. The finite element model is the instrument utilized to map from one space to the other, i.e., the parameters of the finite element model $\vec{P} = [p_1, p_2, ..., p_m]^T$ where m is the

number of considered parameters in the FEM model, form a point in model parameter space, which is mapped to a point in model output space $\vec{O} = [o_1, o_2, ..., o_n]^T$ via a function $f(\vec{O})$, where *n* is the number of effective scaffold properties predicted by the FEM model. While the prediction of behavior is equivalent to mapping point $\vec{P}$ in parameter space to point $\vec{O}$ in output space, model updating is equivalent to mapping in the opposite direction. This mapping procedure is represented mathematically by the following expression [17],

$$\Delta\vec{O} = [S]\Delta\vec{P} \tag{3.9}$$

where movement in the output space $\Delta\vec{O}$ is related to movement in the parameter space $\Delta\vec{P}$. If the function *f* relating $\vec{O}$ to $\vec{P}$ is nonlinear, the sensitivity matrix $[S]$ for each small movement in parameter space must be calculated to linearize the stepped mapping of $\vec{P}$ to $\vec{O}$. Once $\vec{O}$ is known, then this iterative mapping process allows for the eventual determination of $\vec{P}$ from its initial values $\vec{P}_0$.

If the number of model output parameters measured for updating is at least equal to the number of updating parameters, the estimates for the selected updating parameters should be unique and rank sufficient. If there are more updating parameters than measured model output parameters, rank sufficiency for unique estimates of updating parameters can still be achieved by forcing the difference between the updated parameter values and their initial values to be a minimum. Based on the above, the FE model of the tissue scaffold presented previously was updated based on measurements of the tests on the scaffold mechanical properties as they degrade for given biological conditions, as presented in the following section. The FE model with the so-identified time-variable parameters will allow for prediction of the mechanical properties of tissue scaffolds for given biological conditions. Furthermore, this approach possesses some advantages over other methodologies, such as the voxel finite element method. These advantages will be further elaborated upon in the discussion.

3.4: Experiments and Results

3.4.1: Scaffold Fabrication

The biocompatible polymer Polycaprolactone (PCL) was dissolved in Chloroform (25%v/v) to form a polymer solution which was then mixed with Hydroxyapatite (HA) nanoparticles (Sigma Aldrich, Canada) in a 22%v/v fraction of HA/solution. The material was dispensed with pneumatic pressure through a needle into a series of layered patterns with a direct printing fluid dispensing machine (C-720, Asymtek). These patterns are then dispensed layer by layer to gradually build a porous 3D structure. When such a manufacturing method is employed the strand self weight often leads to strand collapse, preventing the formation of overhanging structures [18]. This issue is resolved by either supporting the overhanging structures with a sacrificial layer, or by selecting a material with yield strength sufficient to support its own weight. The yield strength of the biomaterial employed in this study allowed the construction of overhanging structures without permanent deformation or collapse of the strands. The scaffolds manufactured for material testing, as seen in Fig. 3-2, have a controlled microstructure illustrated in Fig. 3-3. An initial group of scaffolds for model validation were manufactured with a strand spacing of $X = Y = 700\mu m$, and elliptical cross section major and minor radii of $R_1 = 150\ \mu m$, and $R_2 = 147\ \mu m$. A second group of scaffolds fabricated for parameter estimation, had a strand spacing of $X = Y = 1000\ \mu m$, and elliptical cross section major and minor radii of $R_1 = 174\ \mu m$, and $R_2 = 170\ \mu m$.

After fabrication and before degradation, the scaffolds were heated to 90 ˚C and held for 30 minutes in order to transition the PCL into a purely amorphous state. The scaffolds were immediately taken from heat and subjected to air cooling at -50 ˚C for several hours in an attempt to freeze the amorphous microstructure. The success of the heat treatment process was then observed by differential scanning calorimetry (DSC).

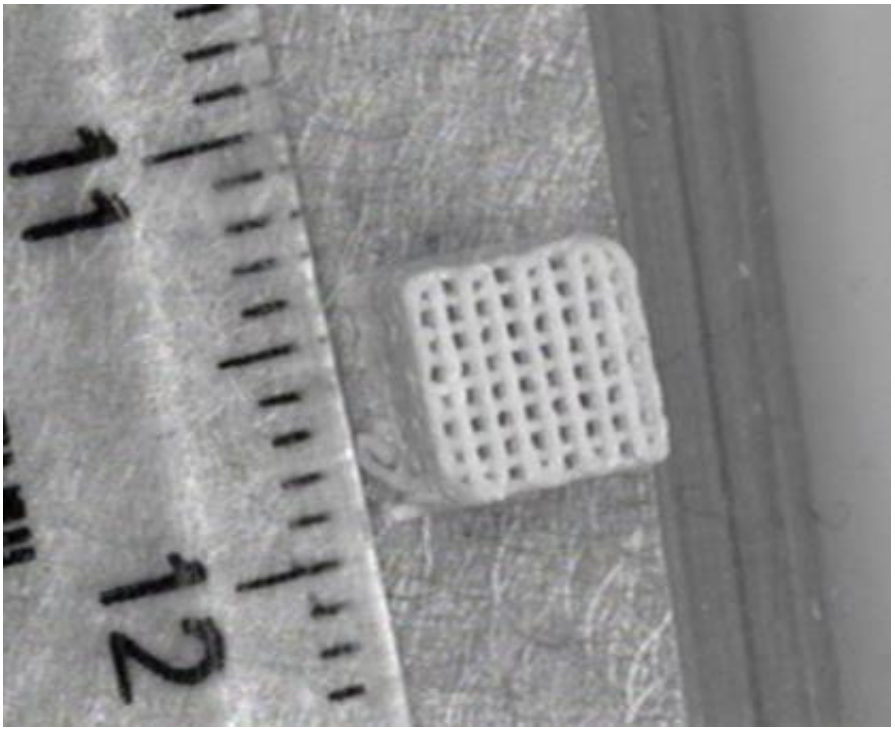

Figure 3-2: Scaffold sample with a size of 5×5×5 mm for mechanical property testing

The initial scaffold batch experienced no statistically significant decrease in crystallinity after heat treatment, but the second group experienced a reduction of over 14%. Both of the scaffold groups experienced recrystallization during quenching. It is possible that the larger pore size of this second scaffold group led to better heat transfer and cooling, supporting less crystallization. The crystallinity of the two scaffold batches after heat treatment were 48.6% and 40.3% respectively.

3.4.2: Parameter Identification and Updating

The time independent model for the semicrystalline polymer (3.1-3.3) was fitted to experimental measurements of the modulus of Polycaprolactone in the wet state for various crystallinities and molecular weights. The best fit

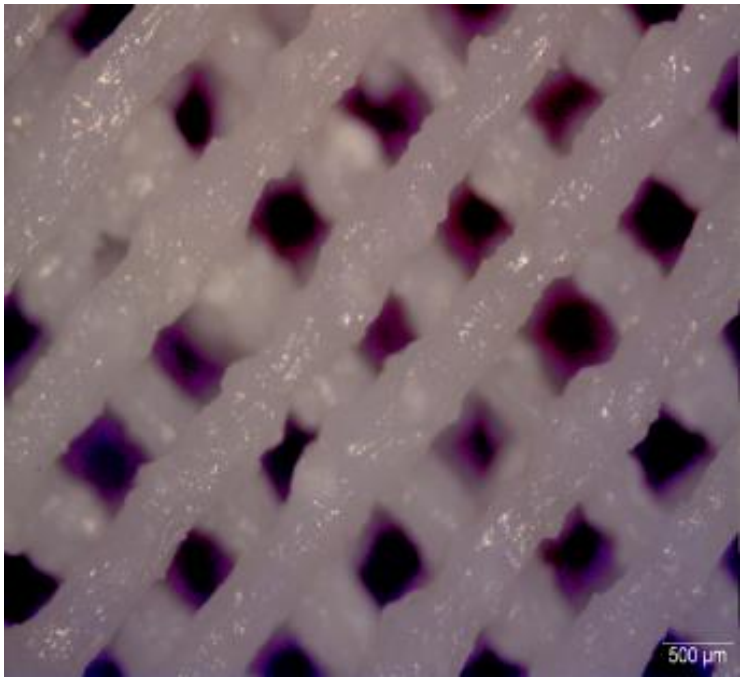

Figure 3-3: Microstructure of scaffold

with the experimental measurements was achieved for E_C = 365.25 MPa, a = 0.025, and b = 0.0035. The plasticization parameter was identified from the observed difference between the elasticity of melt cast and solution cast PCL. Equations (3.1-3.3) with these identified parameters were substituted into the Halpin Tsai model for spherical inclusion reinforced composite (3.4), where the stiffness of Hydroxyapatite was taken to be 81.4 GPa [19]. With a known volume fraction of HA/polymer after solvent evaporation of V_I = 40% v/v, the combined semicrystalline polymer and composite Halpin Tsai models give a prediction of 152.6 MPa for the Young Modulus of the composite. The Poisson ratio of the composite v_{CP} is calculated as volume fraction weighted average of the Poisson ratios of the constituent phases in the composite.

$$v_{CP} = (1 - X_{HA})v_{SC} + X_{HA}v_{HA} \tag{3.10}$$

where ν_{SC} and ν_{HA} are the Poisson ratios of the semicrystalline PCL polymer and the Hydroxyapatite ceramic respectively. The Poisson ratio of Hydroxyapatite is 0.25 [20], and the Poisson ratio of semicrystalline PCL is 0.33 [21]. From (3.10) the effective Poisson ratio of the composite is determined to be 0.29. The two mechanical properties E_{CP}, and ν_{CP}, once calculated, become the material property inputs into the FEM homogenization model as outlined in (3.5-3.8). The end result of this FEM based homogenization process for a scaffold with a pore geometry like that in Fig. 3-1 is an estimate for the scaffold's effective Young modulus and Poisson ratio in both the x and z directions.

The parameters that influence these four mechanical properties may be divided into two categories; (1) geometric parameters, as depicted in Fig. 3-1, such as strand spacing X, Y, and Z, and elliptical strand cross section major and minor radii, R_1, and R_2, and (2) material property parameters such as crystalinity X_C, the average molecular weight M_W of the polymer phase of the scaffold, the volume fraction of Hydroxyapatite X_{HA}, and the Poisson ratio ν of the scaffold composite material.

Since PCL degrades by a bulk mechanism *in vivo*, it is not expected that the geometric parameters of the scaffold will change greatly with time [22]. This was confirmed by measuring the strand radii and spacing with time via optical microscopy. No significant changes in geometry were observed during degradation. Additionally, the nanoparticles of Hydroxyapatite are expected to suppress the formation of additional crystal phase during degradation, maintaining X_C at a constant value [23]. This was confirmed by monitoring the crystallinity of the scaffolds during degradation, which was measured using Differential Scanning Calorimetry. The crystallinity of both the validation and updating scaffolds during degradation is illustrated in Fig 3-4. Finally, the dry weight of the scaffold was measured during degradation, with no significant changes observed over the 19 week degradation period.

The parameter chosen for updating is therefore the average molecular weight of the amorphous phase of PCL, which is the only parameter which is expected to change with time.

Since the geometric parameters of the scaffold are constant, the updating process now becomes a mapping from a point in output space $\vec{O} = [E_1, E_3, v_1, v_3]^T$,to the input space point $P = MW$,

$$\vec{O} = [E_1, E_3, v_1, v_3]^T = \{S\} M_W \tag{3.11}$$

where $\{S\}$ is the sensitivity vector. This sensitivity vector is then linearized by incrementing M_W by a small value and observing the change in the output point of the FEM model over many steps. The algorithm iterates in the direction that decreases the difference between the model predictions and the experimental measurements of E_3 until further iterations no longer lead to improvement.

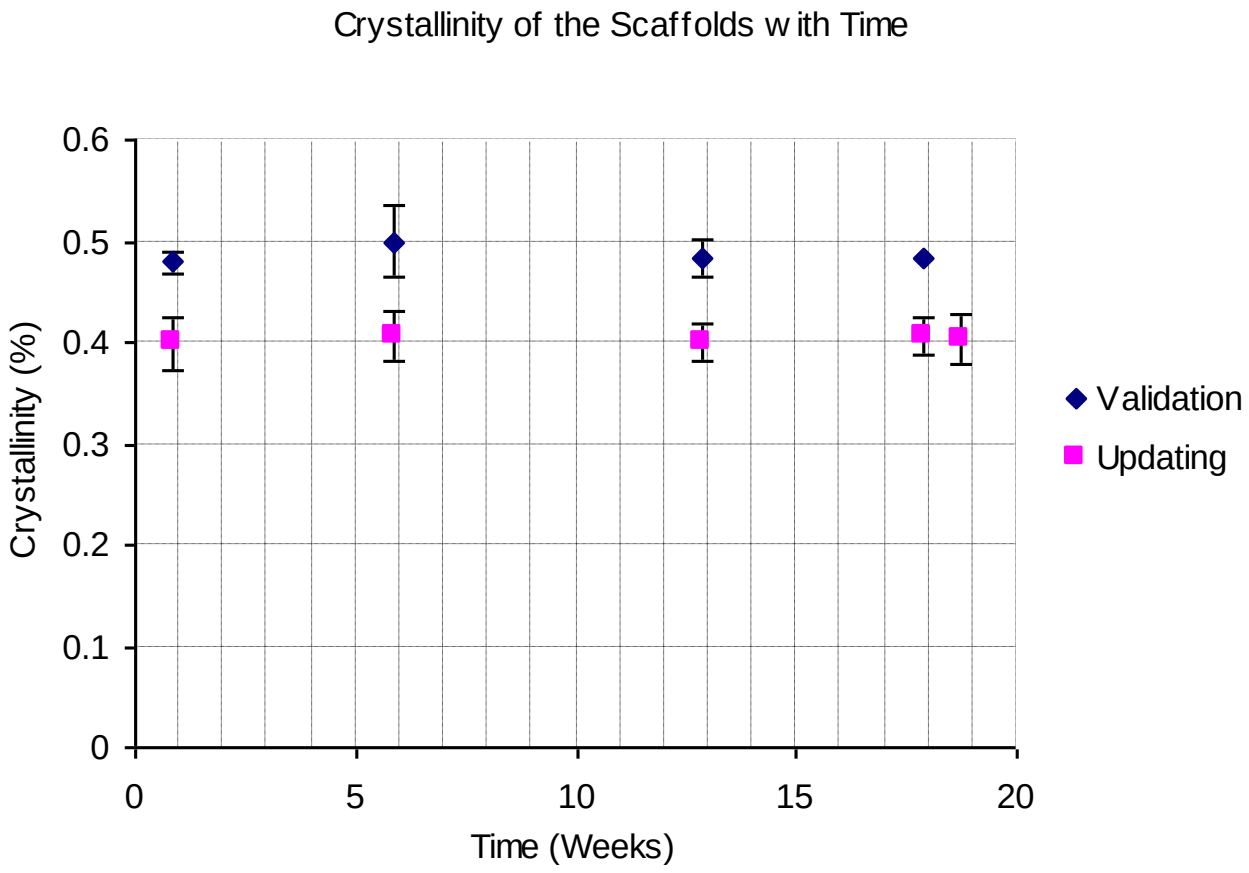

Figure 3-4: Crystallinity of updating and validation scaffolds with time

Experiments were conducted to measure the change in E_3 with time. The degradation of the scaffolds was induced by incubating the scaffolds in phosphate buffered saline at 40˚C over a period of 18 weeks. The temperature of the *in vitro* degradation study was chosen to be 40˚C, since it has been reported that the *in vivo* and *in vitro* degradation of PCL are identical at 40˚C [24].

Experimental measurements of E_3 were taken with a testing machine (1020, Instron) at the conditions of 2 mm/min, and 36% relative humidity at specific points in time (*t* = 1, 6, 13, and 18 weeks), for a scaffold with a strand spacing of 1000μm manufactured with a needle of radius 205μm. For each data point at least two scaffolds were subjected to compression testing. The error bars for each average value in Fig. 3-5 are ± one standard deviation.

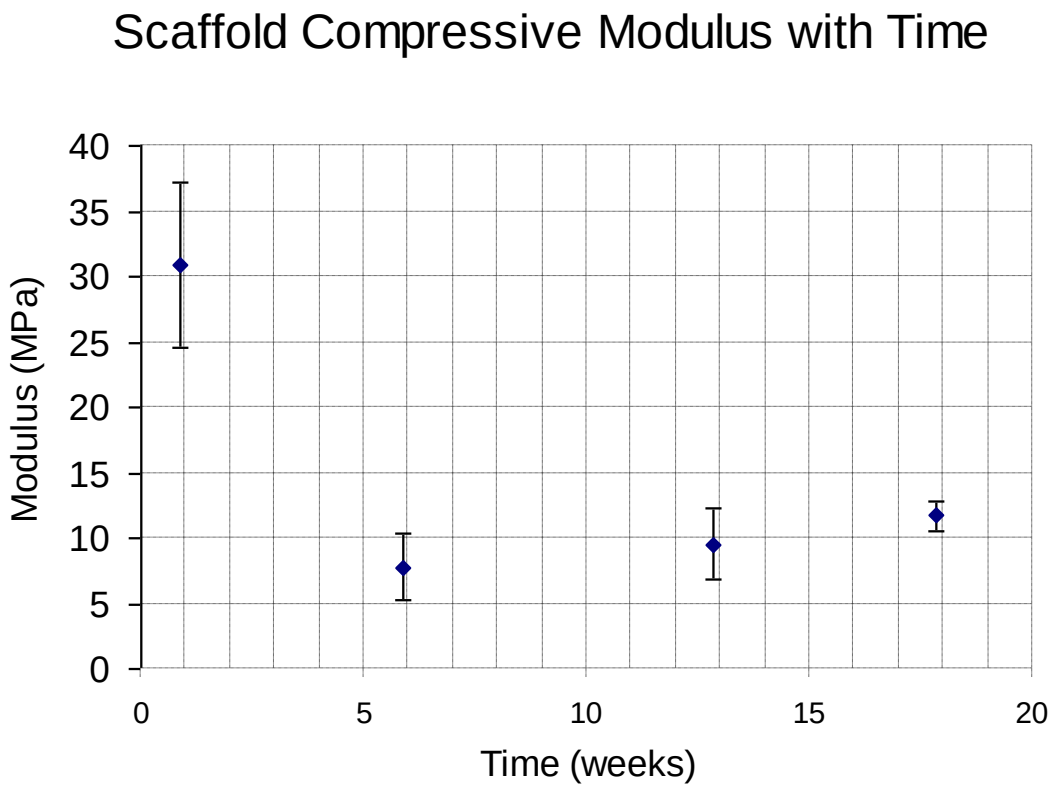

Figure 3-5: Longitudinal compressive modulus of scaffolds with time

These experimental measurements of E_3 with time were utilized in FEM updating to yield the updating parameter MW as a function of time *t*, as illustrated in Fig. 3-6.

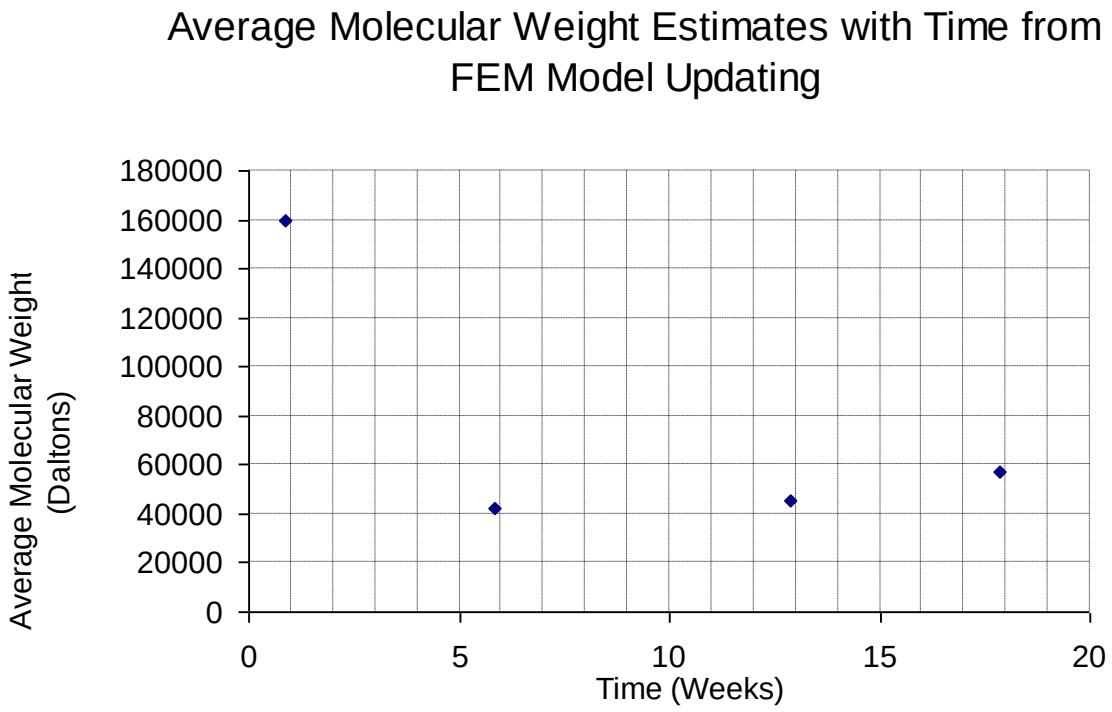

Figure 3-6: Molecular weight estimates for Updating Scaffolds from FEM model updating

The hydrolytic degradation of a biodegradable polymer can be represented mathematically as [3],

$$-dC_e/dt = dC_m/dt = k_1 C_e + k_2 C_e C_m^{\ n} \qquad (3.12)$$

where dC_m/dt is the change in ester bond concentration, C_e with time, dC_m/dt is the increase in monomer concentration with time, C_m is the monomer concentration, n is the byproduct dissociation term, which is the ratio of the concentration of reaction products to the concentration of reactants, and k_1 and k_2 are the non catalysed and catalysed rate constants respectively.

The average molecular weight is related to the current and initial ester bond concentration through,

$$C_e / C_{e0} = M_W / M_{W0} \tag{3.13}$$

where C_{e0} and M_{W0} are the initial ester bond concentration and molecular weight.

The concentration of monomers in the scaffold is a time dependent parameter that is dependent on the diffusion coefficient D_m of monomers inside the scaffold body.

$$dC_m / dt = \frac{dC_m}{dt} + \underset{x_i}{div}\left(D_m grad(C_m)\right) \tag{3.14}$$

As monomers are produced during degradation, the amorphous polymer region of the scaffold increases in porosity. This increase is estimated as [5],

$$p = 1 - \left(C_e + C_m\right) / C_{e0} \tag{3.15}$$

where C_{e0} is the initial ester bond concentration.

The Maxwell Garnett approximation was employed to calculate the effective diffusion coefficient for the monomers with time [25]. For the polymeric porous amorphous region of the scaffold, the effective diffusion coefficient for monomers D_{ap} is calculated from,

$$D_{ap} = D_a\left[1 + \frac{3(D_p - D_a)\rho}{D_p + 2D_a - (D_p - D_a)\rho}\right] \tag{3.16}$$

where D_p is the diffusion coefficient of the inclusion phase, i.e., the pores, D_a is the matrix diffusion coefficient, and ρ is the porosity as calculated from (15). The diffusion coefficient of monomers in the pores is assumed to be that of monomers in water, or 1.23 m^2/s [26], while the diffusion coefficient of monomers in amorphous polymer D_a is taken as 3.6 x 10^{-5} mm^2/hr [27]. An effective diffusion coefficient for the semicrystalline polymer D_{sc} is then calculated from D_{ap}. For the special case where impervious inclusions act as reflective surfaces for the diffusant, (3.16) was adjusted as in [25] to account for an impervious crystalline phase, which is given a diffusion coefficient of zero.

$$D_{sc} = \frac{D_{ap}}{1 - X_C}\left[1 - \frac{3X_C}{2 + X_C}\right] \tag{3.17}$$

Finally, the effective diffusion coefficient for the composite material D_{cp} is calculated from D_{sc} and the volume fraction of hydroxyapatite, which is considered to be impervious to water.

$$D_{cp} = \frac{D_{sc}}{1 - X_{HA}}\left[1 - \frac{3X_{HA}}{2 + X_{HA}}\right] \tag{3.18}$$

The geometry of a scaffold pore was assembled in ANSYS, and the analogy of heat diffusion was employed to estimate C_m in both position and time. Equations (3.12-3.18) were solved at each time step in each element, yielding a history of the average molecular weight of the scaffold with time. The parameter values $n = 1$, $k_1 = 0.00019$ hr^{-1}, and $k_2 = 0.0011$ $hr^{-1}mm^3/mole$ were chosen to force the best possible agreement between the time dependent representation of the scaffold average molecular weight and the results in Fig. 3-6.

3.4.3: Model Validation

Once the updating parameter M_W is known as a function of time, the finite element model with the identified time dependent elastic properties for the scaffold material was utilized to estimate the stiffness of a fluid dispensing assembled scaffold with a strand spacing of $X = Y = 700\mu m$, and a strand radius of 150μm, after 1, 6, and 13 weeks of degradation, and this prediction was compared to the actual stiffness measured during this incubation time.

The stiffness of the PCL/HA scaffold as a function of time as determined by the model is illustrated in Fig. 3-7, plotted alongside the experimentally measured values. The model predictions and experimental values are within experimental error. The coefficient of determination R^2 was calculated and employed to further evaluate the model's agreement with experimental evidence. The calculated value of $R^2 = 0.77$ suggests acceptable agreement between model and experiment.

3.5: Discussion

The ability to evaluate preliminary scaffold designs computationally before manufacture and final testing would represent a major development in the field of tissue engineering, aiding greatly in the eventual development of viable products for clinical practice. The current study performed the back calculation of various parameters of a scaffold from the solution of the inverse problem, when supplied with easily obtained property measurements from the fully assembled scaffold.

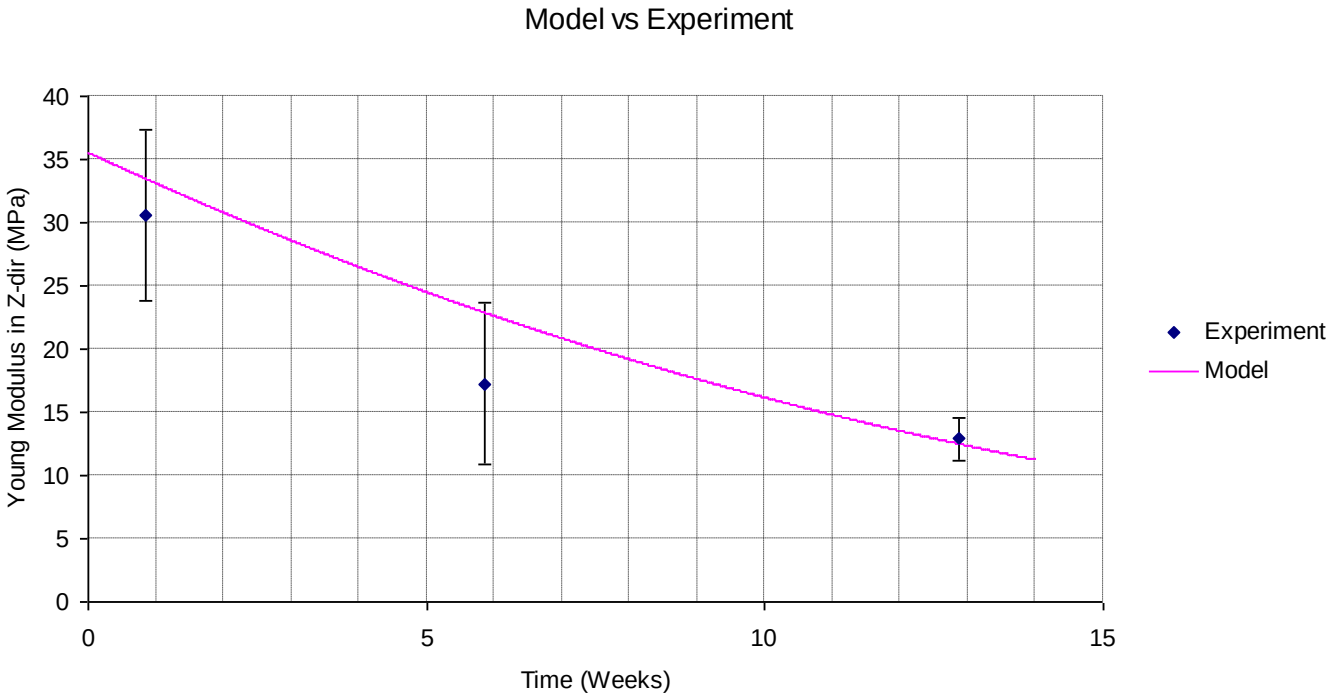

Figure 3-7: Experiment and simulation results of the elasticity modulus of HA/PCL scaffolds

Also, this demonstrated ability to inference the molecular weight from measurements of the scaffold elasticity may allow for the inference of properties that are difficult to measure *in vivo* from more easily obtained measurements of related parameters. For example, the *in vivo* measurement of scaffold modes of vibration may be possible even if the imaging method employed is unable to distinguish tissue from scaffold. The mass accumulation in the pores of the scaffold, and possibly even the scaffold geometry itself, should be inferable from such measurements.

The finite element model updating approach provides some advantages over other methods such as the voxel based finite element method presented in [28, 29]. The elements on the boundary surfaces of the various material phases in the scaffold created by this approach match the irregular geometry of the scaffold and do not need to be divided or smoothed at boundary surfaces like the boundary hexahedral elements in image based meshing approaches [30]. In

addition, examples in literature [29] of the voxel FE approach required more than a million elements for model predictions to be within 15% of experimental measurements. In the current study, models of less than 16,000 elements achieved similar agreement with experiment.

The scope of this study was limited to an initial consideration of only the bulk degradation of the scaffold. In addition to this limitation, a further relevant simplification to the present study was that only the linear elastic behavior of the scaffold at a specific rate of strain was considered. The current study also neglected geometric nonlinearities from large displacements. Additionally, many scaffold materials display surface degradation as well, where both the geometric parameters of the scaffold and the mechanical properties of the scaffold material are time dependent. The presented approach can be extended to include this effect by selecting the geometric parameters in the time independent model as updating parameters. In addition, when the scaffold is seeded with appropriate cells, these will proliferate in response to chemical and physical stimulus, extrude ECM, and generate metabolic wastes, which will diffuse into the scaffold body. These pH raising byproducts of the metabolic process have a significant effect on the degradation of the tissue scaffold. The scaffold degradation and cell proliferation/ECM production are complex interdependent processes which ultimately must be modeled if useful mathematical simulations of tissue scaffold degradation and regeneration are to become a reality. The presented approach is also applicable to the study of both processes simultaneously, which is currently being validated in the authors' lab.

3.6: Conclusions

In this study, an approach based on the concept of finite element model updating was applied to model the time-dependent mechanical properties of a rapid prototyping manufactured scaffold. This approach involved the development of a FE model for the effective mechanical properties of the scaffold, parameterization of the FE model, and the identification of selected parameters as functions of time based on experimental measurements. This approach was validated experimentally by means of scaffolds made from PCL mixed with HA nano-particles. Experimental measurements of the scaffold elasticity degradation with time show agreement with the predictions from the FE model with updated parameters. This indicates that the FE

model updating method is a promising way to predict the time dependent properties of degrading tissue engineered scaffolds. This represents a significant achievement in tissue engineering, as it suggests that one may design/determine a scaffold microstructure with time dependent mechanical properties appropriate for a given application.

Acknowledgements

The present study was supported by the Saskatchewan Health Research Foundation (SHRF) and the Natural Science and Engineering Research Council (NSERC) of Canada.

References

[1] C. V. Blitterswijk, *Tissue Engineering*, Academic Press, 2008.

[2] S. J. Hollister, R. D. Maddox, and J. M. Taboas, "Optimal design and fabrication of scaffolds to mimic tissue properties and satisfy biological constraints," *Biomaterials*, vol. 23, p. 4095-4103, 2002.

[3] E. F. Irwin, K. Saha, M. Rosenbluth,, L. J. Gamble, D. G. Castner, and K. E. Healy, "Modulus-dependent macrophage adhesion and behavior," J. *Biomater. Sci. Polymer Edn*, vol. 19, No. 10, p. 1363–1382, 2008.

[4] K. A. Beningo and Y. L. Wang, "Flexible substrata for the detection of cellular traction forces," Trends in Cell Biology, vol.12, No.2, 2002.

[5] Y. Wang, J. Pan, X. Han, C. Sinka, L. Ding, "A phenomenological model for the degradation of biodegradable polymers," Biomaterials, vol. 30, p. 423–430, 2009.

[6] X. Han, J. Pan, "A model for simultaneous crystallisation and biodegradation of biodegradable polymers," Biomaterials, vol. 30, p. 423–430, 2009.

[7] J. A. Sanz-Herrera, J. M. Garcia-Aznar, M. Doblare, "On scaffold designing for bone regeneration: A computational multiscale approach," Acta Biomaterialia, vol. 21, Issue 6, 2008.

[8] Y. Wang, X. Han, J. Pan, C. Sinka, "An entropy spring model for the Young's modulus change of biodegradable polymers during biodegradation," Journal of the Mechanical Behavior of Biomechanical Materials, vol. 3, p. 14-21, 2009.

[9] G. Perale, P. Arosio, D. Moscatelli, V. Barri, M. Müller, S. Maccagnan, M. Masi, "A new model of resorbable device degradation and drug release: Transient 1-dimension diffusional model," Journal of Controlled Release, vol. 136 p. 196–205, 2009.

[10] J. Milan, J. A. Planell, and D. Lacroix, “Computational modeling of the mechanical environment of osteogenesis within a polylactic acid–calcium phosphate glass scaffold,” *Biomaterials*, vol. 30, p. 4219-4226, 2009.

[11] D. J. Kelly, P. J. Prendergast, “Effect of a degraded core on the mechanical behavior of tissue engineered cartilage constructs: a poroelastic finite element analysis,” *Medical and Biological Engineering and Computing*, vol. 42, No. 1, 2004.

[12] T. D. Fornes, D. R. Paul, “Modeling properties of nylon 6/clay nanocomposites using composite theories,” *Polymer*, vol. 44, p. 4993–5013, 2003.

[13] S. J. Hollister and N. Kikuchi, “A comparison of homogenization and standard mechanics analyses for periodic porous composites,” *Computational Mechanics*, vol. 10, p. 73-95, 1992.

[14] H. Berger, *et al*., “A comprehensive numerical homogenisation technique for calculating effective coefficients of uniaxial piezoelectric fibre composites,”*Materials Science and Engineering A*, vol. 412, p. 53-60, 2005.

[15] S. Nemat-Nasser, M. Hori, *Micromechanics: Overall Properties of Heterogeneous Solids, 1st edition*,” Elsevier Science Publishers, 1993.

[16] J. K. Sinha and M. I. Friswell, “The use of model updating for reliable finite element modeling and fault diagnosis of structural components used in nuclear plants,” *Nuclear Engineering and Design*, vol. 223, p. 11–23, 2003.

[17] X. B. Chen, W. J. Zhang, “Off-Line Control of Time-Pressure Dispensing Processes for Electronics Packaging,” *IEEE Trans. on Elec. Pack. Man*., vol. 26, no. 4, p. 286-293, 2003.

[18] J. P. Li, J. R. de Wijna, C. V. Blitterswijk, K. de Groot, “Porous Ti6Al4V scaffold directly fabricating by rapid prototyping: Preparation and in vitro experiment,” *Biomaterials*, vol. 27, p. 1223–1235, 2006.

[19] M. Akao, H. Aoki, K. Kato, “Mechanical properties of sintered hydroxyapatite for prosthetic applications,” Journal of Materials Science, vol. 16, p. 809-812, 1981.

[20] L. H. He, O. C. Standard, T. T. Y. Huang, B. A. Latella, M. V. Swain, “Mechanical behavior of porous Hydroxyapatite,” Acta Biomaterialia, vol. 4, p. 577–586, 2008.

[21] L. E. Nielsen, *Mechanical Properties of Polymers and Composites*, vol. 2, Marcel Dekker, New York. p. 379–452, 1974.

[22] M. Chasin, R. Langer, *Biodegradable polymers as drug delivery systems*, Marcel Dekker Inc., 1990.

[23] E. Efendiev, N. Gadzhieva, T. Ilyasly, R. Abbasova, F. Yakh’yaev, “Structure of Polyethylene Films Containing Copper Nanoparticles,” *Journal of Applied Spectroscopy*, Vol. 73, No. 3, 2006.

[24] C. G. Pitt, F. I. Chasalow, Y. M. Hibionada, and A. Schindler. Aliphatic polyesters I. the degradation of poly(-caprolactone) in vivo. Journal of Applied Polymer Science, vol. 26, p. 3779–3787, 1981.

[25] J. Kalnin, E. Kotomin, “Modified Maxwell-Garnett equation for the effective transport coefficients in inhomogeneous media,” J. Phys. A: Math. Gen. 31, p. 7227–7234, 1998.

[26] G. Hanna, R. Noble, F. Michel Jr., “Interfacial Resistance for Carboxylic Acid Transfer from Decane to Water,” The Journal of Physical Chemistry, vol. 91, No. 2, 1987.

[27] K. Haik-Creguer, G. Dunbar, B. Sabel,U. Schroeder, “Small drug sample fabrication of controlled release polymers using the microextrusion method,” J. Neurosci. Methods, vol. 80, p. 37–40, 1998.

[28] S. J. Hollister and N. Kikuchi, “Homogenization theory and digital imaging: a basis for studying the mechanics and design principles of bone tissue,” *Biotechnology and Bioengineering*, vol. 43, p. 586-596, 1994.

[29] Y. Chevalier, D. Pahr, H. Allmer, M. Charlebois, P. Zysset, “Validation of a voxel-based FE method for prediction of the uniaxial apparent modulus of human trabecular bone using macroscopic mechanical tests and nanoindentation,” *Journal of Biomechanics*, vol. 40, p. 3333-3340, 2007.

[30] S. K. Boyd, R. Muller, “Smooth surface meshing for automated finite element model generation from 3D image data,” *Journal of Biomechanics*, vol. 39, p. 1287-1295, 2006.

CHAPTER 4

CHARACTERIZATION OF MECHANICAL PROPERTIES OF TISSUE SCAFFOLDS BY PHASE CONTRAST IMAGING AND FINITE ELEMENT MODELING

*****This chapter has been published as "Bawolin, N. K., Dolovich, A. T., Chen, X. B., Zhang, W. J., 2015, Characterization of Mechanical Properties of Tissue Scaffolds By Phase Contrast Imaging and Finite Element Modeling, ASME Journal of Biomechanical Engineering, vol. 137, p. 081004-1 to 081004-8." According to the Copyright Agreement, "the authors retain the right to include the journal article, in full or in part, in a thesis or dissertation".

4.1: Summary

In order to gain a better understanding of how tissue scaffolds behave *in vivo*, experiments will have to be conducted within the living environment to characterize the tissue scaffold behavior with time. One promising approach to this monitoring is called elastography. Briefly, this method involves striking a scaffold with an ultrasonic radiation force to remotely provide loading to the scaffold. Ultrasound is used both to move the scaffold and to measure the resultant deflection of the scaffold. Since force balances can be inserted into tissue analogs and measure the ultrasonic force directly, and this force can also be mathematically modelled, it is reasonable to assume that the loading the ultrasonic beam will apply to the scaffold can be determined. All that is then required to know the material properties of the scaffold from a distance is to measure the deflection of the scaffold under loading. Since ultrasound beams of high frequency which would have good resolution are attenuated greatly by the body, x-ray imaging is proposed along with a phase contrast imaging method to measure the deflection. X-ray methods promise to be able to render the body transparent and detect deflections far smaller than those detectable by ultrasound imaging. A primary safety limit on the intensity of the ultrasound beam in the body constrains how much force may be applied to the scaffold. If the scaffold is stiff enough, the

deflections will not be observable. The limit on scaffold stiffness is a function of the resolution of the deflection measuring technique employed.

The movement of tissue scaffolds remotely can be employed as a method of phase contrast. This imaging method was applied for the first time to image scaffolds. The movement of the scaffold under an ultrasonic load was then employed to measure the stiffness of the scaffold. A finite element model of the scaffold was developed and the loading induced by the ultrasound beam upon the scaffold modelled. A method for deflection detection traditionally used in the field of micro-electromechanical systems was adopted for the first time in the study of tissue scaffolds, and was successfully utilized to measure the deflections of a scaffold deformed under ultrasound loading. The inverse problem was then considered and the minimum amount of unique loading conditions to determine material properties from deflection was determined. In the particular case of a cantilever beam like scaffold deflecting in the presence of an ultrasonic radiation force, a numerically complex iterative process to identify the material properties of the scaffold was discovered to be unnecessary. In some situations, the stress distribution in the body is not a function of material properties and is known *a priori*. When this is the case, the following steps give predictions for the elastic properties of the scaffold: 1) boundary deflections of the scaffold are imaged and then employed to find the average strain in the scaffold, 2) a stress matrix that is independent of the material properties is inverted, and 3) it is then employed with the average strains to rapidly give estimates for the material properties of the scaffold with a non-iterative calculation.

Image subtraction with movement induced by ultrasonic radiation forces was employed as a phase contrast x-ray imaging technique to visualize a tissue scaffold in a liquid medium with a similar density to that of tissue. The periodic microstructure of the scaffold was utilized to detect its movements after it was deformed by a force applied by an ultrasound beam. In detail, the scaffold's sinusoidal profile of intensity in the horizontal direction before and after loading were moved from the spacial domain into the frequency domain. The phase of this signal was then calculated before and after loading. This signal experiences a phase change after loading, and this phase change can be related to the horizontal displacement of the scaffold.

Once the deflections of the scaffold were characterized, a model of scaffold loading from ultrasound was created so that the loading condition of the scaffold was known beforehand. Inverse problem theory calculations were performed to find the number of loading conditions that are necessary to provide a unique and stable estimate for scaffold material properties. A finite element model of the microstructure of the scaffold was then adopted to act as a regularization device and allow the material property estimates to be obtained from a single loading condition. It was discovered that for certain loading conditions, stress in the body is not a function of material properties and is therefore also known beforehand. This allows the use of a simple non iterative calculation to give the material properties of the scaffold from the strain data. The measured deflections and known load were then employed to estimate the material properties of the scaffold. These estimates were then validated with compression testing of the scaffold.

This paper demonstrated the use of ultrasonic radiation force remote palpitation with deflection detection by x-ray imaging as a method for the *in vivo* monitoring of the linear elasticity of tissue scaffolds. This method has clear advantages over other proposed approached to monitoring bulk degradation remotely. Specifically, the method is able to monitor scaffolds with large initial stiffness which prevents their deflection from being detectable with traditional methods like sum of square errors algorithms. This work suggests that cantilever like scaffolds of high stiffness appropriate for bone tissue engineering could be monitored *in vivo* even at the earliest stages of scaffold degradation, providing information on the differences between scaffold degradation in the living environment and their degradation in simple analogs to the living environment like phosphate buffered saline solution or tissue culture medium baths.

4.2: Introduction

A fundamental problem in regenerative medicine is the replacement of the function of damaged tissue and/or organs. Many possible avenues exist for the resolution of this problem, with solutions being both medical and engineering based. Tissue and organ replacement with manmade devices is the first obvious possibility [1,2,3], though without an ability to self-repair. The lifespan of implantable heart replacement pumps, dialysis machines, heart lung replacement

machines, and the like are limited, with repair and replacement entailing surgery. In addition, some organ functions are not currently understood well enough to allow the straightforward design of direct technological replacements. These limitations have led to the search for biological methods for the replacement of damaged organs and tissue. Efforts are underway to affect the immune system so as to prevent rejection directly [4], but these methods, even if successful, will not address the issue of donor tissue scarcity. The ideal biological approach will generate an unlimited supply of tissue for transplant that is not rejected by the patient. This leads to the field of xenotransplantation, where another species is used as an inexhaustible tissue/organ source and the patient's immune system is adjusted, or the donor animal is genetically modified to produce human like tissue/organs [5].

While xenotransplantation may at some point fulfill its promise, it would be ideal to ultimately be able to derive replacement tissue/organs from a patient's own cells alone and not have to rely on an animal source. The existing methods proposed to regenerate tissue/organs from a patient's own cells may be classified into three groups; 1) methods that employ cells alone, 2) methods that employ unaided scaffolds, and 3) methods that utilize both scaffolds and cells [6]. The ability to influence and direct cells to spontaneously regenerate into whole organs is a capability that may need several decades to develop. Unaided scaffolds have demonstrated some success in encouraging regeneration, but are limited by the distances over which cells can migrate [6]. This leaves the final approach, cells and scaffolds combined, as the best near term biological approach to address tissue and organ failure [6].

In this cell and scaffold approach, a scaffold is seeded with cells, which then organize and proliferate into new tissue. The scaffold biodegrades, leaving behind nothing but new tissue. The degradation behavior of the scaffold is related to its performance during the treatment period, since the gradual reduction in scaffold mechanical properties influences the loading of the tissue developing in the scaffold pores, which is known to have an effect on the behavior of seeded cells [7]. In some cases the scaffold is expected to temporarily fulfill the mechanical function of the tissue it replaces and therefore must exhibit assured minimum and maximum mechanical properties, i.e. a minimum yield strength and appropriate Young modulus during the whole treatment process [8].

The state of the art for experimental characterization of tissue scaffold degradation is *in vitro* degradation at body temperature in a biological medium like phosphate buffered saline. However, the observation of degradation is complicated by poor agreement between simple tabletop experiments and full *in vivo* studies [9].

While animal implantation and degradation is currently the standard in the study of *in vivo* degradation, multiple animals must be sacrificed at each time point, and the tissue construct must be explanted for study, leading to multiple possible avenues for error. In addition, gravimetric mass loss measurement and mechanical testing of the explant do not allow location dependent properties to be measured directly. The information given by these techniques is the average quality over the full volume of the scaffold. Methods for monitoring the geometry and mechanical properties of scaffold and regenerating tissue *in vivo* by imaging methods are a promising approach for addressing the limitations of current methods for characterizing *in vivo* mass loss, mechanical property evolution, and time dependent morphology.

The imaging method known as ultrasonic force impulse elastography may permit the characterization and visualization of tissue scaffolds *in vivo*. This method employs two ultrasound beams; 1) a beam for the characterization of tissue deflection, and 2) a beam for the transfer of momentum to the sample, which results in a steady radiation force. This method's primary limitation is that attenuation may prevent the deflection measuring ultrasound beam from reaching deep into the body. In addition, higher resolution measurement requires shorter sound wavelengths, which are more readily attenuated by the body. While there are existing studies on the use of magnetic resonance imaging for the detection of displacements induced by ultrasound for the characterization of mechanical properties *in vivo* [10], to the authors' knowledge no publications exist on the use of in line phase contrast x-ray imaging to characterize tissue scaffold deformation from ultrasound radiation forces.

In this study, a constant acoustic radiation force delivered by a piezoelectric probe deforms a scaffold in a homogeneous approximation to the *in vivo* environment. Propagation based phase contrast imaging at a photon energy of 20 KeV is then utilized to visualize the scaffold at rest and in the deformed state, and the measured deformation is then compared to predictions given

by the forward solution of an FE model. The inverse mapping from the model is employed to estimate modulus from displacement. These estimates are validated by comparison to experimental modulus from compression testing. The FE model is then validated by comparing its predictions to measured scaffold deflection.

4.3: Methodology

4.3.1: Scaffold Fabrication

Polydimethylsiloxane (PDMS) precursor from BASF was dispensed by an Envisiontech bioplotter to form a three-dimensional porous scaffold structure as illustrated in Fig. 4-1. The PDMS precursors polymerize once exposed to airborne water vapor into long chain PDMS. The strand diameter and spacing between strands for these samples was measured by optical microscopy to be 410 ± 6 μm, and one millimeter respectively, with 6 μm being the standard deviation. The cross section of the beam like scaffold was 0.5 cm x 0.5 cm = 0.25 cm^2 and they possessed a length of 3 centimeters. Additional 0.4 cm x 0.4 cm x 0.4 cm cubic scaffolds were fabricated for compressive testing. The coordinate system employed in this work is illustrated in Fig. 4-1.

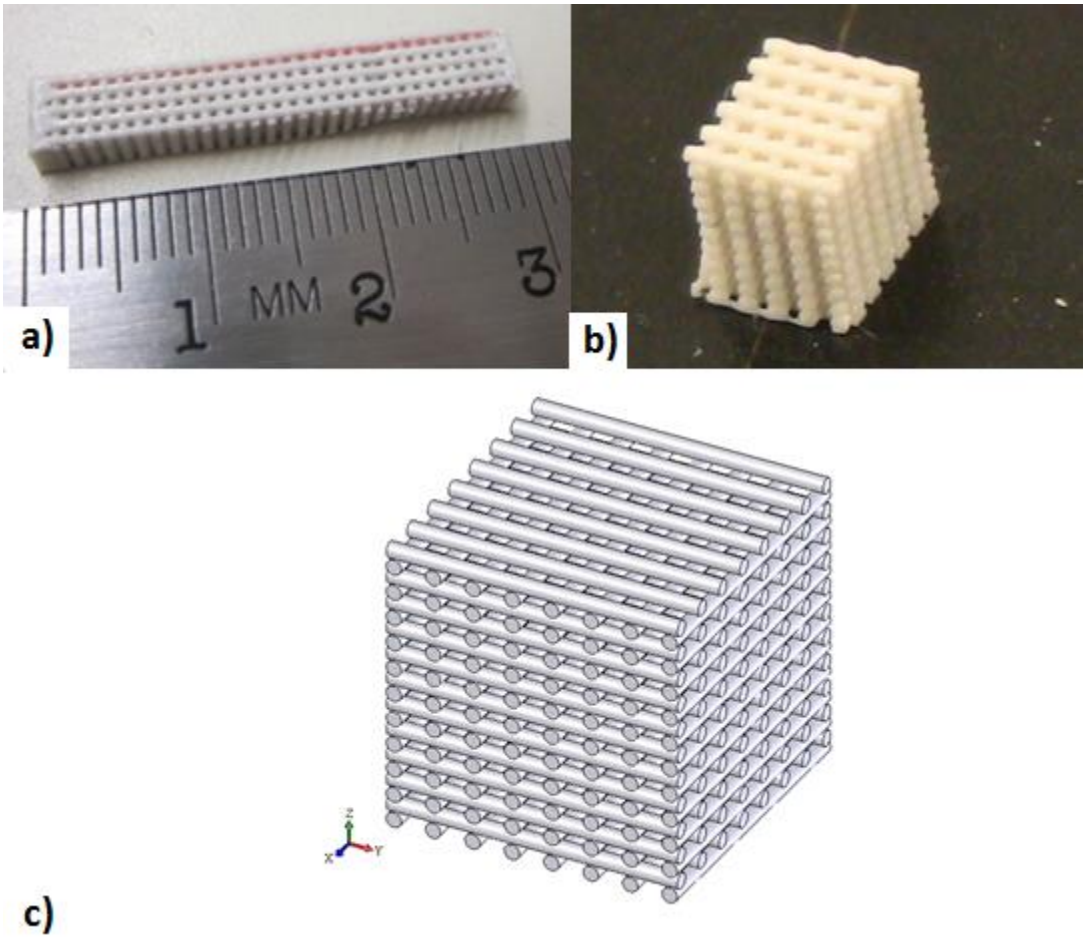

Figure 4-1: a) PDMS Scaffolds Employed for Ultrasonic Radiation Force Bending and Imaging, b) PDMS Scaffolds Employed for Compressive Testing, and c) Coordinate System

This initial experiment employed a very conservative scaffold design in order to guarantee visibility during imaging, with almost unrealistically large strand sizes and pore dimensions. Preliminary imaging revealed that the resolution achievable even when imaging through a two centimeter thick water filled tank was sufficient to resolve features on the order of 20 μm. It seems plausible that this method would be capable of imaging scaffolds with microstructural features on the order of 50-100 μm in size. The future inclusion of an insertion device on the same beamline will ensure that future iterations of this experiment will have even greater resolution. As an additional aside, PDMS was chosen as the scaffold material due to its extended lifespan in the body. This almost inert scaffold would allow the effect of tissue regeneration on a

seeded tissue engineering construct Young's modulus to be isolated and considered apart from the scaffold, without any interfering contribution to mechanical properties from scaffold degradation.

4.3.2: Mathematical Modeling of Ultrasonic Radiation Force

The scaffold was remotely deformed by an ultrasonic radiation force. This force arises from the transfer of momentum from an absorbed sound wave into a target, resulting in a steady distributed load inside the scaffold. In order to derive the material properties of the scaffold from observed deflection, the loading of the scaffold must be approximately known. While this could be measured by some mechanism affixed to the scaffold itself, another approach is to determine loading theoretically. Theoretical expressions for the acoustic radiation pressure and force are derived from the nonlinear equations of fluid dynamics. In [11] simplified expressions valid for plane waves are derived, employing the concept of successive approximations pioneered by Nyborg in 1965. The series expansion of the pressure *p* density ρ and velocity *u* of a wave are given by,

$$\begin{pmatrix} p \\ \rho \\ u(x,t) \end{pmatrix} = \begin{pmatrix} p_0 \\ \rho_0 \\ 0 \end{pmatrix} + \begin{pmatrix} p_1 \\ \rho_1 \\ u_1(x,t) \end{pmatrix} + \begin{pmatrix} p_2 \\ \rho_2 \\ u_2(x,t) \end{pmatrix} + \ldots \tag{4.1}$$

The pressure *p*, density ρ, and oscillatory velocity *u* of a decaying travelling wave may be described, neglecting higher order terms, as an amplitude multiplied by a decaying and oscillatory function,

$$p(x,t) = p_0 + u_0 c_0 \rho_0 \exp(-\alpha x)\cos\left(\omega t - \frac{\omega}{c_0} x\right) \tag{4.2}$$

$$\rho(x,t) = \rho_0 + \frac{u_0 \rho_0}{c_0} \exp(-\alpha x)\cos\left(\omega t - \frac{\omega}{c_0} x\right) \tag{4.3}$$

$$u(x,t) = u_0 + u_0 \exp(-\alpha x)\cos\left(\omega t - \frac{\omega}{c_0} x\right) \tag{4.4}$$

where c_0 is the equilibrium condition speed of sound in the medium (m/s), α is the attenuation coefficient (m^{-1}) , *x* is spatial position

(m), and $\omega = 2\pi f$, where *f* is frequency. By Newton's Second law of motion, it is known that a force is equal to the change in momentum. The mean change in momentum in a unit of volume gives the volume radiation force F^v , which is given by

$$\left\langle \rho \frac{\partial u}{\partial t} \right\rangle = \left\langle \rho \left(\frac{\partial u}{\partial t} + u \frac{\partial u}{\partial x} \right) \right\rangle = \left\langle \rho \left(\frac{\partial u}{\partial t} + \frac{1}{2} \frac{\partial u^2}{\partial x} \right) \right\rangle \tag{4.5}$$

where angular brackets denote average over time, and *x* is position in space. The time average of the change in oscillatory velocity over time is zero, therefore

$$\begin{aligned} \left\langle \rho \frac{\partial u}{\partial t} \right\rangle &= \left\langle \rho \left(\frac{1}{2} \frac{\partial u^2}{\partial x} \right) \right\rangle = \frac{\partial}{\partial x} \left(\frac{1}{2} \rho {u_0}^2 \exp(-2\alpha x) \right) \\ &= \frac{\partial}{\partial x} \left(\frac{I}{c_0} \right) = 2\alpha \left(\frac{I}{c_0} \right) \end{aligned} \tag{4.6}$$

where *I* is intensity. Intensity is the energy per volume of the wave multiplied by its wave speed c_0.

$$I = \left(\frac{1}{2} \rho_0 \langle u \rangle^2 \right) c_0 = \left(\frac{1}{2} \rho_0 {u_0}^2 \exp(-2\alpha) \right) c_0 \tag{4.7}$$

For this particular system, the forward problem is initially considered. For the assumption of plane waves, the body force generated by impinging sound F (N/m^3) [12, 14] is given by (4.6),

where α is the effective attenuation coefficient of the scaffold in m^{-1}, I is the intensity of the ultrasound beam at the scaffold, and c is the effective speed of sound in the scaffold material. Since the scaffold is a composite, composed of both empty space and the surrounding medium, the attenuation and speed of sound of the scaffold are given as volume averages of the properties of alcohol and PDMS. For example, the speed of sound in natural rubber and alcohol is approximately 1600 m/s and 1482 m/s respectively [13]. The scaffold has a porosity of 17%, so the speed of sound is estimated to be 1580 m/s within the scaffold. Likewise, the attenuation of sound in alcohol is 51 x 10^{-15} $m^{-1}Hz^{-2}$ [15], which for a frequency of 1 MHz is 0.051 m^{-1}, and the attenuation in the particular type of PDMS employed was assumed to be similar to that of natural rubber, i.e., 15 m^{-1} [15], leading to an attenuation of 11.26 m^{-1} for the composite. Placing the above values into (4.6) yields,

$$F = R * I \tag{4.8}$$

where R = 0.014 s/m^2.

A finite element model of the beam like scaffold was produced with the commercial software ANSYS, with a model geometry for the scaffold as shown in Fig. 4-2.

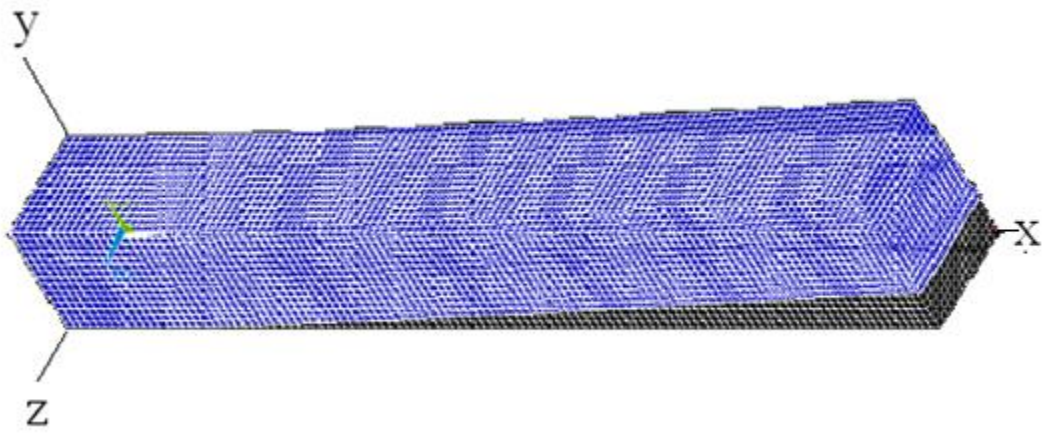

Figure 4-2: Finite Element Model Geometry and Exaggerated Scaffold Deflection under Ultrasonic Loading

The model consists of a beam constrained at one end and subjected to a location dependent body force. The number of elements in the model is 1000 and they are of the type Solid186, which is a 20 node three dimensional solid element. The ultrasonic radiation force was applied as a distributed nodal force in the model. To consider the distance of each element from the source, sound intensity is calculated for each node in the model, and the surrounding volume is employed to calculate a force for each node from (4.8). The path lengths from the source were partitioned into lengths traveled in water and lengths traveled in scaffold. Employing the attenuation coefficients of both scaffold and water, the sound intensity at each node within the scaffold model is calculated. For any given scaffold material properties, the FE model will now predict scaffold deflection caused by the calculated loading from the ultrasonic source.

4.3.3: Imaging

Many phase contrast imaging methodologies have been developed or are in the process of being developed for the characterization of tissue scaffolds/tissue, and could characterize the deflection of the scaffold under known loading. In the review paper [16] a description of various

methodologies is given along with a discussion of the strengths and weaknesses of the reviewed approaches. Two imaging methods are candidates for this study to identify scaffold deflection under a steady acoustic radiation force. A schematic of both methods is illustrated in Fig. 4-3.

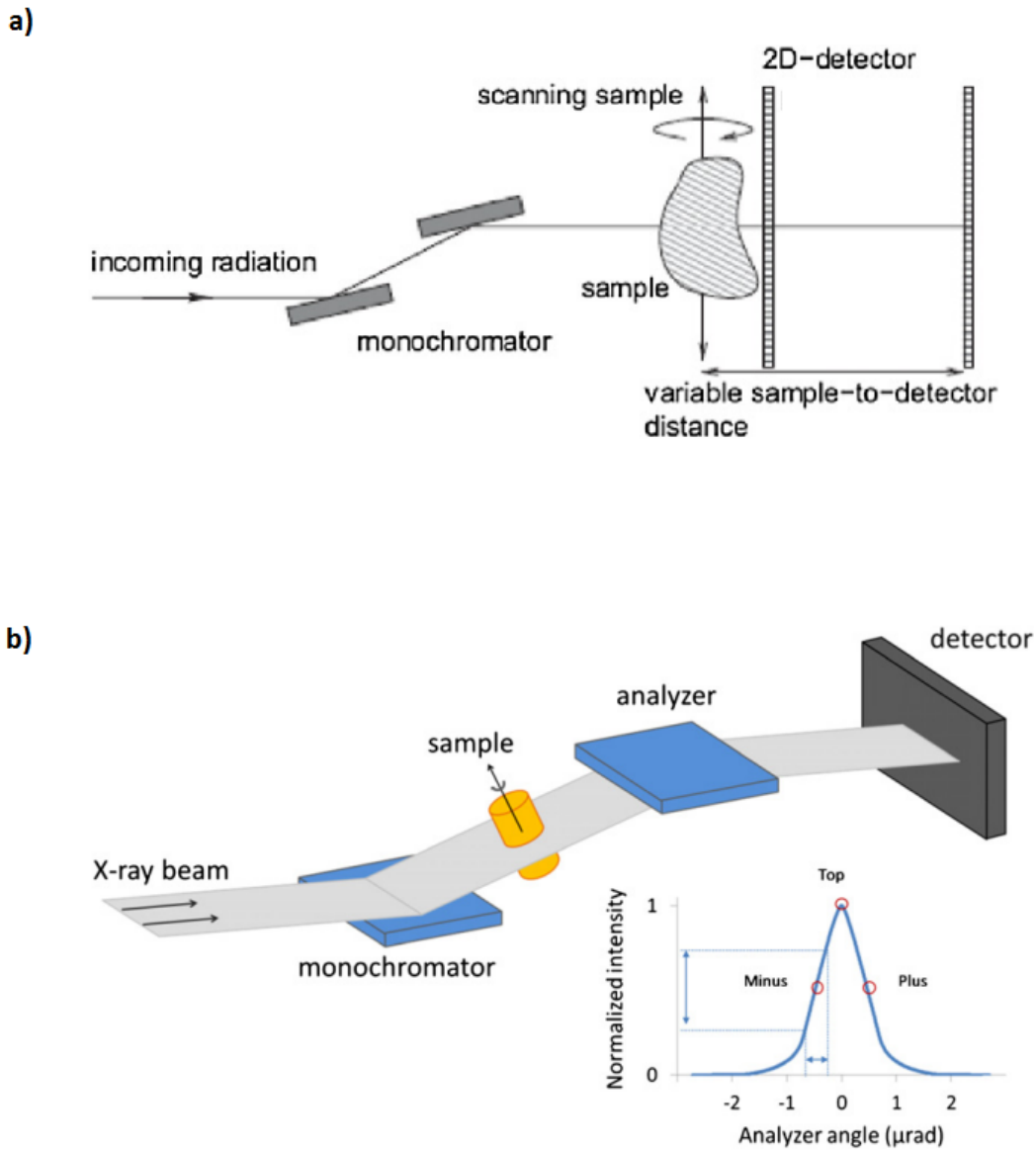

Figure 4-3: Beamline Arrangements for a) DEI [12], and b) PIC [13]

The first method, propagation based in line contrast (PIC), does not involve an analyzer crystal, which avoids micro-radian actuation complexity. In addition, acquiring the image is very simple;

the detector is moved away from the object until destructive interference effects provide acceptable contrast between phases. The method relies on the speed of light variance between different materials, i.e., if parallel beams of light initially in phase take unique paths through the sample, encountering different thicknesses of different phases, they will no longer be in phase after emergence from the sample, and will destructively interfere with each other. These reductions or increases in intensity provide contrast between phases of similar density which are indistinguishable in conventional x-rays based on absorption [17]. A disadvantage of this method is that the contrast depends on photon energy and the distance between the detector and the sample. Tissue and bone have smaller x-ray absorption coefficients for higher photon energies, so a balance must be struck between image quality and dosage. This is especially true with computed tomography which requires multiple exposures as the specimen is rotated in the beam, which allows the reconstruction of a three dimensional image.

Another method of imaging that is not based on absorption is diffraction enhanced imaging/ multiple image radiography (DEI/MIR). An analyzer crystal inserted between the sample and the detector measures the angular distribution of the photons emerging from the sample using the principal of Bragg diffraction. As the crystal is rotated through an angular range, the number of photons diffracted by the crystal is measured by the detector. This yields a rocking curve, and the comparison of this curve before and after sample insertion gives the refraction and the scatter from the presence of the sample. Refraction results in a horizontal shifting of the rocking curve, while scatter increases its horizontal width. Measuring the rocking curve in each pixel of an image gives refraction and scatter contrast images rather than a traditional x-ray absorption based image [18]. In traditional DEI only two points on the rocking curve are employed, while MIR includes many sampling points along the rocking curve to obtain data on scatter and refraction. When the scaffold material and its surrounding environment have similar density, x-ray absorption coefficients, and similar indices of refraction, the geometry of the scaffold is the source of refraction contrast. The circular cross sections of the individual strands of the scaffold microstructure behave like lenses for x-rays, generating great contrast at the strand/water medium boundary. This method has the advantage of providing acceptable contrast at high energy, providing a lower dose than PIC, but suffers from high sensitivity to noise. The percentage of the energy reflected by the main beam is sensitive to the angle of the analyzer

crystal, which allows the detection of the very small changes in angle experienced by x-rays as the pass through the sample. Unfortunately this sensitivity also causes the percentage of the beam diffracted by the crystal to the detector to vary greatly with time due to analyzer crystal vibration. This may be suppressed somewhat by active feedback control of the analyzer crystal. An additional measure that may be taken to combat noise is long exposure times, which has the effect of averaging the photon count in each pixel of the image. DEI also suffers from a need to take many images of a sample as the analyzer crystal is moved. This leads to the possibility of motion artefacts. Also, x-ray scatter is not expected to be a significant source of contrast for the specific scaffolds employed in this study, and the difference between the refractive indices of alcohol and PDMS is sufficient to suggest that propagation based methods are likely ideal for this particular application. While DEI/MIR may be acceptable for future iterations of this study, especially if the scaffold material displays an index of refraction similar to its surroundings, for this preliminary experiment PCI was chosen over the more complex DEI/MIR method.

Scaffolds were immersed within an alcohol filled four centimeter thick polystyrene tank, which represented the *in vivo* environment, and affixed to its floor. Alcohol was employed in order to suppress the formation of bubbles on the scaffolds. Imaging was accomplished with a charge-coupled device (CCD) camera (HAMAMATSU C9300, 4000×2672 pixels) with an effective pixel size of 6 μm. The resolution of a similar imaging setup was less than 18 μm, as measured by 28 line per mm resolution testing phantom [19]. The x-ray photon energy was set at 20 KeV. The detector was located 35 cm from the sample bearing tank. An ultrasound machine delivered a 2.0 W/cm^2 intensity 1 MHz continuous beam into the sample, with the end of the sample positioned directly in the path of the ultrasound beam, and the transducer of the ultrasound machine approximately two centimeters from the centre of the sample.

The scaffold was initially imaged with the ultrasound off. A dark image was acquired with the beamline shutters shut, and then another image was taken of the beam with no sample, which is known as a blank. Finally, an image was taken of the sample. The image of the sample was then normalized with the other two images by the expression,

$$I_{normalized} = \frac{I_{sample} - I_{dark}}{I_{blank} - I_{dark}} \tag{4.9}$$

After five separate images were collected and normalized with expression (4.9), these normalized images were averaged together. All image calculations were performed with the software ImageJ and Matlab. Once this first averaged and normalized image was captured with no ultrasound beam, the ultrasound machine was turned on and a new set of images obtained. These images were then normalized and averaged in the same manner described above.

4.3.4: Image Analysis

The displacement of the free end of the sample when the ultrasound beam was applied was measured by subtracting the deformed and undeformed images from each other. Fig. 4-4 illustrates these two images, one before ultrasound is initiated and one afterwards. The third image in Fig. 4-4 is the subtraction of the two previous images. If the scaffold has been moved by the ultrasound beam, the subtraction of the images of the strained and unstrained state should result in an outline of the scaffold in the direction of motion.

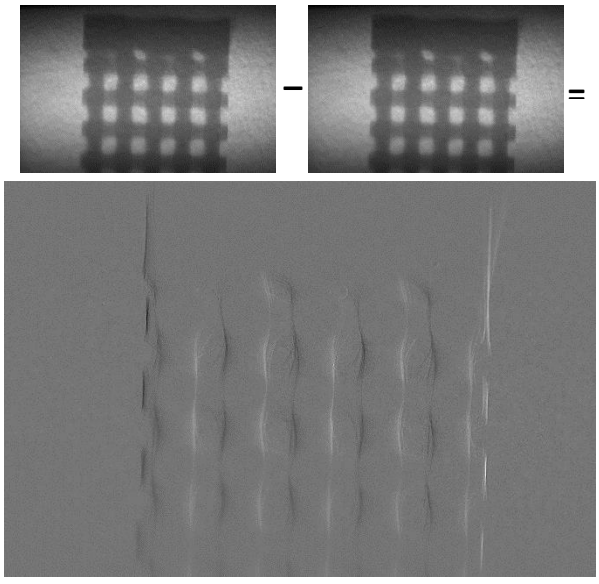

Figure 4-4: Subtraction of Image With and Without Ultrasound Radiation Force to Reveal Scaffold Displacement in the Direction of the Ultrasound Beam.

It is apparent from the resultant images that the scaffold has indeed been deflected by the ultrasonic radiation force in the direction parallel to the beam. Successive images taken without ultrasound give a blank result, indicating that the deflection observed must be from the ultrasound beam alone. It is also observed in the images that the thickness of the outline near the end of the beam is greater than that nearer to its fixed base which is to be expected if the scaffold is behaving as a beam under deflection from a distributed load. Also, the addition of a second transducer or the repositioning of one to a 45 degree angle with the sample may allow displacement in two dimensions, which may be another useful phase contrast imaging approach for scaffold visualization. Some previous work related to this deflection induced phase contrast is present in the literature [20], but to our knowledge the application of this methodology for the imaging of a tissue scaffold is novel.

The thickness of the outline at the top of the sample was measured with ImageJ. The calculated average displacement at the end of the scaffold was 62 ± 8 μm for a set of four scaffold samples, where 8 μm is the standard deviation for the four displacement measurements. An additional method was also employed to measure scaffold displacement known as square sum of errors (SSE). In this method each pixel in the undeformed image is associated with some of its neighbors, which form a unique identifier. This unique identifier is then searched for in the deformed image to find the new location of the pixel. A test parameter for each pixel in the deformed image is calculated and the one with the minimum value is taken as the new location for the pixel in question. This coefficient γ (*x*,*y*) is calculated with the following expression,

$$\gamma(x,y) = \sum_{i=1}^{i=s}\sum_{j=1}^{j=t}\left[U(x+s,y+t) - D(x+s,y+t)\right]^2 \qquad (4.10)$$

where *s* and *t* are the dimensions of the mask matrix *w* composed of the pixels around the one of interest in the undeformed image, *x* and *y* are locations within the deformed image *D*, and U is

the undeformed image. This equation in essence tries to find the *s* x *t* piece in the deformed image that matches a specific *s* x *t* piece taken from the undeformed image. The mask in this study was chosen to be 200 pixels wide and 20 pixels in height. Deflection at the top of the beam was measured for each of the four scaffold samples. For this method of deflection detection, the measured movement of the scaffold was 56 ± 7.5 μm for a set of four scaffold samples, where 7.5 μm is the standard deviation for the four displacement measurements. The two methods of estimating deflection give predictions that are within 11% of each other.

Another method may be employed to evaluate the deflection of a scaffold with a periodic microstructure [21]. The pixel intensity values over a straight horizontal line for such a scaffold take on the form of a sine wave, as shown in Fig. 4-5.

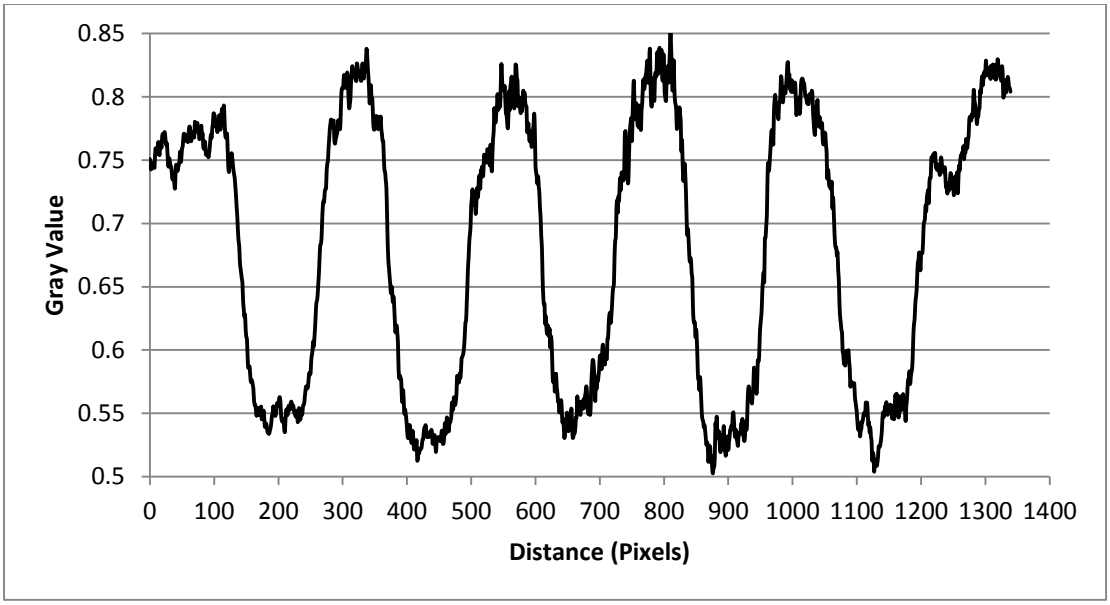

Figure 4-5: Gray Scale Intensity Value Along Horizontal Line in Planar Image of Scaffold with Periodic Microstructure

The areas of greater x-ray intensity are the pores, while the lower intensity regions are where the struts of the scaffold are located.

Taking the Fourier transform of these pixel values leads to a phasor with a specific magnitude and phase angle, i.e., the Fourier transform has a specific real and imaginary component. The continuous Fourier Transform is given by,

$$F(s) = \int_{-\infty}^{\infty} f(x) e^{-j2\pi sx} dx \tag{4.11}$$

where *s* is the frequency of the periodic structure of the scaffold, and *x* is horizontal position in the image. A one dimensional discrete (discretized) section of the deformed and undeformed images are considered. A finite domain *L* is selected for values of *x*, and a finite number of discrete points *N* are sampled in this domain.

$$dx = L/N = \Delta x \tag{4.12}$$

The discrete Fourier Transform is therefore given by,

$$F_{discrete}(s) = \sum_{i=0}^{i=N-1} I(x_i) e^{-j2\pi s_i x_i} \Delta x \tag{4.13}$$

In space, the frequency is the reciprocal of the wavelength of the periodic structure or the number of wavelengths present divided by the domain size *L*. If *n* is defined as the number of wavelengths in *L*, then

$$-j2\pi s_i x_i = -j2\pi(n/N\Delta x)(i\Delta x) = -j2\pi in/N \tag{4.14}$$

The discrete Fourier Transform can now be written as,

$$F_{discrete}(s) = \frac{L}{N} \sum_{i=0}^{i=N-1} I(x_i) e^{-j2\pi in/N} \tag{4.15}$$

The following expressions give the real and imaginary part of the Fourier phasor.

$$\mathrm{Re}\{F(n)\} = \frac{L}{N}\sum_{i=0}^{i=N-1} I(x_i)\cos(2\pi i n / N) \tag{4.16}$$

$$\mathrm{Im}\{F(n)\} = \frac{L}{N}\sum_{i=0}^{i=N-1} I(x_i)\sin(2\pi i n / N) \tag{4.17}$$

To determine an appropriate value for N, we consider the Nyquist criterion that states that the sampling frequency should be greater than twice the maximum frequency in the sampled data.

$$s_{periodic} = n/L,\ s_{sampling} = N/L,\ N > 2n \tag{4.18}$$

If the scaffold is shifted horizontally in space, this leads to a change in the phase angle of the phasor, or a change in the relative sizes of its imaginary and real components. This change in phase angle may be related to the horizontal distance over which the scaffold has moved. The Fourier Transform of the signal in Fig. 4-5 is illustrated in Fig. 4-6, where magnitude is the absolute value of the complex number with real and imaginary components given in (16) and (17).

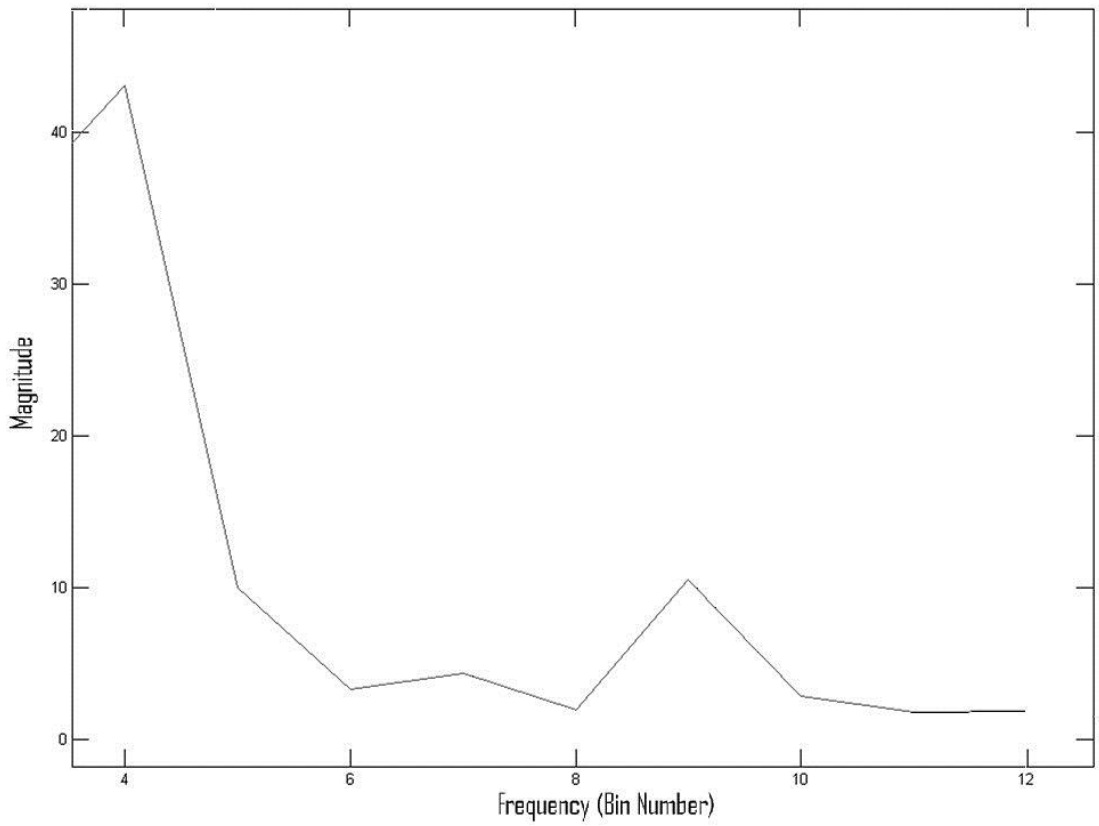

Figure 4-6: Magnitude Component Fourier Transform of Intensity Signal

With this method of image analysis, the deflection of the scaffold was calculated from the experimental data to be 58 ± 13 μm, where the error is given as the standard deviation of the measured deflections for four samples. The phase angle of the signal increased by 0.06 radians as the scaffold deformed. An increase in phase angle was expected as the intensity profile of the scaffold was shifted to the left. The magnitude of this phase change, which is about 0.04, corresponds to a shift to the left of about sixty microns.

4.3.5: Near Subpixel Movement

As the stiffness of the scaffold increases, the size of the deflections that may be observed with a given ultrasonic beam intensity decreases. In order to facilitate the detection of very small deflections, the periodic microstructure of the scaffold and the Fourier transform are employed. Briefly, samples of tissue scaffold were mounted and irradiated with ultrasound as before, but the

intensity of the ultrasound was reduced to half a Watt.

The method of subtracting images resulted in no appreciable outline of the scaffold from deflection, and the application of SSE gave no appreciable deflection. When the SSE was employed to compare an image to itself, the algorithm found a new location with an SSE parameter of zero, which is identical to the starting location. When the SSE algorithm was applied to this particular case, the SSE parameter was nonzero, but the minimum still occurred at the starting location. The SSE algorithm is therefore not able to measure deflection when the changes to the two images, undeformed and deformed, are minor. The images of the scaffold were then evaluated with Fourier analysis as introduced previously, giving a predicted deflection of 7.9 ± 0.5 μm, where 0.5 μm is the standard deviation of deflection measurements for four samples. The observed phase angle increase was about 0.005, and an increase in phase angle was again expected for a shift to the left by the image.

4.3.6: Estimating Material Properties from Deflection and Known Load

Figure 4-4 demonstrates that the deflection of the boundary of the scaffold is observable via PIC imaging. Now that deflection and loading are known, the material properties of the scaffold can be estimated. A direct approach is to iterate the material properties of the scaffold in an FE model of scaffold deflection, and at each iteration compare estimated deflections to those measured experimentally. This approach will give a solution, but is computationally complex. Alternatively, the known deflections on the boundary may be applied and the material properties in the model iterated until the known loading condition is achieved. Since the estimation of the material properties of the scaffold from deflection and known loading is an inverse problem, and the scaffold is an anisotropic material with several material property parameters, the uniqueness, stability, and existence of these estimates must be considered to determine if they can be obtained from the known deflection and loading. Relating the volume averaged strains and stresses in the scaffold to each other through the material properties allows the uniqueness, stability, and existence of a solution to the inverse problem to be examined.

4.3.7: The Orthotropic Case

With known volume averaged strains ε in the *x*, *y*, and *z* directions from boundary displacements, Orthotropic Hooke's law in compliance form can be written as,

$$\{\vec{\varepsilon}\} = [C]\{\vec{\sigma}\} \tag{4.19}$$

where $\{\vec{\varepsilon}\}$ is a 6x1 vector of strains, $\{\vec{\sigma}\}$ is a 6x1 vector of stresses, and $[C]$ is the Compliance matrix. The Compliance matrix is a function of the Young moduli in the x, y , and z directions of the material, and of the Poisson ratios. The form of the compliance matrix for an orthotropic material can be found in [24].

In linear inverse problem theory, the following represents a system of linear equations,

$$\{\vec{y}\} = [X]\{\vec{b}\} \tag{4.20}$$

where $\{\vec{y}\}$ is a vector of experimental observations, and $\{\vec{b}\}$ is a vector of the parameters that are to be estimated. By rearranging (4.19) into the form of (4.20), the material properties, now represented by a vector of estimated parameters $\{\vec{b}\}$, can be determined by simply inverting $[X]$. Also, in (4.20) the matrix $[X]$ does not need to be square. Multiple loading conditions can be included by adding them to $\{\vec{y}\}$ and $[X]$. The unknown in (4.20), $\{\vec{b}\}$, can then be solved using the least squares estimate.

In order to manipulate (4.19) into the form of (4.20), the following relationships between stress and strain are written,

$$(\sigma_x)_i q_1 - (\sigma_y)_i q_4 - (\sigma_z)_i q_6 = (\varepsilon_x)_i \tag{4.21}$$

$$-(\sigma_x)_i q_4 + (\sigma_y)_i q_2 - (\sigma_z)_i q_5 = (\varepsilon_y)_i \tag{4.22}$$

$$-(\sigma_x)_i q_6 - (\sigma_y)_i q_5 + (\sigma_z)_i q_3 = (\varepsilon_z)_i \tag{4.23}$$

where $q_1 = 1/E_x$, $q_2 = 1/E_y$, $q_3 = 1/E_z$, $q_4 = \nu_{xy}/E_x$, $q_5 = \nu_{yz}/E_y$, $q_6 = \nu_{zx}/E_z$, E is Young modulus, ν is Poisson ratio, the subscripts x, y, and z represent material properties directions, i represents different loading conditions from the ultrasonic beam, and σ is the volume averaged stress. The equations (4.21-4.23) may be rewritten in matrix form,

$$A\vec{q} = \vec{\varepsilon} \tag{4.24}$$

When the Young moduli and Poisson ratios are estimated from the known $\vec{\varepsilon}$ one must consider the possibility that many different combinations of material properties may give the known $\vec{\varepsilon}$, i.e., there is no unique solution for the material properties. By examining the rank of matrix A in (4.24), it is apparent that three separate loading conditions from the ultrasound beam, imaged individually to characterize deflection, would allow the Poisson ratios and Young moduli of the scaffold to be estimated uniquely.

4.3.8: The Transversely Isotropic Case

Substituting the Compliance matrix for a Transversely Isotropic material into (4.20) gives the relationship between stress and strain for Transversely Isotropic materials [24]. This standard engineering matrix form is then manipulated into a standard linear parameter estimation problem. With known average strains in the x, y, and z directions, the following equations may be written,

$$(\sigma_x)_i q_1 - (\sigma_y)_i q_3 - (\sigma_z)_i q_4 = (\varepsilon_x)_i \tag{4.25}$$

$$-(\sigma_x)_i q_3 + (\sigma_y)_i q_1 - (\sigma_z)_i q_4 = (\varepsilon_y)_i \tag{4.26}$$

$$-(\sigma_x)_i q_4 - (\sigma_y)_i q_4 + (\sigma_z)_i q_2 = (\varepsilon_z)_i \tag{4.27}$$

where $q_1 = 1/E_x$, $q_2 = 1/E_z$, $q_3 = \nu_{xy}/E_y$, and $q_4 = \nu_{zx}/E_z$.

In a manner identical to the analysis of the Orthotropic case, the rank of *A* indicates a stable and unique solution for only two distinctive loading conditions. One must also consider that all three average stresses and average strains must be nonzero and larger in magnitude than the noise in the system for useful estimates of material properties to be possible.

4.3.9: Direct Inversion to Determine Material Properties

If the stress distribution in the body is not a function of the material properties, then an iterative approach to finding the material properties from deflection and loading is unnecessary. The stresses in the body are determined by employing arbitrary values for the material properties of the scaffold and solving the FE model of deflection for the known loading condition. To test the sensitivity of the stress distribution within the scaffold as a function of material properties, a numerical test was performed with the scaffold FE model. The Monte Carlo method (with Latin Hypercube experimental parameter selection) of sensitivity analysis with ANSYS was employed to select, at random, values for the material properties of the scaffold material. The model was then solved, and the stresses in the beam determined for an identical loading condition during each run. The stress distribution was found to be almost unrelated to the material properties,

meaning that only the average strain and the deflection of the body are strongly related to the material properties in this particular system. The known measured deflections of the scaffold from the imaging data were applied to the FE model's exterior nodes, giving volume average strains within the beam. The known average stress values were then employed with the known volume averaged strains to estimate scaffold stiffness. With the known strain and stresses, the material properties in the *x*-direction were estimated to be E_x = 0.412 MPa and υ_{xy}=0.047. A one percent error introduced into the strain data produced a less than 0.8% change in the estimates for the material properties in the *x*-direction, indicating that this estimate for scaffold properties is stable. Thus with a single loading condition, the material properties of the scaffold can be determined in the *x*-direction from the deflection imaging data.

Since only one shearing stress and normal stress are relevant in the cantilever beam, there is not enough information present to estimate the scaffold material properties in both the *x*-*y* and *z* directions. If the material properties in the *z* direction are desired as well, they must be inferred from an FE model of the tissue scaffold porous structure. An FE model of a similarly manufactured scaffold was adopted from the literature [25] and employed in this study to infer scaffold properties in the *z*-direction from the known modulus in the *x*-*y* directions. This addition of supplementary information to estimate the modulus from those known in the *x*-*y* directions is a form of regularization. For example, the model of the pore gives a modulus in the *x*-direction of 0.412 MPa when the stiffness of the scaffold material itself is 1.7 MPa. This stiffness for the material when placed in the FE model of the pore, gives an estimate of 0.310 MPa for the stiffness of the scaffold in the *z*-direction. If the four separate displacement measurements, one for each sample, obtained experimentally with the SSE deflection measurement technique described previously, are each individually utilized to estimate the scaffold stiffness, four separate estimates are obtained giving 412 ± 97 kPa as the stiffness in the *x*-*y* direction, and 310 ± 65 kPa as the stiffness in the *z*-direction, where the error is plus or minus one standard deviation.

The above strongly suggests that, in some loading cases that could be arranged in the body, an iterative approach to determine material properties from known deflection and loading is not necessary. However, cases where the stress distribution is only a function of geometry and the

ultrasound source output, do not all give sufficient nonzero stresses to estimate all of the material properties in a transversely isotropic or an orthotropic scaffold from known strain. In these cases, additional information from FE analysis of the scaffold pore geometry is necessary. One case in which sufficient stress and strain information is present for direct inversion, and stress is not related to material properties, is a simple cubic scaffold compressed biaxially by ultrasound. The only limitation to this arrangement for *in vivo* scaffold property estimation, is the scaffold stiffness constraints induced by the imaging system's resolution (its ability to characterize deflection). The beam in bending case has the advantage that the end deflection of the beam is sufficiently large that its observation is usually possible.

4.4: Validation

4.4.1: Compressive Testing of Scaffolds

Now that the stiffness of the scaffold has been estimated from the measured deflection and calculated loading, this estimate is validated by comparison to direct stress-strain data. The PDMS scaffold is a transversely anisotropic material, which displays different young moduli in the directions perpendicular and parallel to the stacked scaffold layers. These two Young moduli were measured under compression at a strain rate of 10 mm/min with an Instron Universal Material Testing machine. Three samples were employed per test, giving average stress-strain curves, which are illustrated in Fig. 4-7.

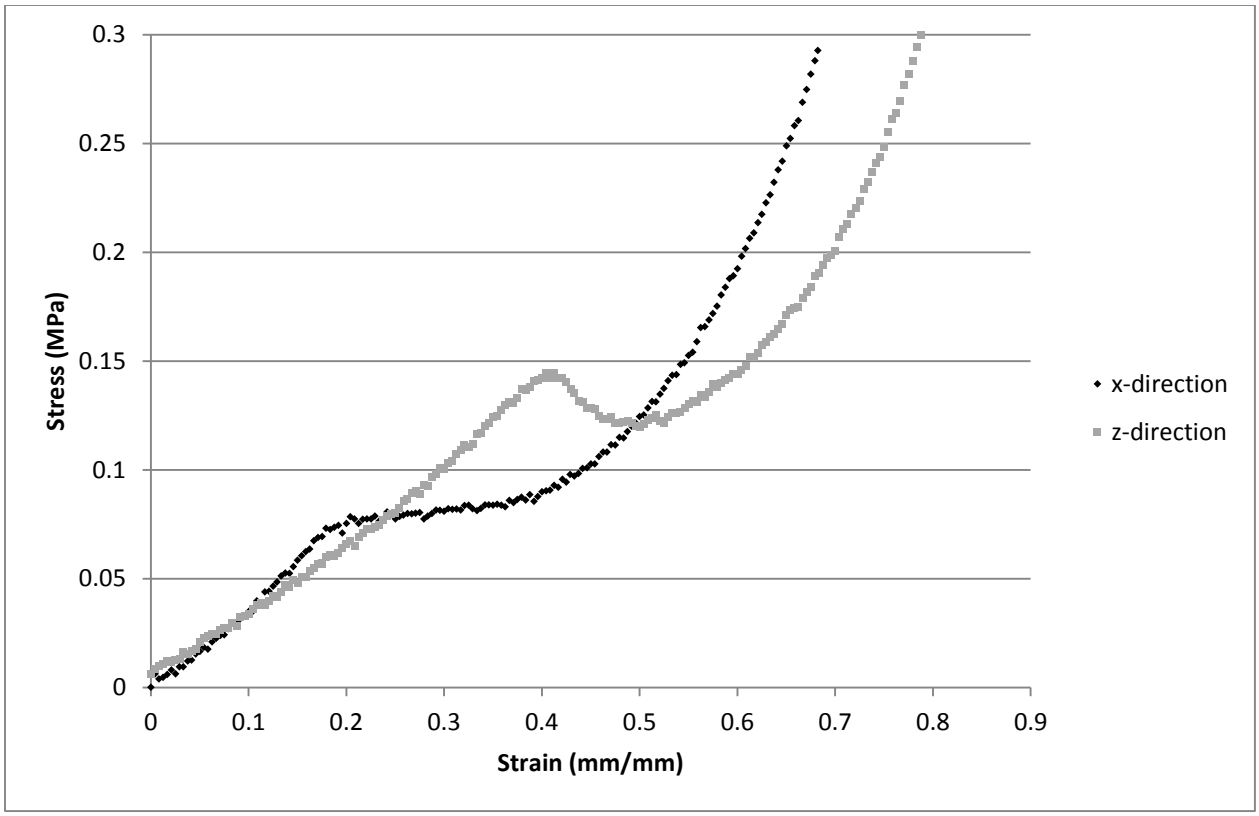

Figure 4-7: Average Compressive Stress-strain Curve for PDMS Scaffold in both the x-dir and the z-direction

From the results of the compressive test, it is estimated that the Young modulus of the scaffold in the *z*-direction perpendicular to the layers is 345 ± 33 kPa, and 364 ± 28 kPa in the *x*-*y* direction parallel to the layers, where the error interval is the standard deviation of the three samples. An F-test reveals that these measured values for modulus are equivalent to those estimated from imaging.

4.4.2: Validation of FE Model of Scaffold Pore

The accuracy of the FE model of the tissue scaffold pore that was employed for regularization was considered. An FE model of an individual pore of the scaffold was created, and the application of periodic displacement boundary conditions was employed to estimate its mechanical properties. Employing the methodology in [25], the homogenization process predicted the following effective material properties for the scaffold with pure PDMS having a

Young Modulus of 2 MPa, a strand radius of 205 μm and a strand spacing of 1000 μm; 1) $Ex = Ey$ = 418 kPa, 2) Ez = 265 kPa, 3) Gxy = 40.6 kPa, 4) $Gxz = Gyz$ = 94.4 kPa, 5) $vxy = vyx$ = 0.045, 6) vyz = 0.26, and 7) vzx = 0.16. The estimated effective transversely isotropic stiffness matrix for the scaffold is given as,

$$[C] = \begin{bmatrix} 440 & 40 & 78 & & & \\ 40 & 440 & 78 & & & \\ 78 & 78 & 290 & & & \\ & & & 94 & & \\ & & & & 94 & \\ & & & & & 41 \end{bmatrix} kPa \qquad (4.28)$$

There is uncertainty in the scaffold's strand diameter and strand spacing, which was measured by optical microscopy to have a standard deviation of ± 8% for strand spacing and ± 2% for strand diameter. With this error, the model Young Moduli predictions have a standard deviation of ± 19%. This error interval is determined by propagating the error of the strand diameters and strand spacings to the estimates for scaffold material properties through the FE model of the scaffold pore. This can be achieved using the probabilistic design application in ANSYS. The numerical model predictions for Young modulus therefore agree with experimental measurements within experimental and model error. The F-test is again utilized to suggest that the two mean values for moduli, one from the finite element model and one from the compression testing of the scaffolds, are in agreement.

4.4.3: Validation of FE Model of Ultrasonic Loading and Deflection

Employing the load-displacement test measured material properties, the deflection of the scaffold subjected to a 2 W intensity ultrasound beam was predicted with the FE model. A convergence study was conducted by increasing the number of elements within the model and observing the change in model predictions. The form of the observed pattern demonstrated that the use of convergence acceleration by means of the Scalar Epsilon Algorithm by Wynn to extrapolate the end deflection of the beam with multiple runs of the model with a coarse mesh is justified, since the parameter of interest displayed exponential decay. The model was run with 950, 1620, and

2597 elements, giving predictions for end deflection of 75, 71, and 68 microns respectively. The Scalar Epsilon Algorithm execution gave a prediction of 50 microns for the end deflection of a finite element model with an infinite number of elements. The model with 21,000 elements took a noticeable amount of time to run even though the problem is linear. This suggests that three runs of coarse mesh models and convergence estimation with the Scalar Epsilon Algorithm gives similar predictions to those given by more computationally demanding FE models with a finer mesh.

The finite element model was run again with the ultrasonic beam intensity changed to 0.5 W, and the Scalar Epsilon Algorithm was used to extrapolate model predictions to an infinite number of elements. The power output of the therapeutic ultrasound machine was within ± 30% of the displayed power output, and the model predictions for deflection were therefore 12 ± 4 μm. The 4 μm standard deviation comes from probabilistic design simulations in ANSYS where the ultrasound power output and the geometric variables are represented as Gaussian distributed design parameters.

4.5: Conclusions

This study has explored the possibility of measuring displacements in an imaging environment similar to that *in vivo* where the implant density and that of its surroundings are similar. In addition, the use of a steady state radiation force for sample deflection has been demonstrated, with measurable displacement successfully imparted to the sample. The forward modeling problem, a function that can map from material properties of the scaffold to predictions of its deflection under the influence of an ultrasound beam, has been solved. The developed mapping was found to estimate the deflection of the scaffold with acceptable accuracy. A preliminary analysis of the inverse problem indicates that three separate loading conditions are required to provide a unique estimate for the stiffness matrix of the scaffold in the orthotropic case, and that two are required when the scaffold is transversely isotropic. Furthermore, the stress distribution in the scaffold is weakly related to material properties in the specific applied boundary conditions employed in this study, allowing the scaffold properties to be estimated by the direct

inversion of the stress matrix A. Furthermore, Fourier analysis of the intensity signal from a tissue scaffold with a periodic structure can be employed to measure its deflection.

4.6: Future Work

In this particular case of a fixed beam like scaffold bending under a distributed load, a question arises as to how great the rotation of the scaffold segment under study can be before the analysis from Fourier analysis no longer is valid. Further research is required to explore this important question. In addition, this approach to scaffold remote material property characterization should be applied to a fully orthotropic tissue scaffold. Finally, the use of Fourier analysis and periodic structures should be applied to situations where the deflections of the scaffold are fully sub-pixel sized to clearly demonstrate Fourier analysis with periodic structures based deflection characterization.

Acknowledgments

The authors acknowledge the support received for the present research from the Natural Sciences and Engineering Research Council (NSERC) of Canada and the Saskatchewan Health Research Foundation (SHRF). Also, the authors acknowledge that the imaging of the scaffolds presented in this paper was accomplished at Canadian Light Source (CLS), which is upported by the Canadian Foundation for Innovation, NSERC, the University of Saskatchewan, the Government of Saskatchewan, Western Economic Diversification Canada, the National Research Council Canada, and the Canadian Institutes of Health Research.

References

[1] Gray, N. A., Selzman, C. H., 2005, Current status of the total artificial heart, American Heart Journal, vol. 152, no. 1, p. 4-10.

[2] Zwischenberger, J. B., Anderson, C. M., Cook, K. E., Lick, S. D., Mockros, L. F., Bartlett, R. H., 2001, Development of an Implantable Artificial Lung: Challenges and Progress, ASAIO Journal, vol. 47, p. 316–320.

[3] Bodell, B. R., Head, J. M., Head, L. R., Formolo, A. J., An Implantable Artificial Lung; Initial Experiments in Animals, 1965, Journal of the American Medical Association, vol. 191, p. 125-127.

[4] Down, J. D., White-Scharf, M. E., 2003, Reprogramming immune responses: enabling cellular therapies and regenerative medicine, Stem Cells, vol. 21, Issue 1, p. 21-32.

[5] Kobayashi, T., Yamaguchi, T., Hamanaka, S., Kato-Itoh, M., Yamazaki, Y., *et al*, 2010, Generation of rat pancreas in mouse by interspecific blastocyst injection of pluripotent stem cells, Cell, vol. 142, p. 787–799.

[6] Atala, A., Kasper, F. K., Mikos, A. G., Engineering Complex Tissues, Tissue Engineering Review B, vol. 4, Issue 160, p. 1-10.

[7] Dado, D., Levenberg, S., Cell–scaffold mechanical interplay within engineered tissue, 2009, Seminars in Cell & Developmental Biology, vol. 20, p. 656–664.

[8] Hollister, S.J., Maddox, R.D., Taboas, J.M., Optimal design and fabrication of scaffolds to mimic tissue properties and satisfy biological constraints, 2002, Biomaterials, vol. 23, p. 4095–4103.

[9] Artzil, N., Oliva, N., Puron, C. Shitreet, S., Artzi, S., *et al*, In vivo and in vitro tracking of

erosion in biodegradable materials using non-invasive fluorescence imaging, 2011, Nature Materials, vol. 10, p. 704-709.

[10] Radicke, M., Mende, J., Kofahl, A. L., *et al*, Acoustic radiation contrast in MR images for breast cancer diagnostics-initial phantom study, 2011, Ultrasound in Med. & Biol., vol. 37, No. 2, p. 253–261.

[11] Nyborg, W. L., Acoustic streaming, In: Mason, W. P., (ed.), 1965, New York, Academic Press.

[12] Torr, G. R., The acoustic radiation force, 1984, Am. J. of Phys., vol. 52, 5, p. 402-408.

[13] Sarvazyan, A.P., Rudenko, O.V., Nyborg, W. L., Biomedical applications of radiation force of ultrasound: historical roots and physical basis, 2010, Ultrasound in Med. & Biol., vol. 36, No. 9, p. 1379-1394.

[14] Tierney, A. P., Dumont, D. M., Callanan, A., Trahey, G. E., Mcgloughlin, T. M., Acoustic radiation force impulse imaging on ex vivo abdominal aortic aneurysm model, 2010, Ultrasound in Med. & Biol., vol. 36, No. 5, p. 821–832.

[15] Tables of Physical & Chemical Constants. 2.1.2 Barometry. Kaye & Laby, Version 1.1, 2008, The National Physical Laboratory, UK.

[16] Appel, A., Anastasio, M. A., Brey, E. M., 2011, Potential for imaging engineered tissues with X-ray phase contrast, Tissue Engineering Part B: Reviews, 17(5), 321-330.

[17] Sztrókay, A., Diemoz, P. C., Schlossbauer, T., *et al*, 2012, High-resolution breast tomography at high energy: a feasibility study of phase contrast imaging on a whole breast, Phys. Med. Biol., vol. 57, p. 2931–2942.

[18] Bravin, A., Coan, P. and Suortti, P., X-ray phase-contrast imaging: from pre-clinical applications towards clinics, Phys. Med. Biol., vol. 58, R1–R35.

[19] Quan-Jie, Jia, et al. "Optimization of the in-line X-ray phase-contrast imaging setup considering edge-contrast enhancement and spatial resolution." Chinese Physics C 36.3 (2012): 267.

[20] Zhong, Z., Thomlinson, W., Chapman, D., and Sayers. D., "Implementation of diffraction-enhanced imaging experiments: at the NSLS and APS." Nuclear Instruments and Methods in Physics Research Section A: Accelerators, Spectrometers, Detectors and Associated Equipment 450, no. 2 (2000): 556-567.

[21] Zhu, N., Chapman, D., Cooper, D., Schreyer, D. J., & Chen, X. (2011). X-ray diffraction enhanced imaging as a novel method to visualize low-density scaffolds in soft tissue engineering. Tissue Engineering Part C: Methods, 17(11), 1071-1080.

[22] Hamilton, T. J., Bailat, C. J., Petruck, C. R., Diebold, G. J., Acoustically modulated x-ray phase contrast imaging, 2004, Phys. Med. Biol. 49, 4985–4996.

[23] Yamahata, C., Sarajlic, E., Stranczl, M., Krijnen, G., Gijs, M., Subpixel translation of MEMs measured by Discrete Fourier Transform analysis of CCD images, 2011, IEEE Solid-State Sensors, Actuators and Microsystems Conference, p. 1697-1700.

[24] Nemat-Nasser, S., Hori, M., Micromechanics: Overall Properties of Heterogeneous Solids, 1st edition, Elsevier Science Publishers, 1993.

[25] Bawolin, N. K., Li, M. G., Chen, X. B., Zhang, W. J., Modeling Material-Degradation-Induced Elastic Property of Tissue Engineering Scaffolds, 2010, ASME Journal of Biomechanical Engineering, vol. 132, 111001_1-111001_7.

CHAPTER 5

SYNCHROTRON BASED *IN SITU* CHARACTERIZATION OF TIME DEPENDENT MASS LOSS FROM EROSION BASED DEGRADATION*

*****This chapter has been submitted as "Bawolin, N. K., Chen, X. B., 2016, Synchrotron Based *In Situ* Characterization of Time Dependent Mass Loss from Erosion Based Degradation, Journal of Functional Biomaterials." According to the Copyright Agreement, "the authors retain the right to include the journal article, in full or in part, in a thesis or dissertation".

5.1: Summary

In the particular case of surface erosion in tissue scaffold degradation, the fundamental properties of the parent material, especially the molecular weight, remain constant throughout the degradation period. All that changes, when scaffolds display this type of degradation, is the internal geometry of the tissue engineering construct. This is significant because it clearly indicates that the mechanical properties of such a tissue scaffold are only a function of a quality which can be observed remotely without removing the scaffold from the body. This indicates that tissue scaffolds of this type may be observed by phase contrast x-ray imaging, and reconstructions of the scaffold geometry will allow its material behavior to be ascertained.

Planar images of Polycaprolactone tissue scaffolds and Polylactic Glycolic Acid were obtained via synchrotron imaging and employed to characterize the remaining volume of parent material left in the scaffold with time. From these volume estimates and known tissue scaffold parent material density, the mass at each time point during degradation was ascertained. A finite element model of erosion was then created, and its parameters estimated from the image based estimates of scaffold mass loss with time.

In this paper, a set of tissue engineering scaffolds manufactured by a rapid prototyping method and cylindrical implants were incubated in an environment that would result in surface degradation. These surface degraded cylindrical implants and rapid prototyping manufactured tissue scaffolds were then imaged via synchrotron x-ray radiation to characterize their time dependent morphologies. From this information, the mass of the scaffolds and implants were estimated from changing geometry. The mass loss of the scaffolds and implants were then validated using conventional gravimetric methods to directly measure the reduction in mass with time for both the scaffolds and cylinders. The estimates for scaffold and implant mass loss as given by geometry monitoring agreed well with the actual direct measurements of mass loss with time.

The scaffold material/degradation medium chosen display surface degradation alone. This has been confirmed in the research of others via the use of gel permeation chromatography, which demonstrates no relevant change in scaffold material molecular weight with time. Mathematical models of the surface degradation of the implants and scaffolds were therefore created, and the parameters in said models were estimated from the experimentally measured mass loss. The mass loss model recreated the geometry of the cylinder or a single pore of the rapid prototyping manufactured scaffold in the finite element modelling software ANSYS. The analogy between heat conduction and diffusion is employed by ANSYS to model the three dimensional transport of chemical species, by merely changing the element option keys to alter elements for heat transfer into elements for conducting diffusion analysis. A set concentration of Sodium Hydroxide and Water is applied to the outside surfaces of the scaffold, and the model then solves the transport equations with the finite element method.

This study demonstrated the remote monitoring of scaffold mass through a signal that can be detected in the living environment with synchrotron radiation imaging methods. This information was then employed to successfully estimate the parameters of a degradation model, which was then able to successfully follow the behavior of the actual scaffolds and cylindrical implants with time.

The degradation behavior of a tissue scaffold or implant is critical to its lifespan and other related features including mechanical strength and mass transport characteristics. This paper presents a novel method based on synchrotron imaging to characterize the time dependent mass loss from the erosion based degradation. Specifically, the surface eroding degradation of cylindrical and rapid prototyping manufactured implants within a representation of the living body was monitored *in situ* by synchrotron based imaging; and the time dependent geometry of the implants was then employed to estimate their mass loss with time based on the mathematical models of surface erosion with the identified model parameter of k_3 . Acceptable agreement between experiment and theory was observed for the estimated model parameters for cylindrical solid PLGA implants, and rapid prototyping manufactured scaffolds. This novel study suggests that geometry evaluation by x-ray diffraction enhanced imaging *in situ*/*in vivo* may allow a better understanding of the difference between simplified *in vitro* experimental representations of degradation and the actual behavior in the environment.

5.2: Introduction

Tissue engineering is a field of research that has as its central goal the development of methods for the replacement of damaged and/or diseased tissue. One of the most promising state of the art methods for creating new tissue is scaffold based tissue engineering. In this treatment process, an artificial matrix, known as a tissue scaffold, is seeded with patient derived cells, forming what is known as a tissue engineering construct. This construct is then either directly implanted within the body, or incubated within an artificial simulacrum of the living environment for a time before implantation. The cells seeded within the scaffold self organize into new tissue/organs, while the underlying scaffold degrades and is usually absorbed and excreted by the body. A critical factor in the design of the tissue scaffold is its degradation behavior, which controls the device's lifespan in the body and other related features such as its mechanical strength and mass transport characteristics, which are both functions of time. Synthetic and natural polymers display two general

types of degradation behavior; 1) bulk degradation and 2) surface degradation. Within the category of bulk degradation there are two additional degradation pathways; 1) uniform degradation and 2) heterogeneous degradation [1].

Part of the volume of the tissue engineering construct is occupied by the tissue scaffold material phase, and the remaining volume is filled by a fluid, seeded cells, and developing tissue. In Fig. 5-1 (a), an example of a unit cell of a tissue engineering scaffold is presented, while Fig. 5-1 (b) , 5-1 (c), and 5-1 (d) illustrate the scaffold material occupied volume in the unit cell, the tissue/cells/fluid occupied volume, and the interface surface between these two volumes, respectively.

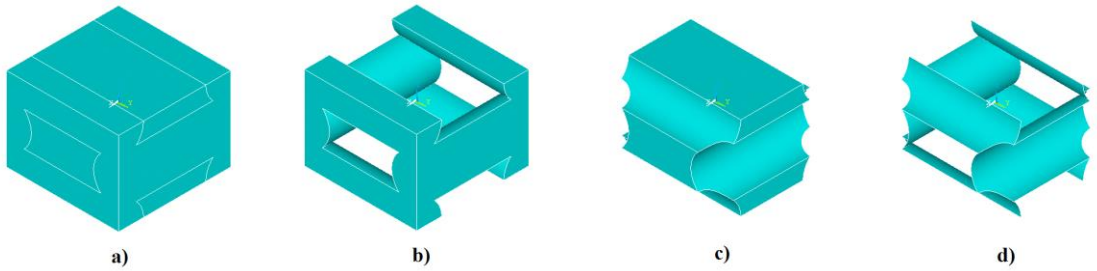

Figure 5-1: Tissue engineering construct unit cell a), scaffold material occupied volume b), tissue/cells/fluid occupied volume c), and interface surface between the two volumes d).

In surface degradation as schematically shown in Fig. 5-2 (a), the scaffold material strongly resists infiltration by the liquid degrading medium, resulting in a steep gradient of medium concentration within the scaffold material, with maximum concentrations occurring very near the interface surface between the scaffold material occupied volume and the volume occupied by tissue/cells/fluid. Each location within the scaffold material occupied volume is some distance from the interface surface. For locations within the scaffold material occupied volume close to the interface surface, the concentration of the degrading medium is high, while far from the interface surface, deep within the scaffold material, the concentration of the degrading medium is less.

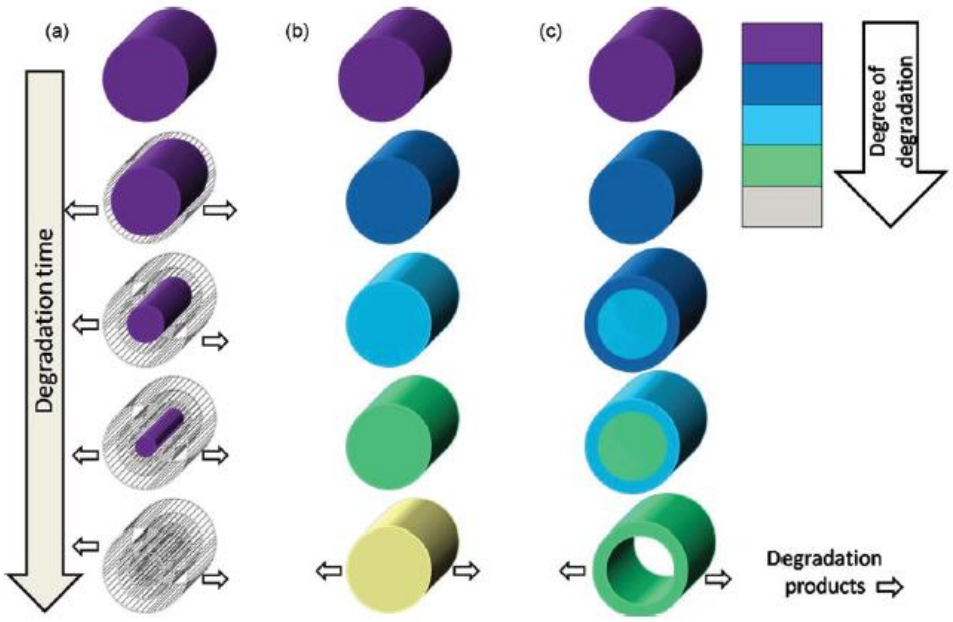

Figure 5-2: Surface degradation (a), homogeneous bulk degradation (b), and inhomogeneous bulk degradation (c) [1].

The degradation chemical reaction (hydrolysis) therefore proceeds at a much higher rate at the interface surface than in the interior of the scaffold material occupied volume, with the molecular weight of the scaffold material only declining at or near the interface surface, which is exposed directly to the degrading medium in the tissue/cells/fluid occupied volume. Once the molecular weight at or near the internal surface of the pore decreases to a critical level, the polymer chains diffuse from the interface surface of the scaffold into the fluid/cell/tissue region. This erosion process changes the geometry of the scaffold material occupied region while leaving the molecular weight, and therefore the mechanical properties, of the scaffold material occupied region of the device unchanged. In essence, small sheet like layers of the scaffold material are dissolved and stripped away, revealing a fresh surface which then in turn is attacked by the degrading medium. Over time the scaffold material

occupied volume decreases in size as the scaffold material is gradually dissolved, and the in solution scaffold materials disposed of by the body. Examples in the literature of scaffolds that display this behaviour may be found in references [2-4]. This degradation behaviour may be highly desirable, especially in the case of hybrid scaffolds, where a framework provides the needed mechanical behavior for the scaffold and a separate hydrogel based scaffold structure contains and organizes the cells. Since the molecular weight, crystallinity, and mechanical properties of the scaffold material remain constant during degradation, only initial molecular weight and initial geometry control degradation and the effective properties of the tissue engineering construct. In addition, the use of a surface degrading polymer for the construction of hybrid scaffolds also introduces the possibility of the mechanical support structure also serving as a drug delivery platform to provide the cells within the hydrogel component of the construct with necessary stimulation with growth factors, nutrients or other possibly beneficial agents.

In contrast, materials that display bulk degradation, as illustrated in Fig. 5-2 (b), permit the medium to easily diffuse throughout the entire scaffold interior, resulting in a significant concentration of medium throughout the entire scaffold. All of the regions of the scaffold are therefore degraded simultaneously, and if random chain scission succeeds in producing a chain of sufficient shortness, it diffuses out of the scaffold. In this manner, mass is removed throughout the entire bulk volume of the scaffold during the degradation process. In [5-7] the scaffolds under study display this type of degradation behavior.

When a polymer chain is scissioned it releases a monomer waste product, which acts as a catalyzing agent for the hydrolysis reaction. If the diffusion coefficient of this monomer waste product is sufficiently high within the scaffold material, the concentration of monomers within the scaffold is low and does not contribute greatly to device degradation. If, however, the diffusion coefficient of the monomer in the scaffold material is sufficiently small, the monomer waste products will build up within the scaffold, and degradation within the core of the device will be much higher

than at the device interface surface, where the monomers can escape into the fluid filled pore. As illustrated in Fig. 5-2 (c), eventually, the interior of the device will be hollowed out. Devices that display this type of degradation behaviour were considered in [8].

The degradation behavior of tissue scaffolds is usually experimentally characterized by *in vitro* tabletop degradation experiments, where a tissue scaffold sample is immersed in phosphate buffered saline (PBS) and incubated at body temperature [9]. While these experiments provide some useful data about degradation, the PBS medium does not perfectly represent *in vivo* degradation. To achieve closer agreement between *in vivo* and *in vitro* degradation experiments, media that includes enzymes and cultured cells have also been employed in degradation testing [10, 11]. It is not yet practical or cost effective to perfectly replicate the living environment *in vitro* by representing every biological and chemical effect found in the body artificially [12].

The differences between *in vivo* degradation, and *in vitro* degradation in PBS, can be characterized by animal testing [13]. Once the desired degradation time is reached, a minimum of three animals would be sacrificed for each time point, and the average molecular weight, mass, and mechanical properties of the implant are then measured [14-16]. This approach requires a large number of animals to evaluate even a small sample size. This analysis of the explant can also only measure the average properties of the entire extracted device; i.e. location specific properties are not measurable [17]. This limitation can be overcome by adopting image based methods to evaluate degradation and mass loss [17]. Any imaging method that can characterize the geometry of the implant, either *in vivo* or *ex vivo*, would be able to visualize surface degradation and infer the resultant mass loss. However, even if imaging based methods are utilized to characterize surface degradation induced sample mass loss, *ex vivo* imaging methods still require the removal of the implant from the animal [18,19,20], which results in some variability from the act of removing the sample and the variation between animals. In [21] the changing density and morphology of bone is evaluated *in vivo* by X-ray micro computed tomography (μ-CT) scans, raising the

possibility that a similar procedure may allow the same type of experimental evaluation to be performed for tissue scaffolds. Unfortunately, this absorption based method has difficulty distinguishing soft tissue from the background, and is only viable because the x-ray absorption characteristics of bone provide sufficient contrast with the soft tissue surroundings. This limitation may be overcome by *in vivo*/*in situ* image based methods that can provide sufficient contrast to visualize the low density polymeric scaffold devices against a tissue background with similar x-ray attenuation properties.

Diffraction enhanced imaging (DEI) is a well-developed imaging method that show promise as a way to monitor implants when they are surrounded by material with similar densities and absorption properties *in vivo* [22]. This imaging method measures the change in the angle of the X-ray photons as they pass through the sample by diffracting them off of a crystal before they arrive at the photon detector. DEI is also able to image samples at high x-ray energies, and since the absorption coefficients of tissue and bone decrease with increasing photon energy, imaging at higher x-ray energies lowers the absorbed *in vivo* dose, which is a significant advantage over other competing imaging methods. In conventional absorption based imaging, lowering the photon energy increases the amount of photons which are absorbed by the sample, which increases the contrast between the sample and the background. This increases the Signal to Noise ratio (SNR) and the resolution [23]. In the DEI method, the SNR is not only related to photon energy but also to the properties of the analyzer crystal [24]. It may therefore be possible with DEI to employ higher x-ray energy to reduce the radiation dose from imaging and still achieve the same SNR as lower photon energy absorption based imaging methods. DEI also generates images based on beam refraction rather than absorption, allowing regions of interest of similar density to the background to be visualized [25]. The beam-line configuration of the DEI imaging method is illustrated in Figure 5-3, where it is compared to that of conventional radiography synchrotron based absorption x-ray imaging.

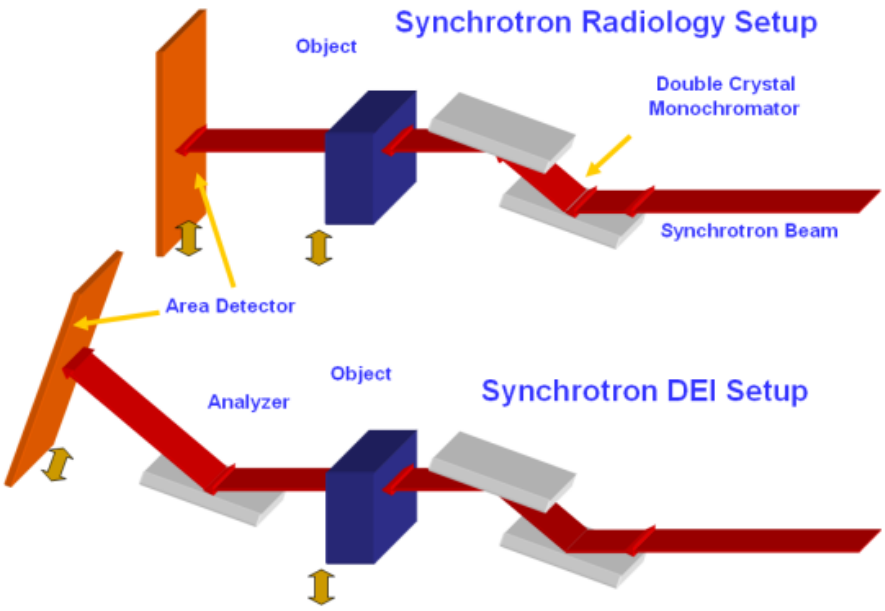

Figure 5-3: DEI/MIR and conventional radiography beamline experimental setups.

In this study, we hypothesize that the DEI imaging method can be employed to characterize the geometry of implants as they erode, and to then infer their mass loss with time. By rotating the sample in the x-ray beam, and imaging the sample at multiple times during this rotation, computed tomography may be employed to reconstruct the scaffold geometry with time. The volume of the remaining scaffold material can be measured at multiple time points during its degradation, and the mass loss inferred from the known density of this scaffold material. While theoretically, it should be possible to detect the porosity that develops in bulk degrading polymers [26], the resolution requirements for this task are not available. Therefore, this method is limited to the consideration of surface degrading tissue scaffolds.

The particular approach proposed above, while possible, raises unresolved issues. In living biological samples, the allowable radiation dose would restrict the number of points in time during the degradation that could be characterized by full computed

tomography image reconstruction [27]. Computed tomography imaging also requires a significant amount of time, on the order of 18 hours or more, especially if high resolution is required [27]. This is especially problematic in situations where the degradation rate is high enough that the mass of the scaffold or drug delivery device changes significantly during the time required to characterize the scaffold volume through imaging. In this work, planar images of the outer surface of the scaffold are employed to determine the average strand diameter of the scaffold with time, and the degradation is then assumed to be uniform throughout the scaffold. The change in strand diameter is employed to estimate the volume of the scaffold with time, and its mass at a specific time is then inferred form this volume and the known density of the scaffold material.

Once *in situ/in vivo* degradation data of a scaffold manufactured from a specific material in a specific environment is known, it may be of interest to predict the performance of the scaffold as a function of initial geometry. A scaffold can then be designed to meet specific mass loss requirements for specific applications. This may be accomplished inefficiently experimentally, or through the development of a model of scaffold degradation to guide the design process. To represent the mass loss, a model is adopted from the literature [28] with the parameters to be identified by means of experimental data capture via DEI.

In this study, scaffolds are manufactured out of a representative biomaterial and degraded in a medium that causes surface degradation to the selected biomaterial. The scaffold is then imaged in a low radiation dose manner in situ by DEI imaging to estimate the remaining volume of the scaffold with time. From the volume change and the known density of the biomaterial, the mass loss of the scaffold is estimated with time. These estimates are then validated by comparison to gravimetric mass loss measurements. A mathematical model of scaffold mass loss is then fitted to this experimental data. This model may then be used as a design tool to calculate the required initial scaffold geometry to achieve specific mass loss behavior for scaffolds composed of the same material and degraded in the same environment.

The polymer Polycaprolactone was chosen as the material employed for rapid prototyping scaffolds, and the degradation medium was chosen to be a 5M base solution of Sodium Hydroxide at a temperature of 55°C. Sodium Hydroxide is chosen as the degradation medium because Sodium Hydroxide ions do not diffuse readily into a wide range of polymer materials, which results in surface degradation behavior [29, 30]. The degradation of devices is also significantly accelerated compared to that experienced in Phosphate Buffered Saline. This particular selection of degradation medium and material can act as a demonstrative system to represent a variety of biologically relevant and general polymer analysis combinations of material and degradation media. To represent an implant with different geometry manufactured out of a different material degraded by a less aggressive degradation medium, PLGA cylinders were degraded as well in a 1M solution of Sodium Hydroxide at 55°C.

In the work of [31] a cylindrical surface eroding polymer implant 4 mm in length with a diameter of 3 mm composed of poly-trimethylene carbonate (PTMC) is degraded within a rabbit animal model. The observed experimental degradation of the PTMC implant by enzymatic surface degradation is related to the degradation of PCL in a 5M solution of NaOH at 55°C, and the degradation of PLGA in a 1M solution of NaOH at 55°C. This allows for the creation of device designs experimentally by employing a representative material/degradation medium that experiences rapid degradation. The behaviour of these analogous devices composed of PCL or PLGA can then be employed to estimate the behaviour of devices composed of PTMC *in vivo*.

5.3: Experiments and Methods

PLGA 50:50 with a viscosity based molecular weight of 100,000 Daltons was purchased from Lactel Corporation. The polymer was raised to an appropriate temperature in a furnace and cast into cylindrical Teflon molds 1 cm high and 0.8 cm in diameter. The samples were removed from their molds with a metal punch and the

surfaces of the plastic cylinders were machined via lathe to achieve consistent sample geometry. 24 samples of PLGA were produced.

Polycaprolactone with an initial number average molecular weight of 80,000 Daltons was purchased from Sigma Aldrich and dispensed into three dimensional tissue scaffolds with an Envisontech bioplotter. The polymer was extruded as a melt at 200° into strands of 500 μm diameter spaced 800 μm apart. Each layer of strands was dispensed 700 μm above the previous layer. These dimensions were verified by optical microscopy, where dimensions were measured with a microscope camera and the software Paxit. The overall dimensions of each scaffold were 5 x 5 x 5 mm.

The sample initial weights were measured and the PLGA and PCL samples were immersed in solutions of NaOH and incubated at 55°C. The PLGA implants were immersed in a 1 Molar solution while the PCL samples were degraded in a 5M solution. Preliminary experiments [32] revealed that these highly basic mediums and elevated temperatures induced accelerated degradation and induce surface degradation in the PLGA and PCL samples. The PLGA samples were degraded for 54 hours with samples removed at t = 0, 12, 24, 30, 36, 42, 48, and 54 hours. For PCL, the scaffolds were removed and characterized at t = 0, 5, 20, 25, 30, 35, and 45 hours. All samples were then reweighed and placed in a 2 cm thick ethanol/water filled tank and imaged at the Canadian Light Source (CLS) Biomedical Imaging and Therapy bend-magnet beam-line (BMIT) at an energy of 40 keV. Three images of each sample were taken; one at the peak of the rocking curve and two at opposite sides of the rocking curve at half intensity. This particular beamline is equipped with a (2,2,0) cut silicon monochromator and analyzer crystal. A copper filter was applied to remove the (2,2,0) reflection leaving only the (4,4,0) reflection at 40 keV to proceed through the sample. The diameter of the deposited strands that make up the layers of the rapid prototyping manufactured scaffold were measured with ImageJ software at twenty separate locations on the scaffold, and these measurements were employed to estimate the remaining volume of the scaffold at each time point.

The semicrystalline PCL samples were not expected to experience crystallization during their degradation in NaOH, since degradation is confined to the interface surface of the scaffolds. But Differential Scanning Calorimetry (DSC) was still performed to ensure that the PCL crystallinity had not changed with time during degradation. The DSC method melts samples of the scaffold and evaluates the heat absorbed by the scaffold during its phase change, which is the conversion of its ordered crystalline phase into a fully amorphous microstructure. By comparing the enthalpy required to transform the samples to their fully amorphous state to that required for a fully crystalline sample, the crystallinity of the scaffold may be obtained [33]. The treatment of the samples involved heating from room temperature to 100°C at a heating rate of 10°C/min and a return to room temperature after stabilization. The phase change initiated at a transition temperature of 60°C which is typical for PCL.

5.4: Modelling

To mathematically represent mass loss, the phenomenological model found in the work of Han and Pan [28] is adopted. Briefly, a hydrolysis reaction reduces the molecular weight of a degrading polymer at some rate $\dot{R}$ which represents the number of polymer chains cut per interval of time.

$$\dot{R} = -dC_e / dt = k_1 C_e C_w + k_2 C_e C_w C_m^{0.5} + k_3 C_e C_w C_m C_{NaOH}^{0.63} \quad (5.1)$$

$$M_w / M_{w0} = C_e / C_{e0}$$

This rate of chain destruction is dependent upon the concentration of ester bonds C_e, the concentration of water C_w, and the concentration of any media that may change the local pH of the surroundings. These may include the acidic byproducts of degradation C_m or some substance present in the surrounding medium, such as basic sodium hydroxide C_{NaOH}. It may also include the byproducts of metabolism generated

by the cells seeded in the scaffold. In the particular degradation conditions selected for this study, the degradation rate from the presence of water and weak acidic degradation byproducts is much less pronounced than that induced by the presence of the sodium hydroxide. Therefore, the simplified model of degradation may only consider this chemical species and its mass transport inside the implant. The hydrolysis rate parameters for water and monomers k_1 and k_2 may be ignored leaving only k_3 as an unknown parameter in the degradation model that must be estimated from the experimental data. The terms above the concentration of monomers and sodium hydroxide are dissociation terms, relating concentration to the amount of the species that dissociates in solution. The diffusion coefficient of the species within the implant increases with time due to the increase in the porosity of the material. The porosity of the polymer is approximated by,

$$\rho = 1 - C_e / C_{e0} \tag{5.2}$$

and the effective diffusion coefficient of the degrading polymer is estimated by the Maxwell Garnett expression for the effective properties of a mixture, when the inclusions of the second phase in the mixture are spherical [34].

$$D_{ap} = D_a \left[1 + \frac{3(D_p - D_a)\rho}{D_p + 2D_a - (D_p - D_a)\rho} \right] \tag{5.3}$$

where D_p is the diffusion coefficient in the pores, D_a that in the amorphous phase of the material, and ρ the time dependent porosity of the amorphous polymer phase. At a critical molecular weight, the polymer is assumed to become soluble in the degrading medium and diffuse out of the implant. For PLGA this critical molecular weight has been experimentally determined to be 15,000 Daltons [35]. For PCL this critical molecular weight is 5000 Daltons [36]. In each element of the model, the scission rate is calculated, and a random parameter is assigned as the fraction of scissions that have

produced polymer chains less than the critical molecular weight in size. The mass loss in each element is then calculated as,

$$\frac{M_t}{M_0} = \frac{N_t}{N_0} \tag{5.4}$$

where M_t is the mass at time t, M_0 is the initial mass of the element, and N_t and N_0 are the number of polymer chains in each element with molecular weights greater than the critical molecular weight respectively. For PLGA, the diffusion coefficient of NaOH was chosen to be similar to that of a carboxyl monomer in an amorphous polymer; 3.6×10^{-7} cm^2/hr. For PCL, the diffusion coefficient of NaOH was chosen to be higher, since the PCL displayed bulk degradation. A value of 8.29×10^{-4} cm^2/hr was chosen, which is equal to the measured diffusion coefficient of water in PCL. In order to estimate the unknown parameter in the model, an objective function was defined and minimized.

$$Obj(k_3) = \sum_{t=0}^{t=k} abs(M_{\exp}(t) - M_{model}(t)) \tag{5.5}$$

where *t* is degradation time, *k* is the time at the end of sample degradation, $M_{\exp}(t)$ is the experimentally measured mass loss as a function of time, and $M_{model}(t)$ are the time dependent model predictions for mass loss.

5.5: Results and Discussion

Monitoring of PCL scaffold crystallinity yielded the following results, illustrated in Fig. 5-4, which indicate that there is no appreciable crystallization of the sample during surface degradation.

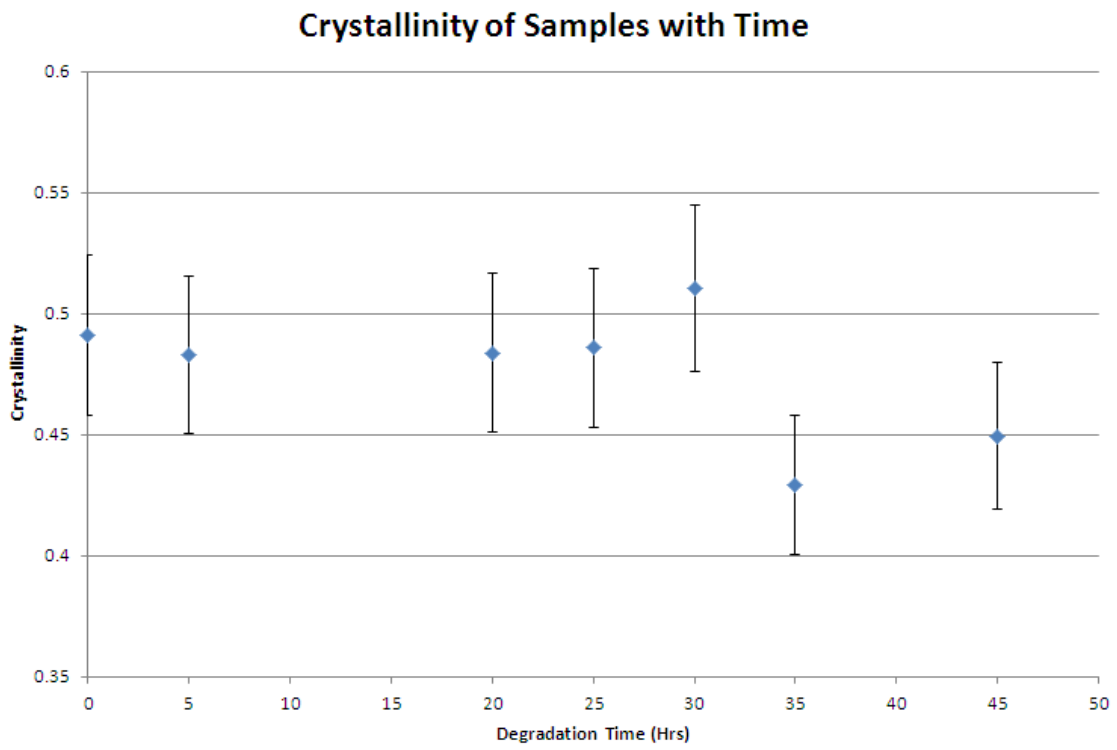

Figure 5-4: Crystallinity of PCL scaffolds with time

Monitoring of the geometry was employed successfully to measure changes in the diameter of the PCL tissue scaffold layer by layer strands, and the diameters of the PLGA cylinders, and to correlate these changes with mass loss in a challenging environment where the samples are surrounded by a medium of similar density and x-ray absorption characteristics. A representative example of the DEI images gained of the scaffolds and implants are shown in Fig. 5-5.

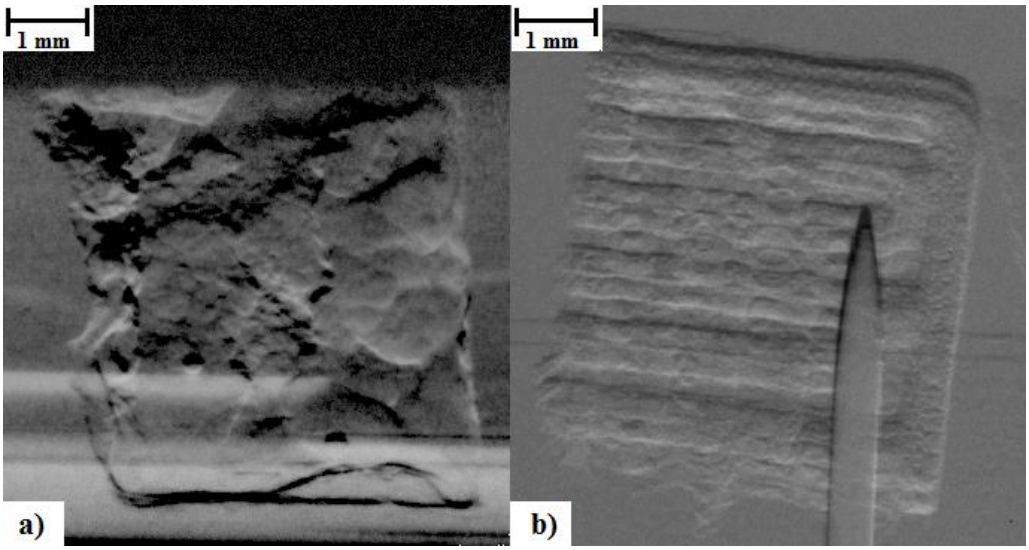

Figure 5-5: DEI image of PLGA cylinder a), and PCL tissue scaffold b)

In order to estimate mass from the images, the program ImageJ was employed to measure an average strand/cylinder diameter in the scaffold/implant. These average diameters were then utilized to estimate the remaining volume of the scaffold/implant, with the known density of PCL or PLGA giving the remaining mass from the image based time dependent volume estimate.

The experimental data from both this approach and traditional gravimetric analysis were in acceptable agreement, with a percent error of less than 9% observed between the two methods, as illustrated in Figures 5-6 and 5-7.

Once experimental data on the mass loss with time was available, the parameters of the finite element model of mass loss were adjusted using the Cyclic Coordinate Descent Algorithm [37] until the best agreement between model predictions and the actual observed behavior was obtained. The objective function (5) reached a minimum value of 47.1 for the PLGA implants and a minimum value of 33.3 for the PCL scaffolds. When these minimum values for (5) were obtained, the free parameter k_3 was set to 3.74 $hr^{-1}$for the PLGA cylinders and 0.28 hr^{-1} for the PCL scaffolds. These

model parameters are valid for devices manufactured out of PLGA and PCL and degraded in 1M and 5M NaOH solutions at a temperature of 55°C respectively. These models with the identified parameters were able to return the observed mass loss in the experimental data. The geometry of the devices as predicted by the mass loss model are presented in Figures 5-8 and 5-9, where red regions indicate full absorption, green indicates partial degradation, and blue regions retain their initial molecular weight. The maximum observed difference between model predictions and experiment was 20%.

The degradation of PCL and PLGA cylindrical implants in NaOH at 55°C was simulated mathematically with the above estimated values for k_3, and the implant geometry found in [31]. It was found that the 20% mass loss *in vivo* for PTMC implants after 8 weeks is expected to occur in the analogous accelerated degradation system of PCL/NaOH at 55°C after 36 hours, and after 9 hours for PLGA/NaOH at 55°C. These results suggest that a PLGA or PCL scaffold in NaOH can be employed as an analogous system to PTMC *in vivo* without the need for an approximately 56 day period to evaluate each potential scaffold design. This experimental approach to scaffold design may be of interest if the scaffold degradation is influenced by both the area of the interface surface and the movement of the degradation medium. If the degradation medium is not static but rather in motion, the current mathematical degradation model is unable to consider the resultant enhancement to the degradation of the scaffold or the possibility of heterogeneous rather than uniform degradation. In this case, an experimental study of the scaffold degradation with an analogous system may allow this effect to be explored for multiple scaffold geometries within a practical degradation time.

Finally, the developed degradation model was fitted to the *in vivo* experimental data found in [31]. The degradation model was able to successfully represent the mass loss of a PTMC implant when $k_3 = 0.00144$ hr^{-1}, as illustrated in Fig. 5-10, with an R^2 value of 0.957. The model with this value for the free parameter k_3 was then employed to simulate the degradation of a PTMC rapid prototyping scaffold. The model's

estimate for the lifespan of such a scaffold in the living environment is presented in Fig. 5-11.

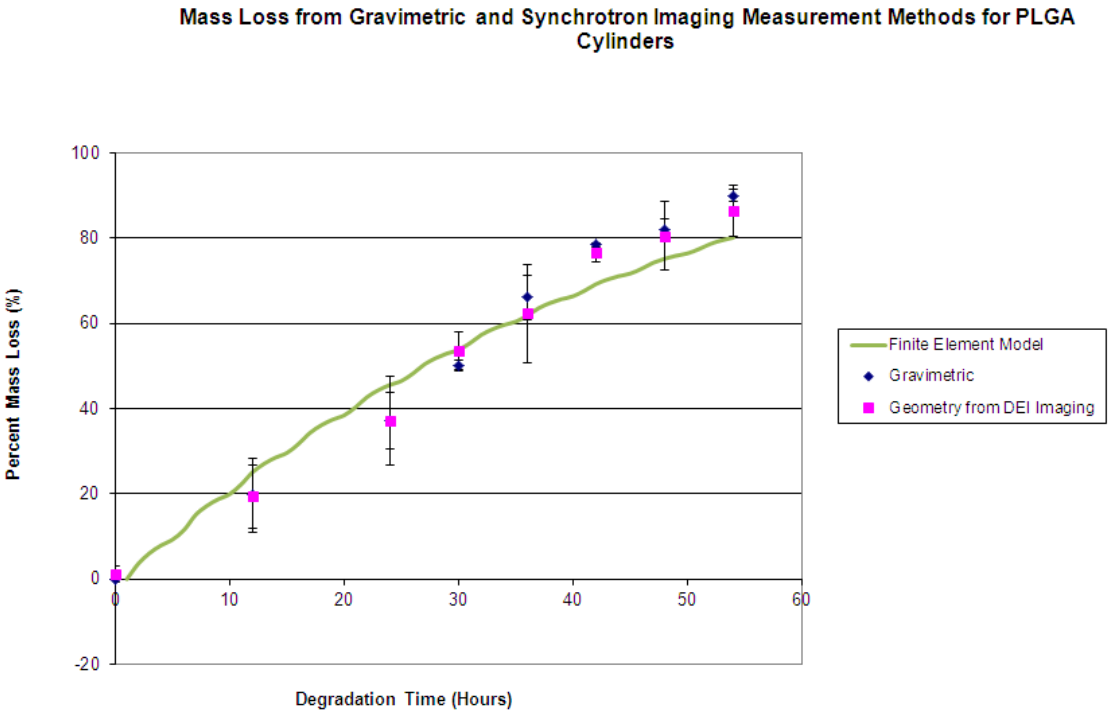

Figure 5-6: Mass loss for PLGA cylinders characterized by DEI imaging and traditional gravimetric experimental methods

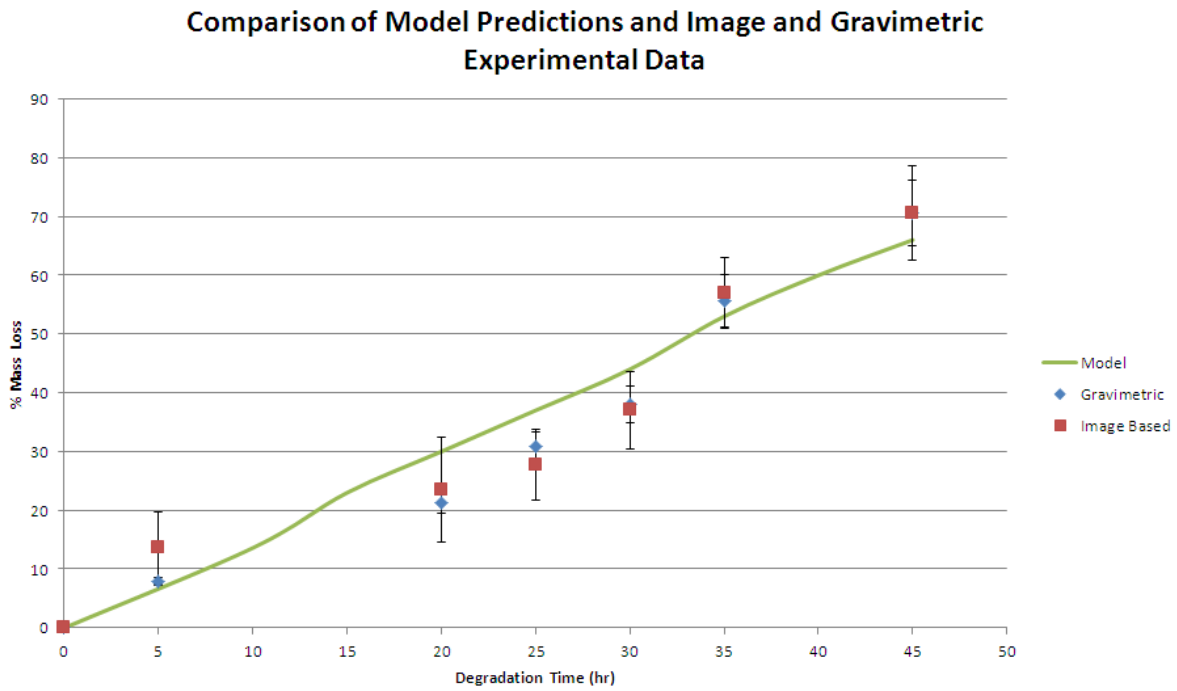

Figure 5-7: Mass loss for PCL scaffolds characterized by DEI imaging and traditional gravimetric experimental methods for model validation, and the predictions of model when k_3 = 0.28 hr^{-1}.

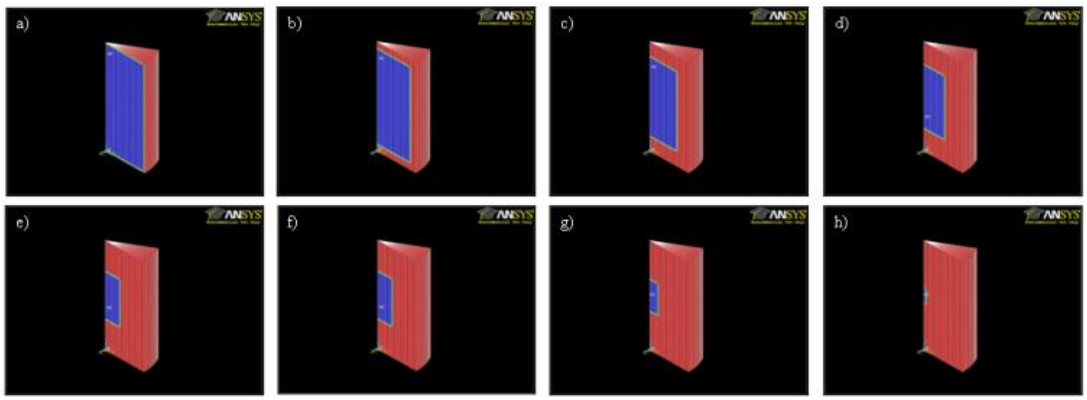

Figure 5-8: Geometry after a) 1, b) 8, c) 16, d) 24, e) 32, f) 40, g) 48, and h) 60 hours of degradation for PLGA cylinders.

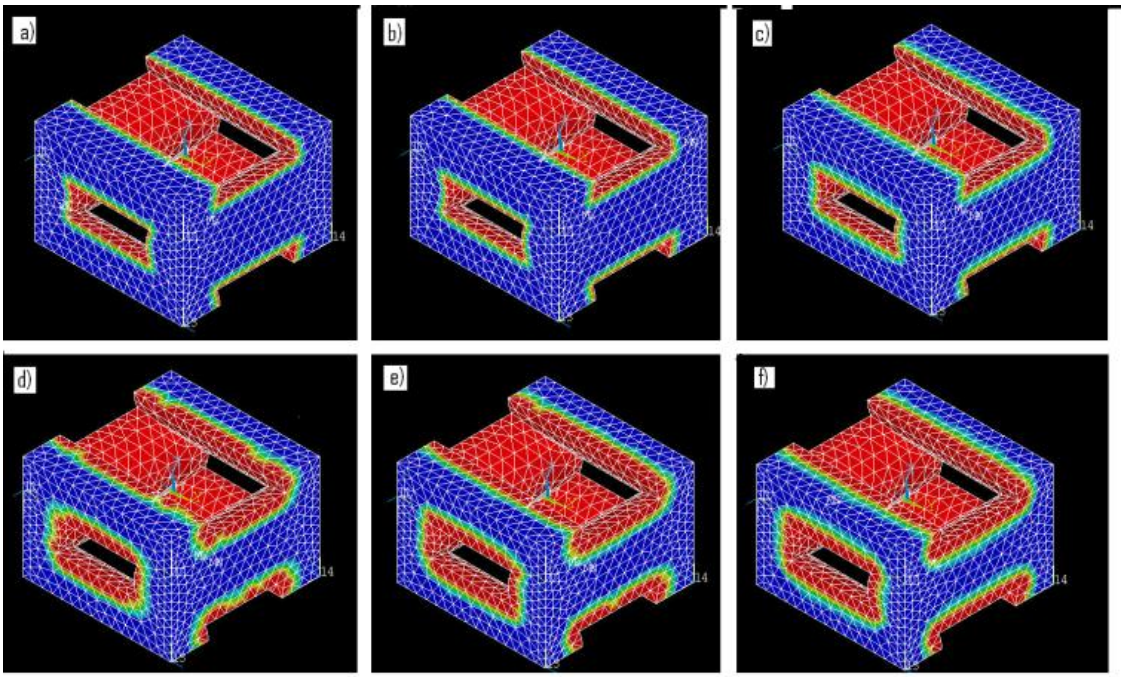

Figure 5-9: Geometry after a) 1, b) 5, c) 10, d) 15, e) 30, and f) 45 hours of degradation for PCL rapid prototyping scaffold samples.

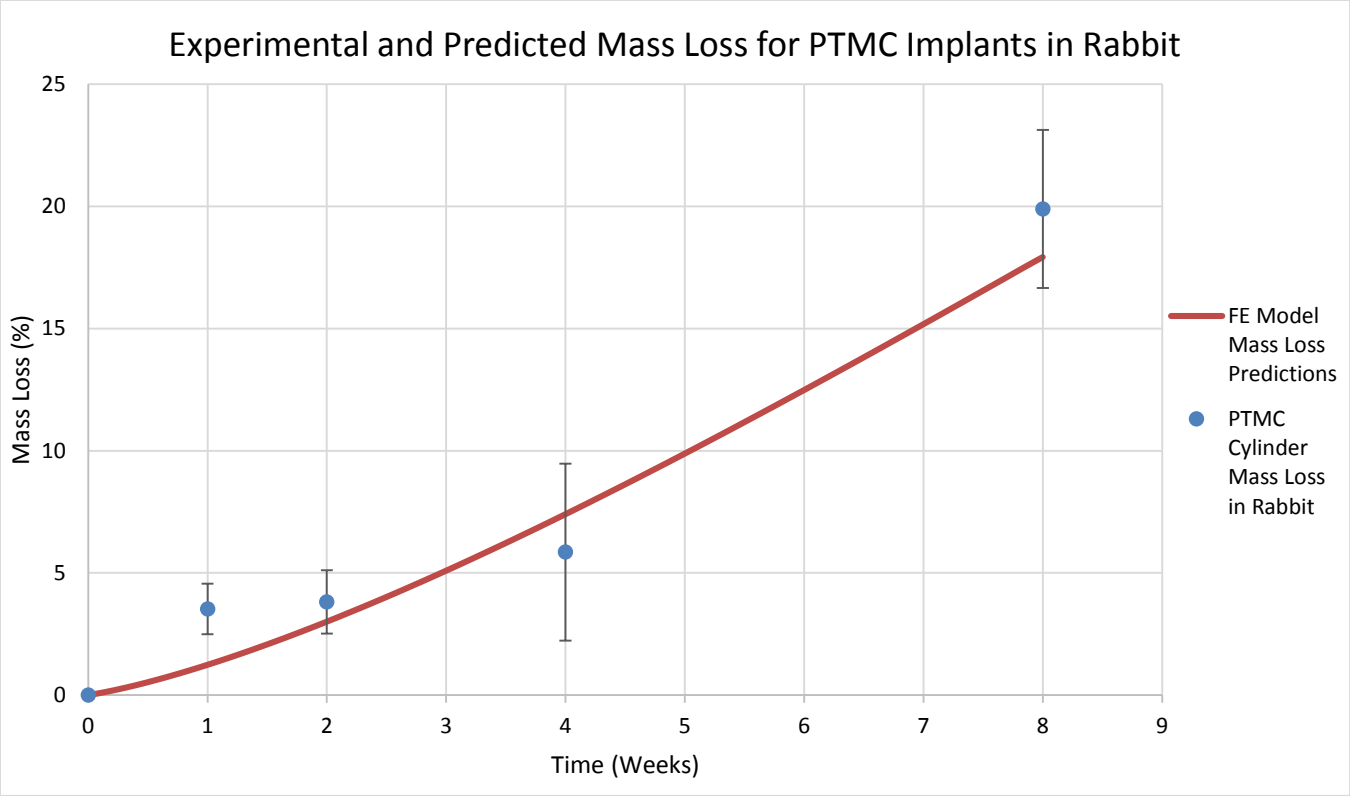

Figure 5-10: Experimental measurements of mass loss for PTMC cylindrical implant and mass loss model predictions when k_3 = 0.00144 hr^{-1}.

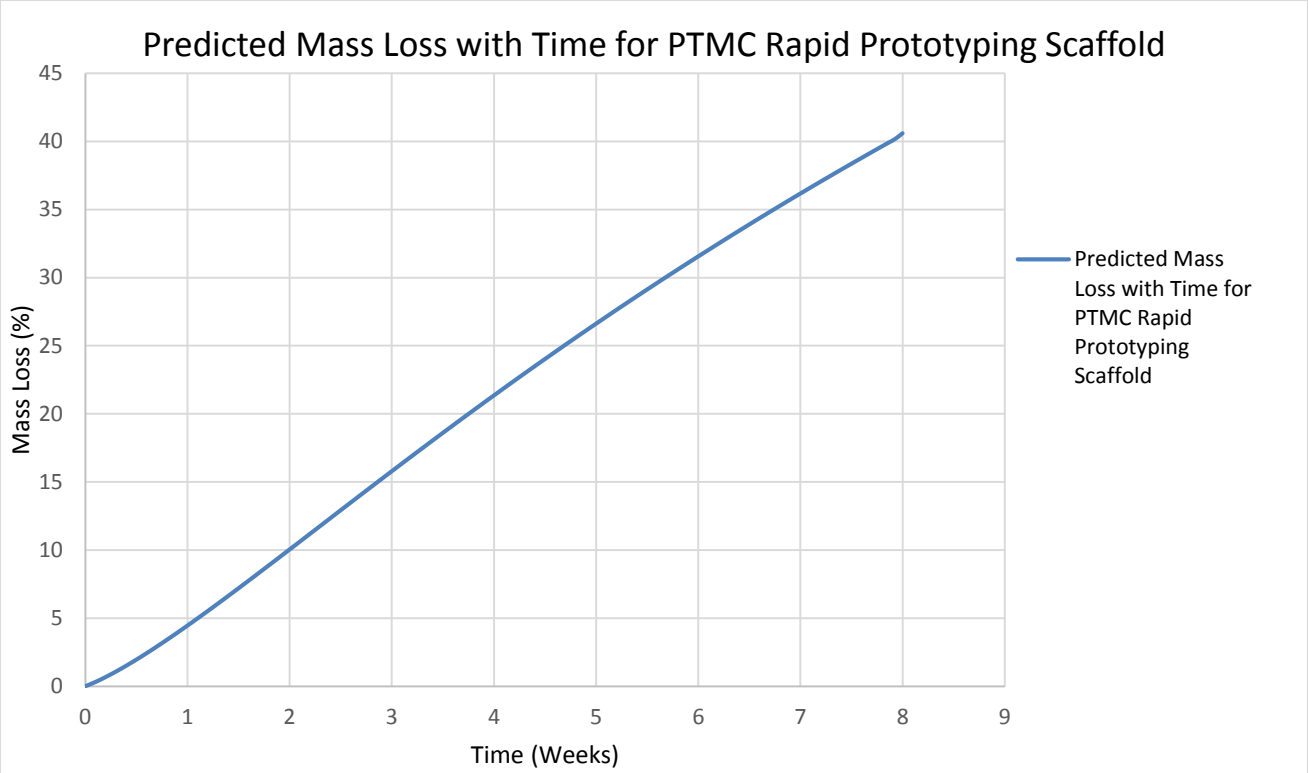

Figure 5-11: In vivo degradation behavior of PTMC rapid prototyping scaffold within rabbit as predicted by mass loss model with k_3 = 0.00144 hr^{-1}.

It is clear from Figures 5-6 and 5-7 that the geometry signal of the scaffold is sufficient to remotely infer the mass of the scaffold without having to explant the device, as is the traditional method for mass loss monitoring. Furthermore, there is no need to add substances or tracers, radioactive or otherwise, to the scaffold to track the movement of mass in the body, as is necessary for some of the other approaches to monitoring mass loss *in vivo* [38, 39]. However, since the volume of an object is proportional to its dimensions to the third power, any error in the measurement of the geometric parameters of the scaffold will be magnified in the prediction of mass from geometry measurements. The resolution of the imaging system must therefore be sufficient to achieve an acceptable error in the estimation of scaffold/implant mass. The existing imaging system was capable of estimating mass within 25% of the actual mass as characterized by gravimetric methods. The way is now clear to begin

applying this approach to examining the *in vivo* surface erosion of devices and comparing these observed results to those obtained in simple analogs to the living environment such as phosphate buffered saline or cell culture medium immersions.

5.6: Conclusions and Future Work

Diffraction enhanced imaging was successfully employed to visualize PLGA and PCL devices in an imaging environment similar to that of a living body, where both the density of the surroundings and implant are similar. Monitoring of the geometry with time allowed the volume and hence the mass of the implant to be estimated as a function of time. These estimates of mass agreed reasonably with the directly measured mass loss. This data was then able to allow the estimation of the parameters in a mass loss mathematical model. Future work will include the application of this method to implant structures that display bulk degradation, where the initial formation of interior voids will be the critical state employed to estimate model parameters. In addition, the next stage in the validation of this approach for mass loss characterization is the evaluation of a PTMC rapid prototyping fabricated scaffold *in vivo* with the same imaging methodology outlined in this study. Also, the use of leave one out cross validation for parameter estimation, with an averaging of the estimations for the parameter k_3, and the use of a smaller step-size may improve agreement between the FE models and experiment.

Acknowledgments

Research described in this paper was performed at the Canadian Light Source. The Canadian Light Source is supported by the Natural Sciences and Engineering Research Council of Canada, the National Research Council Canada, the Canadian

Institutes of Health Research, the Province of Saskatchewan, Western Economic Diversification Canada, and the University of Saskatchewan.

References

1. Woodruff, M. A., Hutmacher, D. W., 2010, "The return of a forgotten polymer : Polycaprolactone in the 21st century", *Progress in Polymer Science*, vol. 35(10), pp. 1217-1256.
2. Zhuang, H., Han, Y., Feng, A., 2008, "Preparation, mechanical properties and in vitro biodegradation of porous magnesium scaffolds", *Materials Science and Engineering C*, vol. 28, pp. 1462–1466.
3. Ibim, S. E., Uhrich, K. E., Attawia, M., Shastri, V. R., El-Amin, S. F., Bronson, R., Langer, R., Laurencin, C. T., 1998, "Preliminary in vivo report on the osteocompatibility of poly(anhydride-co-imides) evaluated in a tibial model", J Biomed Mater Res, vol. 43, pp. 374–379.
4. Ibim S. E., Uhrich, K. E., Bronson, R., El-Amin, S. F., Langer, R. S., Laurencin, C. T., 1998, "Poly(anhydride-co-imides): In vivo biocompatibility in a rat model", Biomaterials, vol. 19, pp. 941–951.
5. Lam, C. X. F., Hutmacher, D., W., Schantz, J. T., Woodruff, M. A., Teoh, S. H., 2009, "Evaluation of polycaprolactone scaffold for 6 months in vitro and in vivo", Journal of Biomedical Materials Research Part A, vol. 90A, Issue 3, pp. 906-919.
6. Holy, C. E., Dang, S. M., Davies, J. E., Shoichet, M. S., 1999, "In vitro degradation of a novel poly(lactide-co-glycolide) 75/25 foam", Biomaterials, vol. 20, pp. 1177-1185.
7. Gough, J. E., Christian, P., Unsworth, J., Evans, M. P., Scotchford, C. A., Jones, I. A., 2004, "Controlled degradation and macrophage responses of a fluoride-treated polycaprolactone", J Biomed Mater Res A., vol. 69(1), pp. 17-25.
8. Paolo Arosio, Valentina Busini, Giuseppe Perale, Davide Moscatelli, Maurizio Masi, "A new model of resorbable device degradation and drug release - part I:zero order model", 2008, Polym Int, vol. 57, pp. 912–920.
9. Juan Pena, Teresa Corrales, Isabel Izquierdo-Barba, Antonio L. Doadrio, Maria Vallet-Regi, 2006, "Long term degradation of poly(3-caprolactone) films in biologically related fluids", Polymer Degradation and Stability, vol. 91, pp. 1424-1432.
10. Juan Pena, Teresa Corrales, Isabel Izquierdo-Barba, M. Concepcion Serrano, M. Teresa Portoles, Raffaella Pagani, Maria Vallet-Regi, 2006, "Alkaline-treated poly(ε-caprolactone) films: Degradation in the presence or absence of fibroblasts", Journal of Biomedical Materials Research Part A, vol. 76A, issue 4, pp. 788–797.

11. Franklin R. Tay, David H. Pashley, Cynthia K.Y. Yiu, Joyce Y.Y. Yau, Mak Yiu-fai, Robert J. Loushine, R. Norman Weller, W. Frank Kimbrough, Nigel M. King, 2005, "Susceptibility of a Polycaprolactone-Based Root Canal Filling Material to Degradation. II. Gravimetric Evaluation of Enzymatic Hydrolysis, JOE, vol. 31, num. 10, pp. 737-741.

12. Molly M. Stevens, Robert P. Marini, Dirk Schaefer, Joshua Aronson, Robert Langer, V. Prasad Shastri, 2005, "In vivo engineering of organs: The bone bioreactor", PNAS, vol. 102 no. 32, pp. 11450–11455.

13. Lichun Lu, Susan J. Peter, Michelle D. Lyman, Hui-Lin Lai, Susan M. Leite, Janet A. Tamada, Shiro Uyama, Joseph P. Vacanti, Robert Langer, Antonios G. Mikos, 2000, "In vitro and in vivo degradation of porous poly(DL-lactic-co-glycolic acid) foams", Biomaterials, vol. 21, pp. 1837-1845.

14. C.G Pitt, M. M. Gratzl, G. L. Kimmel, J. Surleas, A. Schindler, 1981, "Aliphatic polyesters II: The degradation of poly (DL-lactide), poly (ε-caprolactone) and their copolymers in vivo", Biomaterials, vol. 2, pp. 215-220.

15. C. Doyle, E.T. Tanner, W. Bonfiel, 1991, "In vitro and in vivo evaluation of poly-hydroxy-butyrate and of poly-hydroxy-butyrate reinforced with hydroxy-apatite", Biomaterials, vol. 12, pp. 841-847.

16. Hans Pistner, Harald Stallforth, Ralf Gutwald, Joachim Muhling, Jiirgen Reuther, Christian Michel, 1994, "Poly(L-lactide): a long-term degradation study in vivo Part II: Physico-mechanical behavior of implants", Biomaterials, vol. 15, no. 6, pp. 439-450.

17. Saey Tuan Ho, Dietmar W. Hutmacher, 2006, "A comparison of micro CT with other techniques used in the characterization of scaffolds", Biomaterials, vol. 27 pp. 1362–1376.

18. L. Ciocca, I. G. Lesci, O. Mezini, A. Parrilli, S. Ragazzini, R. Rinnovati, N. Romagnoli, N. Roveri, R. Scotti, 2015, "Customized hybrid biomimetic hydroxyapatite scaffold for bone tissue regeneration", J Biomed Mater Res Part B: Applied Biomaterials, DOI: 10.1002/jbm.b.33597.

19. Hoi Man Wong, Paul K. Chub, Frankie K.L.Leung, Kenneth M.C.Cheung, Keith D.K.Luka, Kelvin W.K.Yeung, 2014, "Engineered polycaprolactone–magnesium hybrid biodegradable porous scaffold for bone tissue engineering", Progress in Natural Science: Materials International, vol. 24, pp. 561–567.

20. K. Klodowski, J. Kaminski, K. Nowickab, J. Tarasiuk, S. Wronski, M. Swietek, M. Blazewiczb, H. Figiel, K. Tureka, T. Szponder, Micro-imaging of implanted scaffolds using

combined MRI and micro-CT, Computerized Medical Imaging and Graphics, vol. 38, pp. 458–468.

21. D. W. Wagner, D. P. Lindsey, G. S. Beaupre, 2011, “Deriving tissue density and elastic modulus from microCT bone scans”, Bone, vol. 49, issue 5, pp. 931-938.

22. Chapman, D., Thomlinson, W., Johnston, R. E., Washburn, D., Pisano, E., Gmür, N., Zhong, Z., Menk, R., Arfelli, F., and Sayers, D., “Diffraction Enhanced x-ray Imaging,” 1997, Phys. Med. Biol., vol. 42, p. 2015.

23. Dierker, J., Joite-Barfub, S., Sabel, M., Editor: Aichinger, H., 2012, “Radiation Exposure and Image Quality in X-ray Diagnostic Radiology: Physical Principles and Clinical Applications”, Springer-Verlag, Berlin, Germany.

24. Brankov, J. G., Saiz-Herrandez, A., Wernick, M. N., 2004, “Noise analysis for diffraction enhanced imaging”, Proceedings of the 2004 IEEE International Symposium on Biomedical Imaging: From Nano to Macro, pp. 1428-1431.

25. Muehleman, C., Li, J., Connor, D., Parham, C., Pisano, E., Zhong, Z., 2009, “Diffraction-Enhanced Imaging of Musculoskeletal Tissues Using a Conventional X-Ray Tube”, Academic Radiology, vol. 16, issue 8, pp. 918–923.

26. Chhaya Engineer, Jigisha Parikh, Ankur Raval, 2011, “Review on Hydrolytic Degradation Behavior of Biodegradable Polymers from Controlled Drug Delivery System,” Trends Biomater. Artif. Organs, vol. 25(2), pp. 79-85.

27. M.A. Webb, G. Belev, T.W. Wysokinski, D. Chapman, 2013, “Diffraction enhanced imaging computed tomography (DEI-CT) at the BMIT facility at the Canadian Light Source”, 7th Medical Applications Of Synchrotron Radiation Workshop (MASR 2012) Shanghai Synchrotron Radiation Facility (SSRF), pp. 1-5, DOI:10.1088/1748-0221/8/08/C08002.

28. Wang, Y., Pan, J., Han, X., Sinka, C., and Ding, L., 2008, "A Phenomenological Model for the Degradation of Biodegradable Polymers," *Biomaterials*, vol. 29, pp. 3393–3401.

29. K.C. Ang, K.F. Leong, C.K. Chua, M. Chandrasekaran, 2007, “Compressive properties and degradability of poly(e-caprolatone)/hydroxyapatite composites under accelerated hydrolytic degradation”, J Biomed Mater Res A., vol. 80(3), pp.655-660.

30. Christopher X. F. Lam, Monica M. Savalani, Swee-Hin Teoh, Dietmar W. Hutmacher, 2008, “Dynamics of in vitro polymer degradation of polycaprolactone-based scaffolds: accelerated versus simulated physiological conditions”, Biomed. Mater. vol. 3, p. 034108-034122.

31. Zheng Zhang, Roel Kuijer, Sjoerd K. Bulstra, Dirk W. Grijpma, Jan Feijen, 2006, “The in vivo and in vitro degradation behavior of poly(trimethylene carbonate),” Biomaterials, vol. 27, p. 1741–1748.

32. Bawolin, N. K., 2013, “Synchrotron based imaging for mass loss characterization”, Canadian Congress of Applied Mechanics, Saskatoon, Saskatchewan, Canada.

33. Guo Q. and Groeninckx G., 2001, “Crystallization Kinetics Poly(e-caprolactone) in Miscible Thermosetting Polymer Blends of Epoxy Resin and Poly (e-caprolactone)”, *Polymer*, vol. 42, p. 8647-8655.

34. Bawolin, N. K., Li, M. G., Chen, X. B., Zhang, W. J., 2010, "Modeling Material-Degradation-Induced Elastic Property of Tissue Engineering Scaffolds," *Journal of Biomechanical Engineering*, vol. 132, pp. 111001-1-111001-7.

35. Husmann M., Schenderlein S., Luck M., Lindner H., Kleinebudde, 2002, "Polymer erosion in PLGA microparticles produced by phase separation method," *International Journal of Pharmaceutics*, vol. 242, number 1, pp. 277-280(4).

36. Wang, S., Lu, L., Yaszemski, M. J., 2006, “Bone Tissue-Engineering Material Poly(propylene fumarate): Correlation between Molecular Weight, Chain Dimensions, and Physical Properties,” *Biomacromolecules*, vol. 6, p. 1976-1982.

37. Bezdek, J. C., Hathaway, R. J., 2002, “Some notes on alternating optimization”, In: N. R. Pal, M. Sugeno, (ed.), “Advances in Soft Computing, vol. 2275 of Lecture Notes in Artificial Intelligence”, Springer-Verlag, pp. 288–300.

38. Sun, H., Mei, L., Song, C., Cui, X., Wang, P., “The in vivo degradation, absorption and excretion of PCL-based implant”, 2006, Biomaterials, vol. 27, p. 1735–1740.

39. Artzi1, N., Oliva, N., Puron, C., Shitreet, S., Artzi, S., Ramos, A., Groothuis, A., Sahagian, G., Edelman, E., 2011, "In vivo and in vitro tracking of erosion in biodegradable materials using non-invasive fluorescence imaging," *Nature Materials*, vol. 10, pp. 704-709.

CHAPTER 6

REMOTE DETERMINATION OF STIFFNESS OF SCAFFOLDS DURING SURFACE DEGRADATION BY GEOMETRIC PARAMETER MEASUREMENT WITH TIME VIA SYNCHROTRON RADIATION IMAGING*

*****This chapter has been submitted as "Bawolin, N. K., Chen, X. B., 2016, Remote Determination of Stiffness of Scaffolds During Surface Degradation by Geometric Parameter Measurement With Time Via Synchrotron Radiation Imaging, ASME Journal of Biomechanical Engineering." According to the Copyright Agreement, "the authors retain the right to include the journal article, in full or in part, in a thesis or dissertation".

6.1: Summary

Tissue scaffolds fulfilling certain geometric requirements will display degradation behavior known as surface erosion. If the material is sufficiently thin and/or the hydrolysis inducing medium cannot diffuse readily into the scaffold, only the outer surface of the scaffold will be destroyed and abolished by the surrounding liquid medium. The scaffold will therefore degrade layer by layer, its internal volume protected from the medium by material that prevents contact by all but the outermost layer of scaffold material with the degrading medium. When this degradation mode dominates, the mechanical properties of the scaffold become dependent solely on the geometry of the internal struts in the scaffold composed of the parent material. Since geometry can be characterized successfully by synchrotron x-ray imaging, The external observation of the scaffold in the living environment can be achieved, and from this data the stress-strain behavior of the scaffold can be inferred.

A finite element model of tissue scaffold stress-strain behavior was updated with time with geometry data obtained from the imaging of a degrading scaffold. Imaging as achieved in a challenging imaging environment similar to that found in the in vivo environment. A surface erosion model was then fitted to the experimentally observed shape of the scaffold inner

structure. Since Polycaprolactone (PCL) scaffolds were semicrystalline, they did not display very pronounced nonlinear behavior. A non-biodegradable but biocompatible scaffold was therefore constructed out of a biomaterial that displayed relatively generic nonlinear behavior with initial linear behavior, yielding, and then strain hardening. Nonlinear finite element models were then employed to relate the image based measurements of scaffold internal strand diameter to the complete large deformation nonlinear material behavior of a scaffold.

PCL scaffolds were degraded in an environment established to induce surface degradation. The scaffolds were then imaged by synchrotoron radiation to characterize the geometric properties of the scaffold with time. The internal scaffold morphology was then related to mechanical behavior through finite element modelling. These predictions for stress-strain behavior were then validated by compression testing of the actual scaffold. For PCL scaffolds and the nonlinear case, the imaging data derived predictions for elastic property agreed with experiment with an R^2 value of 0.9 in the z-direction, and an R^2 value of 0.7 in the x-y plane. In the nonlinear case tissue scaffold models with parameters measured by imaging gave very good agreement in the z-direction, but x-direction predictions of nonlinear behavior were only within 25% of each other.

Measurements of internal tissue scaffold geometry with time for surface eroding scaffolds were related to the material stress-strain behavior of the scaffolds in the transverse and longitudinal directions. Finite element models with geometric data from imaging as inputs successfully reconstructed the stress-strain curves of the transversely isotropic scaffolds in both primary directions. In the nonlinear case, the full stress-strain curve with yielding and strain hardening was reconstructed from the model, but acceptable agreement between the FE model predictions with imaging data input and the actual stress-strain curves was only achieved in the longitudinal direction.

6.2: Introduction

Illness and injury that results in damage or failure of organs and tissue requires for treatment a replacement of the lost tissue/organ. The challenge of replacing damaged or diseased tissue for the effective treatment of illness or injury has led to the proposal and development of the tissue

scaffold with cells based tissue engineering procedure. This treatment assembles an artificial scaffold to act as a prosthetic extracellular matrix (ECM), and seeds this construct with human cells. Over time, the artificial ECM degrades and is absorbed and replaced by a true ECM manufactured by the proliferating cells in the scaffold [1]. The behavior of scaffolds has been shown to differ in the *in vitro* and *in vivo* environments [2]. The mechanical properties of the scaffold play an important role in the behavior of a tissue engineering construct (TEC) [3], which introduces the need for a method to characterize these properties of the scaffold during the treatment timeframe.

In the work of Frier et al., [4] implants were degraded within a Winstar rat and then surgically explanted after the sacrifice of the animal at various time periods during the treatment period, the authors noted that various different animal models give different degradation behaviour. The *in vivo* degradation behaviour was observed to be significantly faster than *in vitro* degradation with the rat implanted sample displaying about 70% of the initial molecular weight after two weeks while samples *in vitro* still retained upwards of 95% of their initial molecular weight. By 28 weeks the molecular weight of the two samples are essentially identical, indicating that both degradation rates eventually become similar. In the work of Kenley et al., [5] implants are incubated *in vivo* and *in vitro* and the pH of the *in vitro* environment is decreased until the two rates of degradation are identical. The *in vivo* experiment again employed a mouse model and involved the sacrifice of the animal and the removal of the device at certain times during the treatment process. In [6] another *in vivo* study involved the direct removal and analysis of scaffolds after implantation, and observed faster molecular weight decline *in vivo* than that observed *in vitro*. This was speculated to be the result of metabolic waste byproducts produced by cells encapsulating the implant, the accumulation of acidic degradation byproducts in the vicinity of the scaffold, and by the presence of enzymes that were not present in the *in vitro* degradation medium.

From the above studies, it is possible to identify some shortcomings with the methods employed to characterize in vivo degradation. The methods in question do not allow the direct measurement of position dependent characteristics and instead only give the overall averaged properties of the whole scaffold. These methods also do not permit the sequential measurement

of the same specimen which guarantees that a specific degradation environment is being maintained. One must also consider the effect of removal and processing on the scaffold properties before they are measured. For example, in [7] the in situ measurement of tissue properties a significantly different measured value for mechanical properties of tissue than when the tissue was excised and characterized *in vitro*. This is possibly due to the inability to perfectly replicate the living environment outside of the body. It is also likely that living tissue displays different behaviour than dead tissue and that the preconditioning of tissue for *in vitro* evaluation changes the mechanical properties of tissue [8].

In [9] scaffolds created via solvent casting and particle leaching were implanted in rats and removed after degradation. The scaffolds were dissolved in solvent and evaluated with Gel Permeation Chromatography to measure their molecular weight decline with time. Some of the scaffolds were then frozen and sectioned histologically to characterize some of the location dependent properties of the scaffold over an eight week period. It is known that histological sectioning of a scaffold to obtain location specific properties introduces deformations in the scaffold due to cutting [10,11], and that the process of trying to compensate for this damage with imaging data and computational reconstruction is not straightforward. In order to overcome these limitations, *in situ in vivo* techniques have been proposed and employed to evaluate the characteristics of scaffolds without its removal from the body.

In [12] a radioactive scaffold is implanted into a rat and allowed to degrade. The excretions of the rat are then monitored and the radioactivity observed is related to scaffold mass loss. Theoretically, this mass loss could then be related to molecular weight and therefore, material properties of the scaffold with time. The drawbacks of this method are the possibility that the tracer may influence the properties of the scaffold, radiation dosage issues, and the rather indirect way in which the signal detected outside of the body is related to the mechanical properties of the scaffold. In [13] fluorescent additions to the scaffold allow the optical tracking of mass within the body of a rat. This technique has some limitations regarding allowable tissue depth and the need to add fluorescing materials to the scaffold, possibly influencing its behaviour.

In the work of [14] magnetic resonance is employed to measure the sound wave speed through tissue to determine its elasticity. The limitations of this approach include the inconvenient presence of strong magnetic fields around the subject and possible resolution restrictions due to magnetic field strength limitations. It should be noted here that x-ray imaging could fill the same role as magnetic resonance imaging in this method, if the data acquisition rate was sufficient to observe the movement of sound waves through the sample. In [15,16] a method known as photoacoustic imaging is employed to monitor a scaffold *in vivo*. The scaffold is rapidly heated with electromagnetic radiation and its expansion and contraction result in sound waves which can be measured and used to reconstruct an image of the scaffold. The intensity of the electromagnetic radiation used to rapidly heat the scaffold *in vivo* is constrained by safety issues, limiting the energy in the ultrasound wave given off by the vibrating scaffold, and therefore the depth of tissue this signal can pass through before it is undetectable. This method therefore suffers from significant depth and resolution limitations. It does however possess the advantage of employing readily available instrumentation that could easily be employed in a clinical setting.

In the work of Kim et al., [17] and Yu et al.,[18] the scaffold is deformed within a mouse by a load externally applied to the mouse body. The deflections induced in the scaffold are then quantified by ultrasonic measurement. Such an approach as this is subject to limitations on the ability to apply a known force internally within the body from external loading. The resolution and penetration depth of the ultrasonic imaging employed to characterize scaffold deformation are also significant limitations to this method. In [19] a tissue scaffold was incubated in a simulation of the in vivo environment and ultrasound was employed to observe the scaffold deflection from a pulsatile fluid pressure. A pressure sensor upstream characterized the load applied to the scaffold. While it is possible that knowledge of the initial scaffold mechanical properties could be employed to ascertain the loading environment from initial deflection measurements, the inability to directly measure the loading of the scaffold is a significant limitation to this approach.

Another very popular *in vivo* characterization technique found in the literature is the use of x-ray computed tomography for the assessment of scaffold geometry [20-22]. In [20] iron and ceramic

based scaffolds for bone tissue engineering are evaluated *in vivo* with x ray analysis and the absorption of the scaffolds is related to mass loss *in vivo*. It is unlikely that this approach will be applicable for soft tissue engineering where the scaffold and background possess similar density. In [21] micro-tomography is employed to track tissue scaffold morphology and tissue ingrowth after the scaffold is removed from the in vivo environment and dried in order to give sufficient absorption contrast to visualize the scaffold. In [22] tissue scaffolds were removed from a mouse model after degradation, and sectioned histologically to evaluate tissue accumulation and scaffold degradation. Dried samples were also imaged via computed x-ray tomography to characterize scaffold degradation and tissue development. In the above studies, the limitations on scaffold depth for *in vivo* visualization are significantly reduced. It is straightforward to utilize x-ray imaging and computed tomography to evaluate scaffolds and implants that display significantly different density than their surroundings, which usually is related to the atomic number of the elements the scaffold material is composed of. In the case of hydroxyapatite scaffolds, the presence of Calcium results in high contrast between soft tissue and scaffold, similar to that observed in conventional x-ray radiography between bone and surrounding tissue. When the scaffold has a density near that of the surroundings, imaging via x-rays with attenuation as the only source of contrast becomes difficult. Fortunately x-ray techniques exist which rely on more than just absorption/attenuation to generate an image.

The technique known as in-line propagation based phase contrast (IPC) relies on the dependence of the speed of light in a material on its index of refraction. The x-ray beam enters the target with every parallel beam of light in phase, but as they take different paths through different thicknesses of various phases within the object being imaged, the formerly in phase waves of light are rendered out of phase, and begin to destructively interfere. This destructive interference leads to differences in intensity which reveal the boundaries of regions of differing refractive index within the imaged object. Since refraction is caused by both geometry and the movement of light from one phase to the other, as well as by density, this imaging method is capable of visualizing scaffolds within the body, the shape of the scaffold components aiding in their visibility to this particular imaging method [23, 24, 25,26]. The IPC method suffers from some drawbacks. Unfortunately the optimum contrast is achieved at a specific imaging x-ray energy and x-ray detector to sample distance. Another method that may be employed to collect

experimental data on geometry change due to bioerosion is the diffraction enhanced imaging method/multiple image radiography (DEI/MIR). In this method, an analyzer crystal is placed between the beam emerging from the sample and the x ray detector. It is known from Bragg's law that a silicon crystal will diffract a beam of x rays at a critical angle. As this analyzer crystal is rotated, the percentage of the x ray beam falling on its surface that is reflected by the crystal into the detector will change [27, 28]. The ratio of incident photon count to reflected photon count as a function of crystal angle is known as the rocking curve of the imaging system, and a typical rocking curve is illustrated in Fig. 6-1.

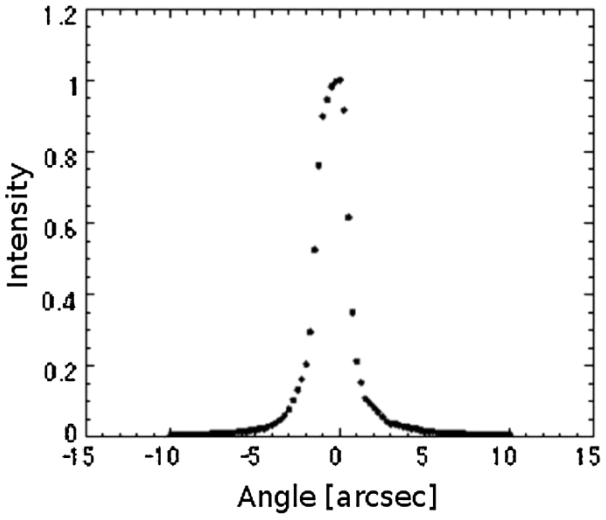

Figure 6-1: Experimentally measured rocking curve for the (3,3,3) reflection of silicone analyzer crystal [29]

By examining the rocking curve of each pixel of the detector before and after a sample has been placed within the beam, the absorption, refraction, and scatter of the sample can be characterized. Absorption is just a decrease in the height of the rocking curve after the insertion of an object into the beam, refraction causes the centre of the rocking curve to move, and scatter is an

increase in the width of the curve. Calculating the rocking curve before and after the insertion of the sample is accomplished by taking multiple image captures as the analyzer crystal is rotated. The absolute minimum number of images is three, and it is usually sufficient to image at five points along the rocking curve; i.e. at the intensities of 0.25, 0.5, and 1 on both the low angle and high angle tails of the rocking curve. From these images, the rocking curve in each pixel of the detector can be assembled and used to calculate a value for refraction, absorption and scatter. These values for each pixel can then be employed to generate images based on absorption, x ray refraction, and x ray beam spreading. Two of these images, the refraction and scatter images, do not depend on density for contrast genration, and therefore may be used to visualize scaffolds which have similar density to their tissue surroundings.

A new method is now developed for monitoring the mechanical proeprties of tissue scaffolds *in vivo*. In the case of surface degrading scaffolds, the surface morphology of the tissue scaffold is characterized with time with synchrotron radiation based imaging. In particular the phase contrast imaging method employed is multiple image radiography/ diffraction enhanced imaging (MIR/DEI), and propagation based in line phase contrast imaging (PCI). The characterized changing morphology of the scaffold is then related to its mechanical properties with finite element modelling. This new approach allows the full stress strain curve of the scaffold to be inferred indirectly *in situ* without its removal from the body. This proposed method is an improvement over existing state of the art in the following ways; 1) it places very little restriction on the location of the scaffold since the energy of the photons used for imaging is very high, and 2) it does not require the scaffold and the surroundings to have significantly different absorption contrast as is required in micro-CT, and 3) it is able to monitor seperately the supporting surface degrading skeleton in a hybrid tissue scaffold and the cell bearing hydrogel phase.

In this study, the phase contrast and diffraction enhanced imaging methods are utilized to observe the morphology of a surface degrading scaffold, and these imaging characterized geometric parameters are then mapped to predictions for the elastic property and nonlinear stress-strain curve of the scaffold with time. The elastic property and stress-strain behavior as estimated from imaging and numerical modelling is then validated by direct experimental measurement via stress strain testing.

6.3: Methods

6.3.1: Material and Degradation Medium

While ultimately the material used in the creation of skeletal frameworks for hybrid polymer/hydrogel TECs will be a material that displays surface degradation in an aqueous medium, such as the Polyanhydride or Polytrimethylene Carbonate family of biomaterials, the material chosen in this study is the same as in [30], the Polycaprolactone/NaOH system. Since Polycaprolactone (PCL) is a brittle material and displays linear stress-strain behavior, a material that exhibits nonlinear behavior known as FullCure720 was chosen for the experiment to demonstrate the inference of nonlinear scaffold behavior from imaging measured geometric parameters. The PCL scaffolds were immersed in a 5M solution of NaOH and incubated at 55°C for 45 hours for the evaluation of degradation from imaging data. PCL scaffolds were removed at 0, 5, 10, 15, 20, 25, 30, 35, 40, and 45 hours, and then rinsed with deionized water.

6.3.2: Scaffold Fabrication

Polycaprolactone (M_n of 80,000 Daltons) was purchased from Sigma Aldrich and fashioned into three dimensional porous scaffolds via an Envisiontech bioplotter rapid prototyping machine. This device consists of a Cartesian actuator with an end effector which consists of a molten polymer reservoir and an extrusion needle. The molten polymer is extruded through the needle and employed to construct the three dimensional tissue scaffold layer by layer. The scaffolds were $4 \times 4 \times 4$ mm cubes with an initial strand diameter of 424 ± μm and a strand spacing of 800 ± μm. The scaffold and the coordinate system employed for material property directions is shown in Fig. 6-2.

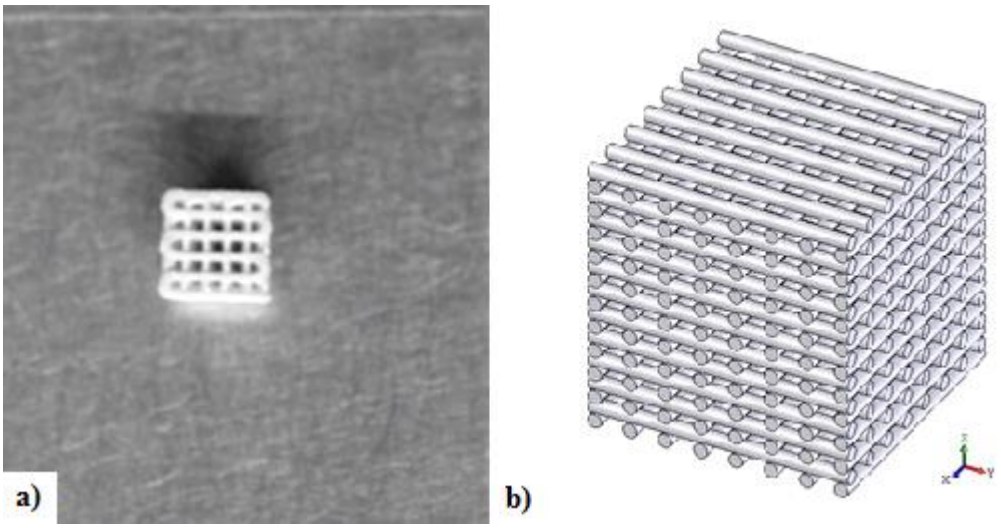

Figure 6-2: PCL tissue scaffold a) and b) coordinate system utilized

In order to characterize the stress strain behaviour of PCL directly, to provide input to the FE scaffold model, three solid cubes of PCL with 1 cm length sides were also fabricated using the bioplotter. In order to test the estimation of material properties from x-ray imaging in the material and geometric nonlinear case, compression samples of FullCure720 tissue scaffold material and full tissue scaffold samples were assembled using a Polyjet rapid prototyping machine. The FullCure720 scaffolds had a strand diameter of 348 ± 44.9 µm and a strand spacing of 892 ± µm.

6.3.3: Imaging

The imaging for this study was performed at the Canadian Light Source Biomedical Imaging and Therapy Beamline (BMIT). Phase contrast imaging (PCI) was performed with a bend magnet source at an energy of 20 KeV, with the detector positioned 35 cm from the sample, while diffraction enhanced imaging (DEI) was performed at a photon energy of 40 keV. The samples were immersed in a water/detergent mixture, with the detergent added to eliminate the formation of bubbles on the scaffolds. This approximation of the living environment caused the scaffold to be indistinguishable from the background when employing conventional x-ray imaging, which was simulated by reducing the distance between the detector and sample to less than 3 cm. Even in this case, the quality of imaging exceeds that of a conventional x-ray tube due to the unique

characteristics (superior photon intensity and collimation) of the synchrotron x-ray source. Once imaging was complete, the software ImageJ was employed to measure the average scaffold strut diameter with time. Distances in the images were determined by pixel count, with the conversion factor between distance in µm and pixel number determined by measuring a known geometric parameter. In this case it was the known strand spacing of 800 µm. Examples of PCI and DEI images acquired during this study are shown in Fig. 6-3.

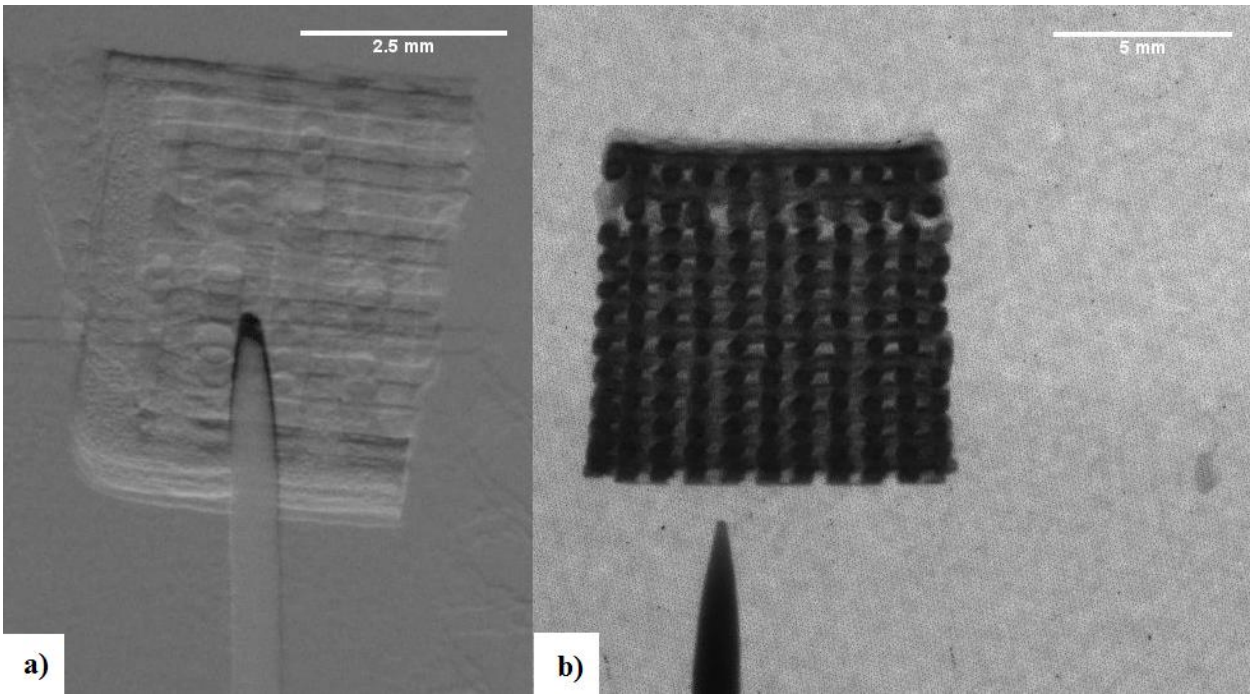

Figure 6-3: a) DEI image of scaffold and b) PCI image of scaffold

6.3.4: Differential Scanning Calorimetry

Surface degrading scaffolds display a thin degradation zone near the surface of the scaffold material that is exposed to the degradation medium. While it is expected that the crystallinity of the bulk scaffold material will remain constant during the degradation process, it was necessary to confirm this assumption and ensure that crystallinity change would not have a significant effect on scaffold surface degradation. The scaffold crystallinity was evaluated by differential scanning calorimetry (DSC), with a specific enthalpy of 81.6 J/g [31] for a fully crystalline sample. The heating history of the samples was a steady rise in temperature at a rate of

10°C/min. from room temperature to 100°C. The transition of the crystalline phase to a fully amorphous state occurred at about 60°C.

6.3.5: Compressive Testing

An Instron 4505 test instrument was employed to compress the PCL and FullCure720 scaffolds at a strain rate of 10 mm/minute. Three scaffold samples of each type were tested. To capture the transversely isotropic stiffness parameters of the scaffolds, they were tested along both the z-axis and along the x-axis, as defined in Fig. 6-2. In order to determine the mechanical properties of the nonporous scaffold bulk material, solid blocks of PCL and FullCure720 were assembled with the Envisiontech bioplotter and subjected to a load displacement test at a crosshead speed of 10 mm/minute.

6.3.6: Finite Element Modelling

Tissue scaffolds are very complex heterogeneous composite materials that possesses several structural levels. For example, at the smallest length scale, the scaffold consists of individual polymer chains. At the next higher structural level, the amorphous randomly oriented polymer chains and the crystalline folded chains are arranged in a specific microstructure. This spherulitic structure of the semicrystalline polymer is shown in Fig. 6-4, as imaged by optical microscopy.

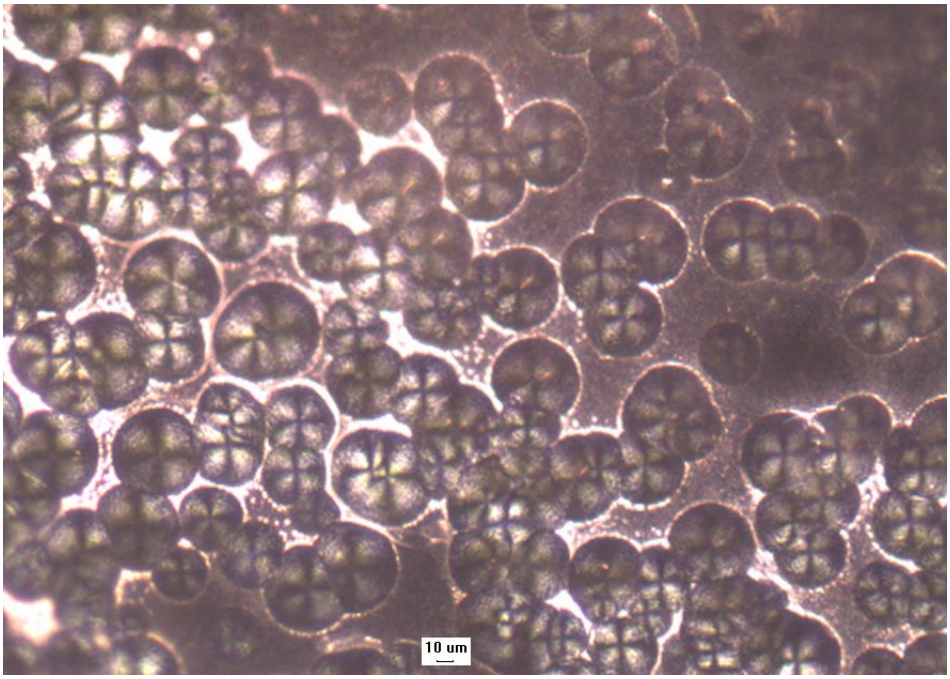

Figure 6-4: Spherulite microstructure of tissue scaffold material PCL

Following the semicrystalline structure of the scaffold bulk material in length scale, there is then the porous scaffold structure itself, and finally, at the largest lengthscale, is the entire scaffold body, contoured to fit the wound area. Ideally, a finite element model of the scaffold would be able to encompass all of the length scales in the scaffold and model every structural detail, no matter how minute, in a single finite element model, but computational limitations make this approach difficult. A way around this difficulty is to represent each structural level as its own model and find the effective properties for each structural level. Each structural level can then be regarded as an equivalent homogeneous material. The model of the next structural level can then consider the previous structural level as a simplified homogeneous material and not include all of the geometric and material property details of the previous structural level. To accomplish this homogenization, a representative volume (RV) of the scaffold was modelled in ANSYS with periodic deflection boundary conditions and subjected to a computational load displacement test. An image of this finite element model for a single pore of the rapid prototyping scaffold is illustrated in Fig. 6-5.

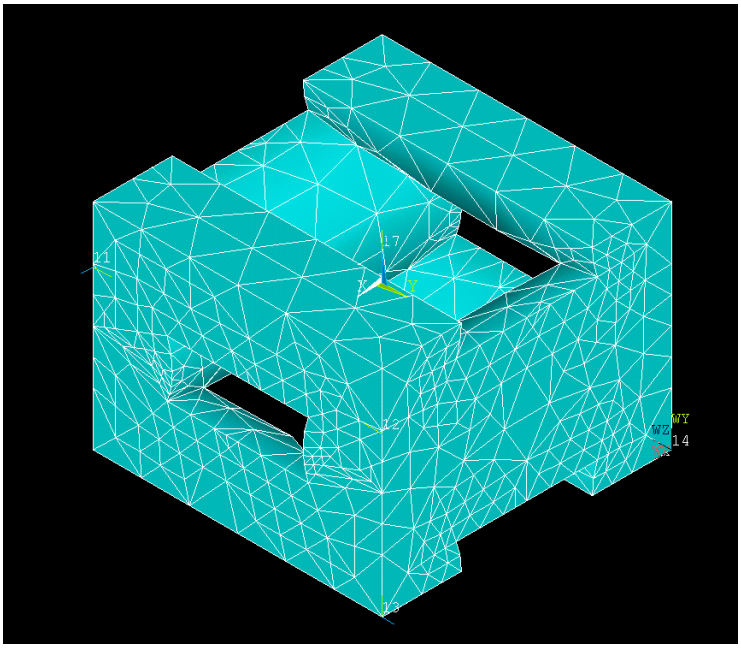

Figure 6-5: Finite element model of an isolated individual tissue scaffold pore

Periodic deflection boundary conditions were established in ANSYS by writing a script in the APDL language to force the deflections of corresponding nodes on opposite sides of the RV to be identical. The volume averaged strain and stress at each strain load-step in the RV were calculated by the following expressions [32];

$$\bar{S}_{ij} = \frac{1}{V}\int_{V} S_{ij} dV \qquad (6.1)$$

$$\bar{T}_{ij} = \frac{1}{V}\int_{V} T_{ij} dV \qquad (6.2)$$

where $\bar{S}_{ij}$ is the average strain in the RV, $\bar{T}_{ij}$ is the average stress in the RV, and V is the RV volume.

In the following manner a theoretical prediction for the stress strain curve of the scaffold was created. At each time step, the model was run three times with increasing element number, and

the prediction at an infinite number of elements was extrapolated using the Scalar Epsilon Algorithm of Wynn [33]. In order to evaluate the mesh quality of the finite element model, convergence and mesh refinement studies were conducted. The model predictions were plotted with respect to increasing element number, and the convergence of the solution was considered. The results of this study are shown in Fig. 6-6, and it is apparent that the model predictions are converging.

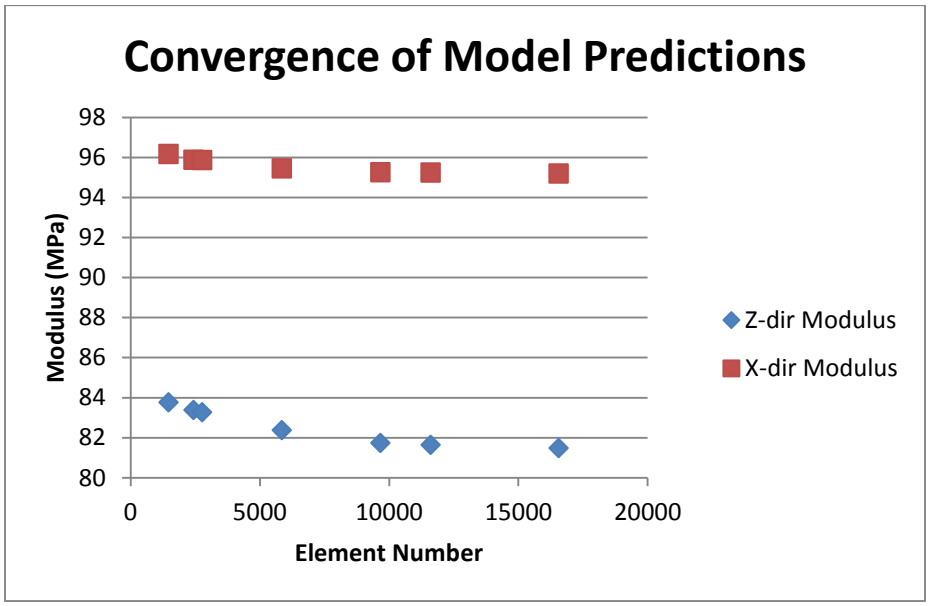

Figure 6-6: Convergence of FE predictions for stiffness

Similarly, the influence of a refined mesh at suspected points of stress concentration on model predictions was considered. Mesh refinement Increases the number of elements in regions suspected of displaying rapidly changing stress values, in order to more accurately capture the actual mechanical behavior of the scaffold. In Fig. 6-7, the effect of mesh refinement is illustrated.

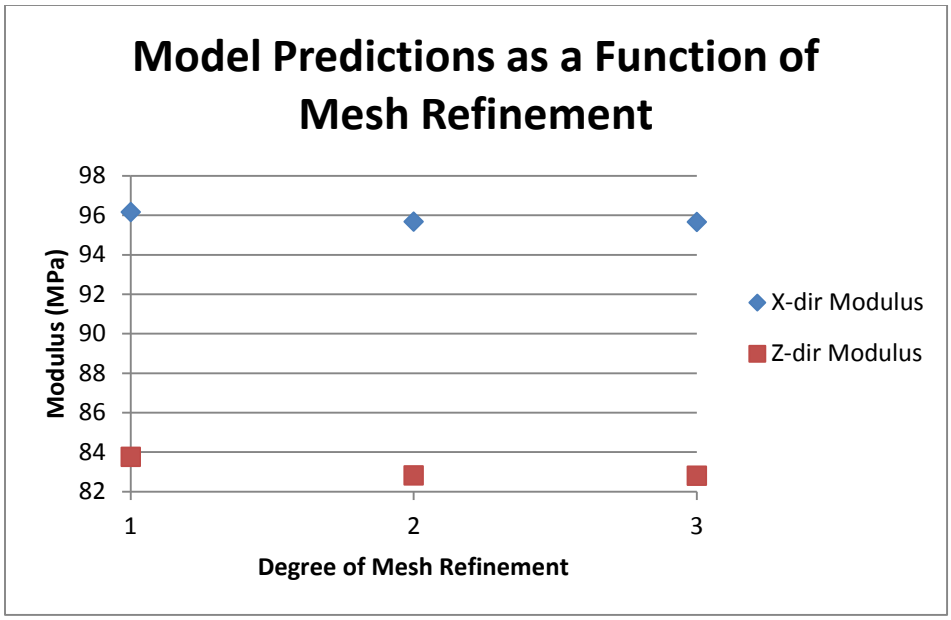

Figure 6-7: Mesh refinement effect on Young Modulus predictions

This observed behavior of the model suggests that the modelled microstructure of the scaffold pores does not concentrate stress sufficiently to require an exceptionally fine mesh to accurately represent the stress distribution.

6.4: Results

6.4.1: Differential Scanning Calorimetry

As expected, the crystallinity of the PCL scaffold material remained the same within experimental error during the entire 45 hour long degradation period. Before the start of degradation the crystallinity of the PCL scaffolds was 49.1 ± 2.9%, and at 45 hours the crystallinity was 44.9 ± 2.7%. As expected, changes to the Young Modulus of the scaffold are therefore singularly the result of geometry changes, with negligible contribution from changes in the bulk crystallinity or molecular weight of the scaffold material. These results are presented in Fig. 6-8.

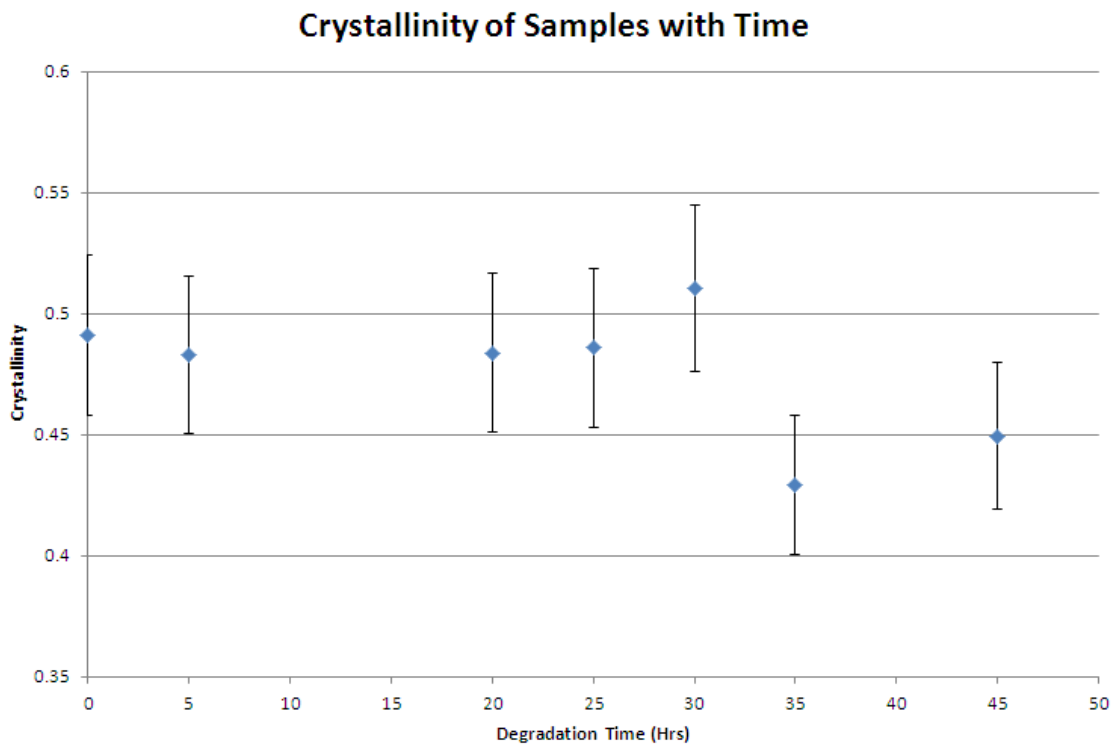

Figure 6-8: Crystallinity of PCL scaffolds with time

6.4.2: Compressive Testing

The following stress strain curves were observed for the PCL and FullCure720 bulk materials.

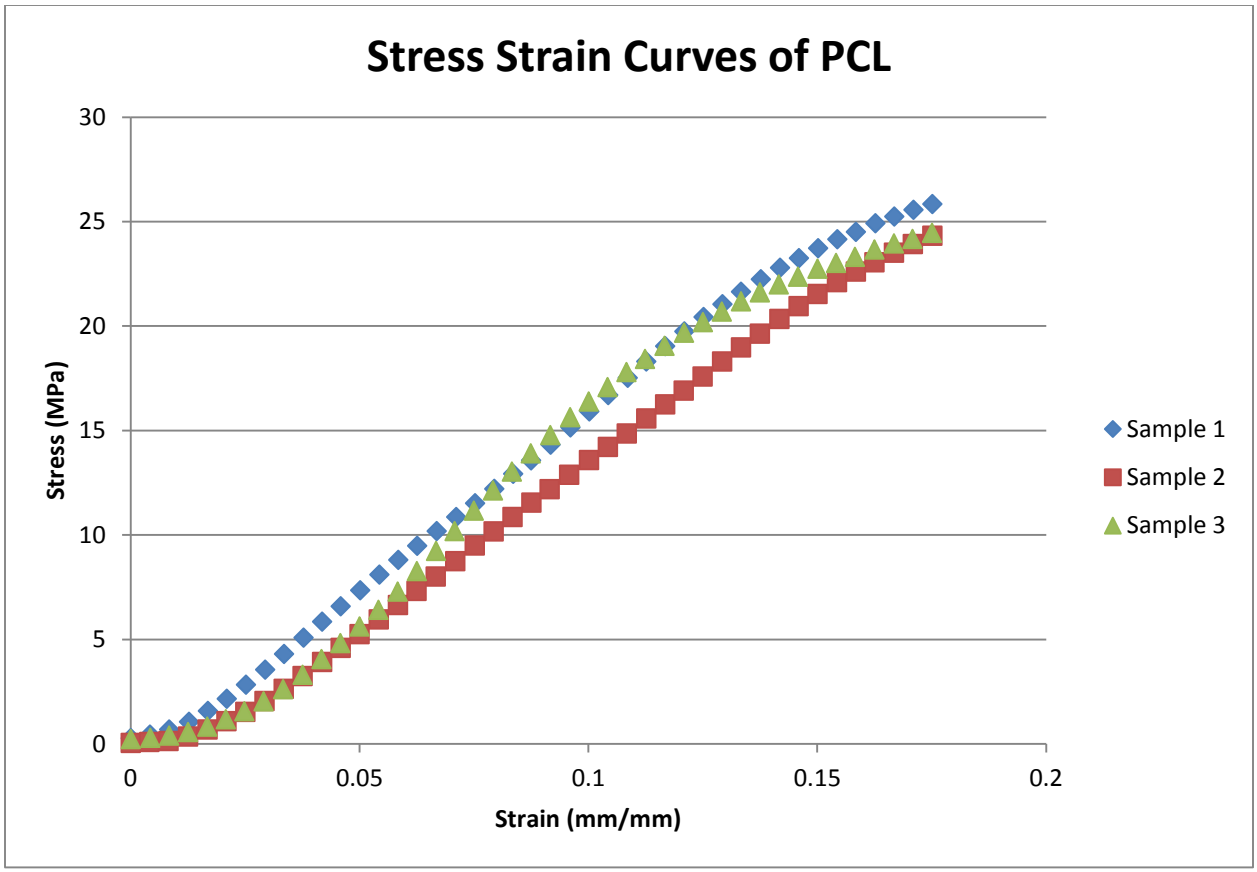

Figure 6-9: Stress-strain curves of PCL

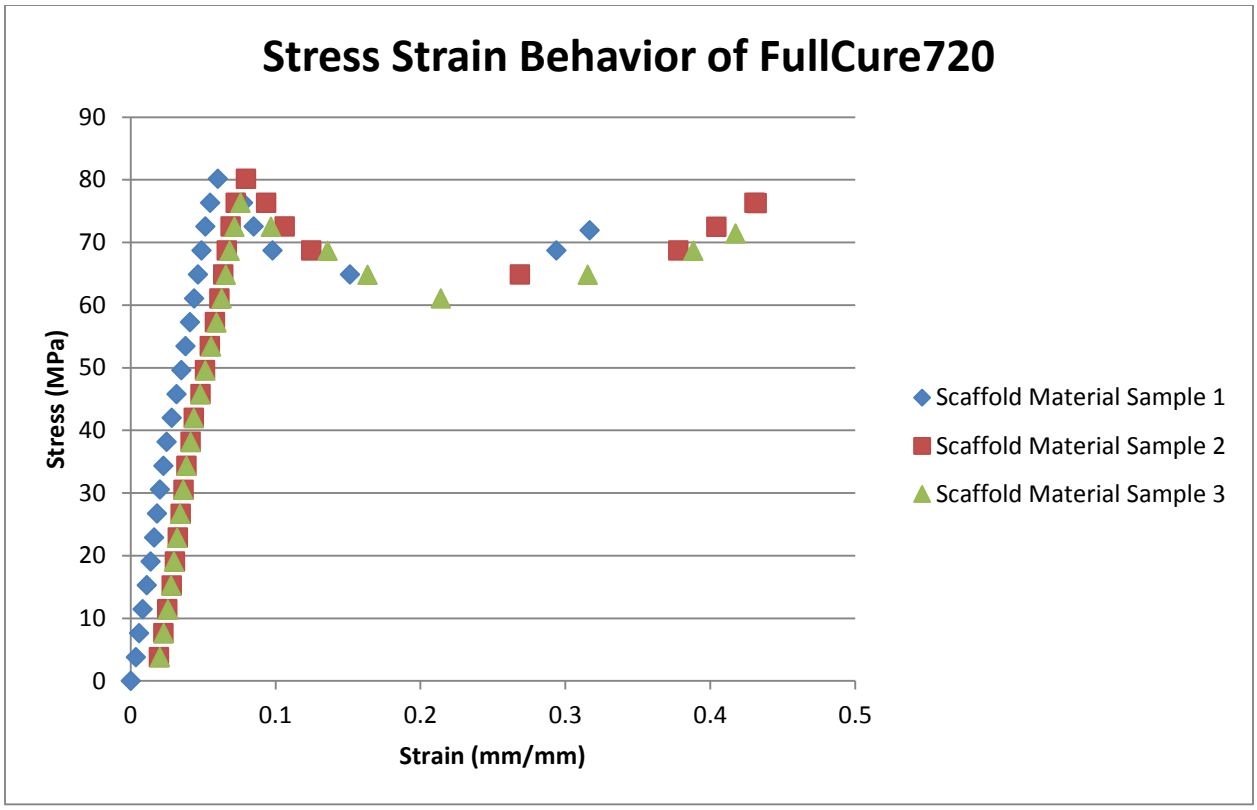

Figure 6-10: Stress-strain curves of FullCure720 material

It is observed that the semicrystalline polymer PCL displays brittle behavior, while the FullCure720 material yields and then experiences strain hardening. The PCL scaffolds are expected to therefore display essentially linear stress-strain behavior, while the FullCure720 scaffolds will have a nonlinear stress strain curve. The stress-strain curves of the FullCure720 and PCL scaffolds are presented in Fig. 6-11.

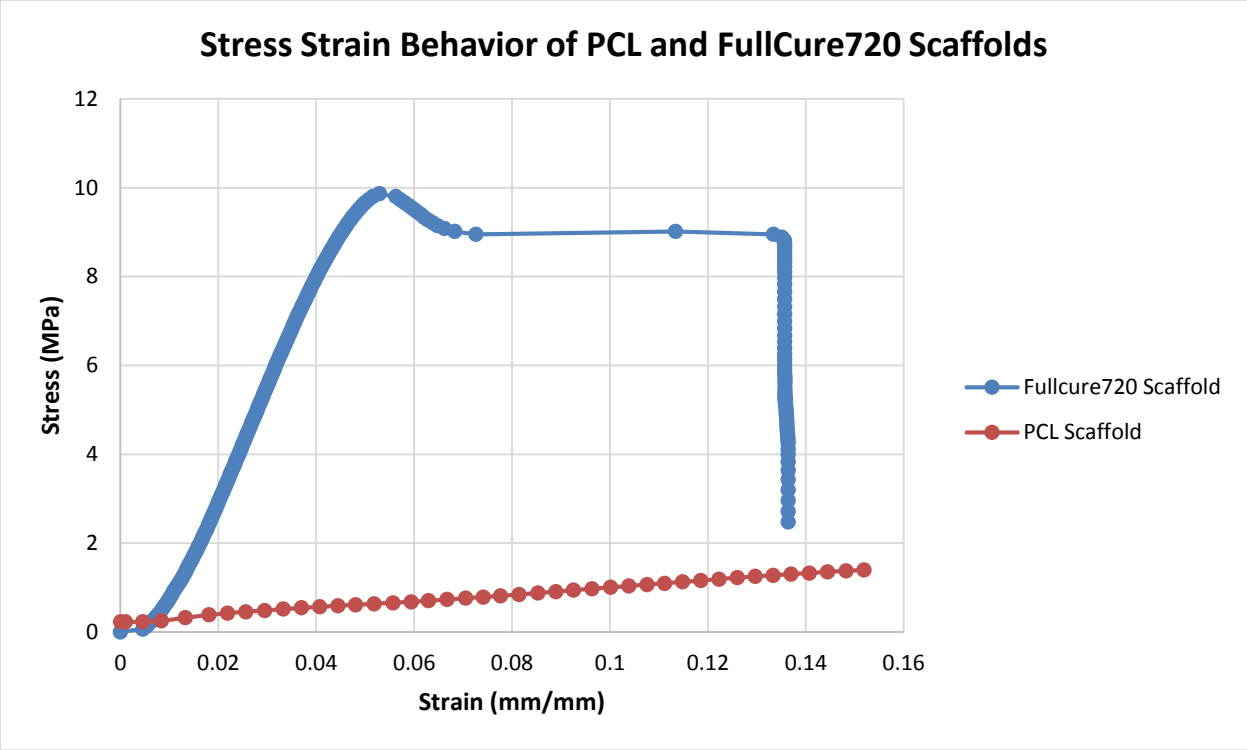

Figure 6-11: Stress-strain behavior of PCL and FullCure720 scaffolds

6.4.3: Imaging and Scaffold Elastic Property Estimation

The following geometric changes in the average strut diameter of the PCL scaffolds were observed with time and are presented in Fig. 6-12.

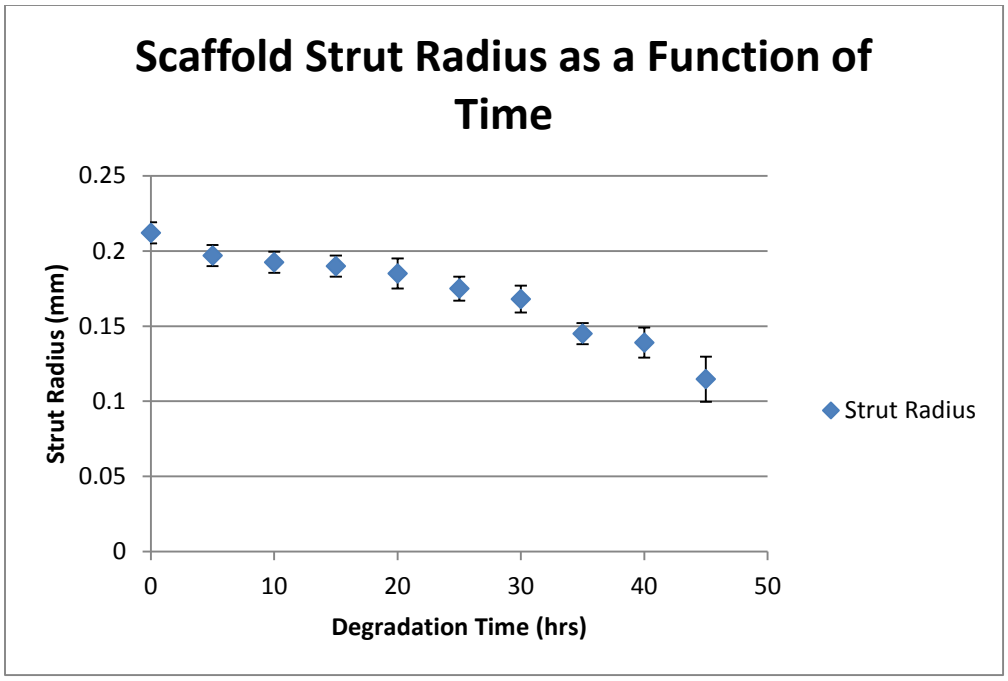

Figure 6-12: Observed geometry of scaffold changing with time

These observed changes to the diameter/radius of the tissue scaffold's strands (struts) were entered in the finite element model of the scaffold's stiffness properties, yielding predictions for the scaffold properties with time. These predictions of stiffness were then compared to actual direct measurement of the scaffold stress-strain curve via compressive load-deflection testing. These results are illustrated in Figures 6-13 and 6-14.

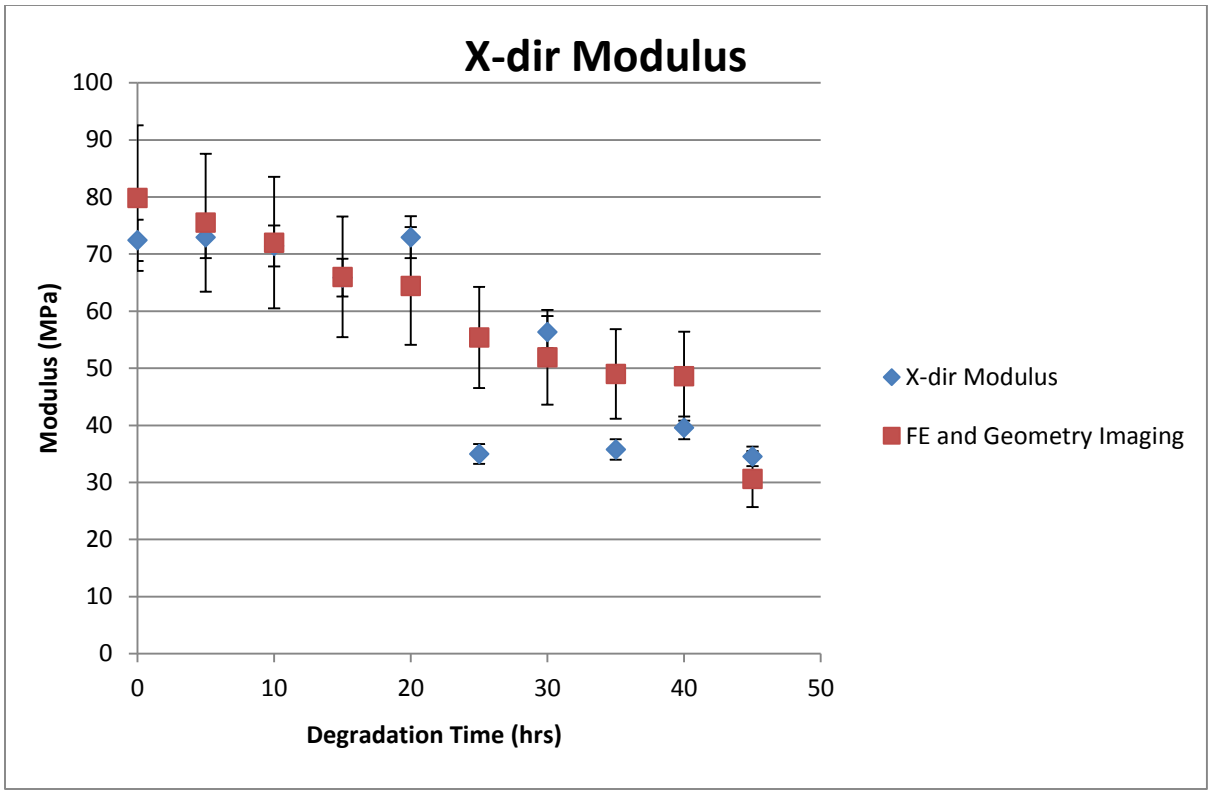

Figure 6-13: Comparison between theoretical Young Modulus from imaging data and FE analysis and direct mechanical testing of stiffness for the scaffold stiffness along the x-direction

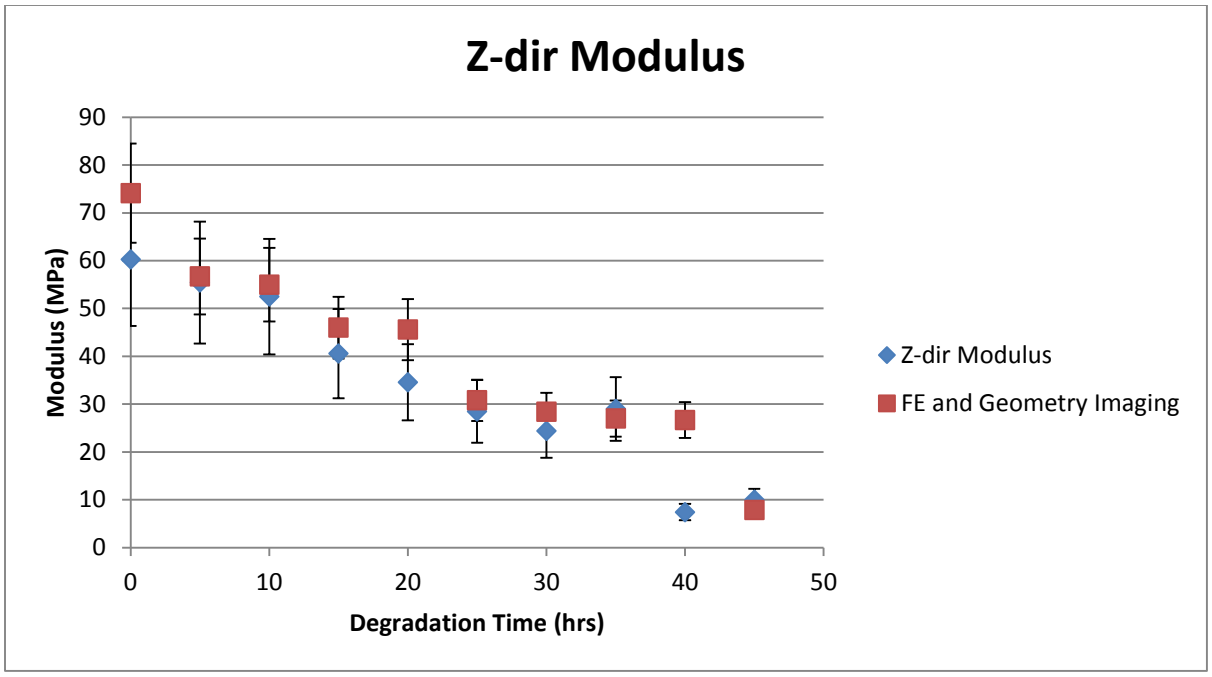

Figure 6-14: Comparison between theoretical Young Modulus from imaging data and FE analysis and direct mechanical testing of stiffness for the scaffold stiffness along the z-direction.

The R^2 values of image and FE analysis derived stiffness and the actual material testing measurements of scaffold stiffness are R^2=0.746 for elastic properties in the Z-direction, and R^2=0.885 for elastic properties in the X-direction. The actual elastic properties of the scaffold were estimated with acceptable accuracy by the use of imaging data and FE modelling.

6.4.4: Nonlinear Stress Strain Behaviour from Imaging

The strand diameter of the FullCure720 tissue scaffolds were measured to be 348 ± 44.9 µm. A finite element model of the FullCure720 scaffolds with 27 unit cells, 85,524 Solid95 elements, and periodic large deflection boundary conditions was then executed in ANSYS to predict the nonlinear stress-strain behavior of the scaffolds in the longitudinal and transverse directions. This predicted behavior was then compared to that given by stress-strain testing. These results are presented in Fig. 6-15. The R^2 value of FE model predictions to experimental nonlinear stress-strain behavior in the Z-direction was 0.929. The FE model therefore gives acceptable

agreement between theory and experiment when predicting scaffold stress strain curves in the Z-direction.

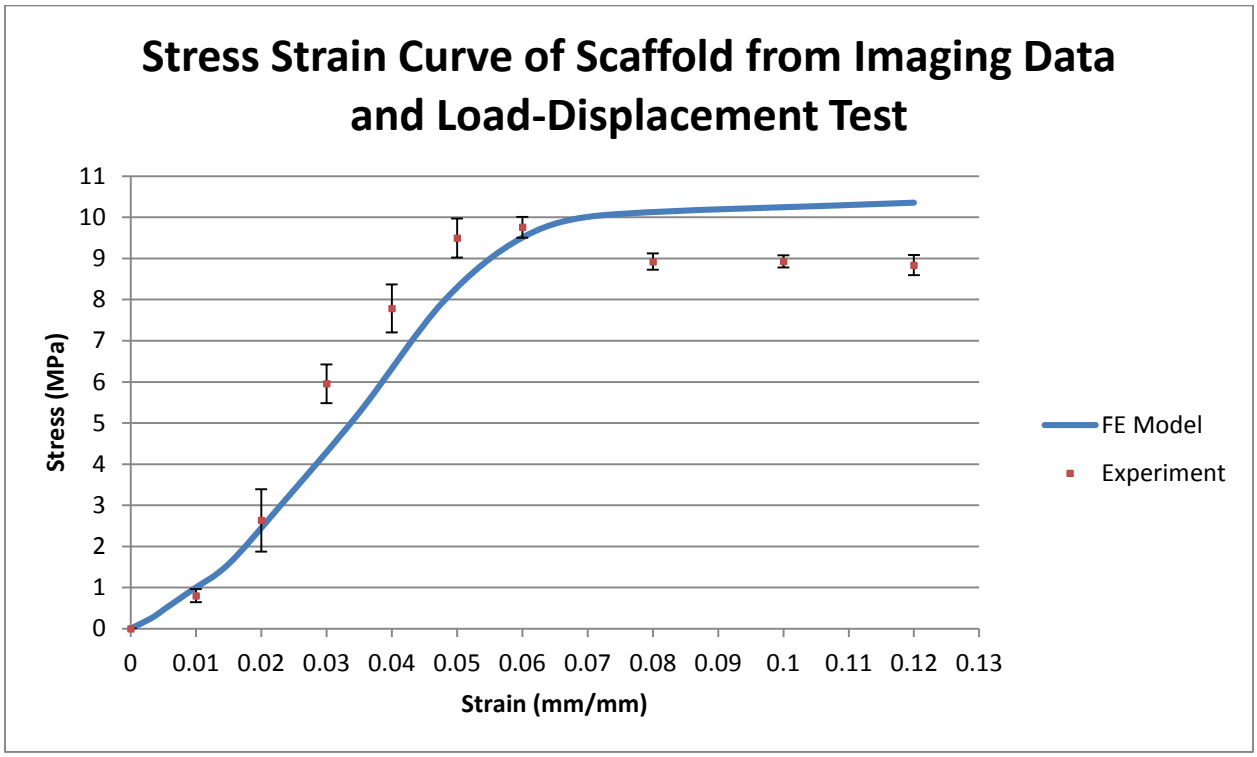

Figure 6-15: Comparison of predictions of nonlinear FE model with imaging data derived geometry and experimental results from stress-strain test

6.5: Discussion and Future Work

The morphology changes of tissue scaffolds with time were monitored remotely by synchrotron imaging and employed as the input of finite element models to give estimates for the effective stiffness of a tissue scaffold experiencing surface erosion/degradation. Planar two dimensional images of tissue scaffolds were taken in a challenging environment similar to that encountered *in vivo*, and with the assumption that surface degradation was uniform throughout the scaffold, the average diameter of the scaffold's strands was measured. From these direct measurements of geometry, the scaffold elasticity was estimated by numerical modelling of the scaffold with time dependent known geometric parameters. The model estimates for elasticity of the scaffold with

time were then compared to direct experimental measurement of the scaffold elasticity. In this way it was demonstrated that the remote measurement of a parameter that can be characterized while a scaffold is within the living environment could be combined with mathematical modelling to estimate a tissue scaffold quality that cannot always be measured directly *in vivo*.

This preliminary study utilized planar two dimensional imaging only. While this limits the dose necessary to characterize the tissue scaffold geometric changes, it also assumes that surface degradation is uniform throughout the entire porous scaffold structure. Full three dimensional computed tomography (CT) image reconstruction would give a more powerful measurement of what parts of the scaffold still remain and contribute to its overall effective mechanical properties at any given time-point during scaffold degradation. In addition, in some cases of surface degradation, an intermediate region sheaths the fully undegraded component of the scaffold. The dimensions of this region, its contribution to the mechanical properties, and whether this region can be identified via a DEI or absorption based signature should be considered in future studies. In addition, future studies should also focus on the imaging of the second phase of the scaffold, the cell bearing hydrogel. The volume fraction occupied by tissue in this phase may be estimated by imaging and employed to predict the mechanical properties of this part of the scaffold with time as well.

6.6: Conclusions

Current state of the art hydrogel scaffolds for cartilage engineering do not possess ideal mechanical properties for this application. One possible way to enhance the mechanical properties of these scaffold types is the hybrid scaffold approach where a polymeric skeletal structure provides the mechanical support necessary to temporarily replace and provide the functionality of cartilage, while a separate hydrogel component of the scaffold provides the biocompatible ideal environment for regenerating cartilage tissue. In this way, the design of the biological and structural components of the scaffold are decoupled from each other and may be altered to suit a wide range of values without influencing or interacting with the performance of each other. Furthermore, surface degrading scaffolds are of interest because of their simple straightforward degradation behavior and the fact that the changing geometry of such scaffolds

can be visualized through *in vivo* imaging methods. In this study, a tissue scaffold material, with a limited diffusion rate in relation to the degradation medium, experienced hydrolytic surface degradation with time, and were imaged at specific time points during the degradation period. From this geometric data, which can be measured in very challenging imaging environments where the surroundings and target are of the same or nearly the same density, estimates for the stiffness property of the scaffolds with time were made. These estimates were then validated by an alternative method of scaffold Young Modulus characterization, clearly demonstrating a viable method *for in vivo* prediction of scaffold stiffness from characterized scaffold geometry.

Acknowledgement

Research described in this paper was performed at the Canadian Light Source. The Canadian Light Source is supported by the Natural Sciences and Engineering Research Council of Canada, the National Research Council Canada, the Canadian Institutes of Health Research, the province of Saskatchewan, Western Economic Diversification Canada, and the University of Saskatchewan.

References

[1] Atala, A., Bauer, S. B., Soker, S., Yoo, J. J., Retik, A. B., "Tissue-engineered autologous bladders for patients needing cystoplasty," *Lancet*, vol. 367, p. 1241–46, 2006.

[2] Nama, J., Johnson, J., Lannutti, J., and Agarwal, A.,"Modulation of embryonic mesenchymal progenitor cell differentiation via control over pure mechanical modulus in electrospun nanofibers," *Acta Biomaterialia*, vol. 7, issue 4, p. 1516-1524, 2011.

[3] Sun, H., Zhu, F., Hu, Q., Krebsbach, P. H., Controlling stem cell-mediated bone regeneration through tailored mechanical properties of collagen scaffolds, *Biomaterials*, vol. 35, Iss. 4, p. 1176–1184, 2014.

[4] Freier, T., Kunze, C., Nischan, C., Kramer, S., Sternberg, K., Sa, M., Hopt, U. T., Schmitz, K. P., In vitro and in vivo degradation studies for development of a biodegradable patchbased on poly(3-hydroxybutyrate), *Biomaterials*, vol. 23, p. 2649–2657, 2002.

[5] Kenley, R. A., Lee, M. O., Mahoney, T. R., Sanders, L. M., Poly(1actide-co-glycolide) Decomposition Kinetics in Vivo and in Vitro, *Macromolecules*, vol. 20, no. 10, 1987, p. 2398-2403.

[6] Grayson, A. C. R., Voskerician, G., Lynn, A., Anderson, J. M., Cima, M J., Langer, R., Differential degradation rates in vivo and in vitro of biocompatible poly(lactic acid) and poly(glycolic acid) homo- and co-polymers for apolymeric drug-delivery microchip, *J. Biomater. Sci. Polymer Edn.*, vol. 15, no. 10, p. 1281-1304, 2004.

[7] Miller, K., Chinzei, K., Orssengo, G., Bednarz, P., Mechanical properties of brain tissue in-vivo: experiment and computer simulation, *Journal of Biomechanics*, vol. 33, p. 1369-1376, 2000.

[8] Gefen, A., Margulies, S. S., Are in vivo and in situ brain tissues mechanically similar?, Journal of Biomechanics, vol. 37, p. 1339–1352, 2004.

[9] Lu, L., Peter, S. J., Lyman, M. D., Lai, H. L., Leite, S. M., Tamada, J. A., Uyama, S., Vacanti, J. P., Langer,R., Mikos, a. G., In vitro and in vivo degradation of porous poly(DL-lactic-co-glycolic acid) foams, *Biomaterials*, vol. 21, p. 1837-1845, 2000.

[10] Ourselin, S., Roche, A., Subsol, G., Pennec, X., Ayache, N., Reconstructing a 3D structure from serial histological sections, *Image and Vision Computing*, vol. 19, p. 25–31, 2000.

[11] Lebenberg J., Hérard, A.S., Dubois, A., Dauguet, J., Frouin, V., Dhenaina, M., Hantraye, P., Delzescaux, T., Validation of MRI-based 3D digital atlas registration with histological and autoradiographic volumes: An anatomofunctional transgenic mouse brain imaging study, *NeuroImage*, vol. 51, p. 1037–1046, 2010.

[12] Sun, H., Mei, L., Song, C., Cui, X., Wang, P., The in vivo degradation, absorption and excretion of PCL-based implant, *Biomaterials*, vol. 27, p. 1735–17402005, 2006.

[13] Artzi1, N., Oliva, N., Puron, C., Shitreet, S., Artzi, S., bon Ramos, A., Groothuis, A., Sahagian, G., Edelman, E. R., In vivo and in vitro tracking of erosion in biodegradable materials using non-invasive fluorescence imaging, *Nature Materials*, vol. 10, p. 704-709, 2011.

[14] Goss, B. C., McGee, K. P., Ehman, E. C., Manduca, A., Ehman, R. L., Magnetic Resonance Elastography of the Lung: Technical Feasibility, *Magnetic Resonance in Medicine*, vol. 56, p. 1060–1066, 2006.

[15] Zhang, Y. S., Cai, X., Yao, J., Xing, W., Wang, L. V., Xia, Y., Non-Invasive and In Situ Characterization of the Degradation of Biomaterial Scaffolds by Volumetric Photoacoustic Microscopy, *Angew. Chem. Int. Ed.*, vol. 53, p. 184 –188, 2014.

[16] Park, D. W., Ye, S. H., Jiang, H. B., Dutta, D., Nonaka, K., Wagner, W. R., Kim, K., In vivo monitoring of structural and mechanical changes of tissue scaffolds by multi-modality imaging, *Biomaterials*, vol. 35, p. 7851e7859, 2014.

[17] Kim, K., Jeong, C. G., Hollister, S. J., Non-invasive monitoring of tissue scaffold degradation using ultrasound elasticity imaging, *Acta Biomaterialia*, vol. 4, p. 783–790, 2008.

[18] Yu, J., Takanari, K., Hong, Y., Lee, K. W., Amoroso, N. J., Wang, Y., Wagner, W. R., Kim, K., Non-invasive characterization of polyurethane-based tissue constructs in a rat abdominal repair model using high frequency ultrasound elasticity imaging, Biomaterials, vol. 34, p. 2701-2709, 2013.

[19] Dutta, D., Lee, K. W., Allen, R. A., Wang, Y., Brigham, J. C., Kim, K., Non-Invasive Assessment Of Elastic Modulus Of Arterial Constructs During Cell Culture Using Ultrasound Elasticity Imaging, *Ultrasound in Med. & Biol*., vol. 39, no. 11, p. 2103–2115, 2013.

[20] Ulum, M.F., Arafat, A., Noviana, D., Yusopa, A.H., Nasutiona, A.K., Abdul Kadir, M.R. Hermawan, H., In vitro and in vivo degradation evaluation of novel iron-bioceramic composites for bone implant applications, Materials Science and Engineering C, vol. 36 (2014) p. 336–344.

[21] Jones, A. C., Arns, C. H., Sheppard, A. P., Hutmacher, D. W., Assessment of bone ingrowth into porous biomaterials using MICRO-CT, Biomaterials, vol. 28, p. 2491–2504, 2007.

[22] Saito, E., Suarez-Gonzalez, D., Rao, R. R., Stegemann, J. P., Murphy, W. L., Hollister, S. J., Use of Micro-Computed Tomography to Nondestructively Characterize Biomineral Coatings on Solid Freeform Fabricated Poly (L-Lactic Acid) and Poly (e-Caprolactone) Scaffolds In Vitro and In Vivo, Tissue Engineering: Part C, vol. 19, num. 7, p. 507-517, 2013.

[23] Langer M., Liu Y., Tortelli F., Cloetens P., Cancedda R., Peyrin F., Regularized phase tomography enables study of mineralized and unmineralized tissue in porous bone scaffold., J Microsc. vol. 238, p.230-239, 2010.

[24] Zehbe, R., Riesemeier, H., Kirkpatrick, C. J., Brochhausen, C., Imaging of articular cartilage – Data matching using X-ray tomography, SEM, FIB slicing and conventional histology, Micron, vol. 43, iss. 10, p. 1060–1067, 2012.

[25] Rack, A., Developments in High-Resolution CT: Studying Bioregeneration by Hard X-ray Synchrotron-Based Microtomography, Comprehensive Biomaterials, vol. 3, p. 47–62, 2011.

[26] Appel, A., Anastasio, M. A., and Brey, E. M., Potential for Imaging Engineered Tissues with X-Ray Phase Contrast, Tissue Engineering Part B: Reviews., vol. 17(5), p. 321-330, 2011.

[27] Thurner, P., Karamuk, E., Müller, B., 3-d characterization of fibroblast cultures on PETT textiles, *European Cells and Materials*, vol. 2. , p. 57-58, 2001.

[28] Zhu, N., Chapman, D., Cooper, D., Schreyer, D. J., Chen, X., X-Ray Diffraction Enhanced Imaging as a Novel Method to Visualize Low-Density Scaffolds in Soft Tissue Engineering, *Tissue Engineering Part C: Methods.*, vol. 17, no. 11, p. 1071-1080, 2011.

[29] Alessandro, S., Serge, H., Geoffroy, A., Fabio, C., Joel, C., A Scheme for Solving the Plane–Plane Challenge in Force Measurements at the Nanoscale, *Nanoscale Research Letters*, vol. 5, iss. 8, p. 704-709, 2010.

[30] Christopher X. F. Lam, Monica M. Savalani, Swee-Hin Teoh, Dietmar W. Hutmacher, Dynamics of in vitro polymer degradation of polycaprolactone-based scaffolds: accelerated versus simulated physiological conditions, *Biomed. Mater.* vol. 3, p. 034108-034122, 2008.

[31] Guo Q. and Groeninckx G., Crystallization Kinetics Poly(e-caprolactone) in Miscible Thermosetting Polymer Blends of Epoxy Resin and Poly (e-caprolactone), *Polymer*, vol. 42, p. 8647-8655, 2001.

[32] Berger, H., Kari, S., Gabbert, U., Rodríguez-Ramos, R., Bravo-Castillero, J., and Guinovart-Díaz, R., "A Comprehensive Numerical Homogenisation Technique for Calculating Effective Coefficients of Uniaxial Piezoelectric Fibre Composites," *Mater. Sci. Eng., A*, vol. 412, p. 53–60, 2005.

[33] P. R. Graves-Morris, D. E. Roberts, A. Salam, "The epsilon algorithm and related topics," *Journal of Computational and Applied Mathematics*, vol. 122, p. 51–80, 2000.

CHAPTER 7

GENERAL DISCUSSION

Organ failure currently does not have an ideal medical amelioration. While donor organs may in some cases be available, current state of the art requires immunosuppressive drug therapies to control the tendency of the body to reject donor tissue as foreign. A wide variety of medical and engineering efforts have been directed at this particular problem, and one of the most promising methods that may in the future yield fully functional organs derived from a patient's own cells is called scaffold based tissue engineering.

The mechanical properties of the tissue engineering construct play a vital role in its proper behavior during the treatment time period. In some treatment approaches, the scaffold will be immediately implanted after cell seeding, and will be required to provisionally fulfill the mechanical function of the tissue it is replacing for a time. In situations where the scaffold is pre-treated by a period of *in vitro* incubation, the seeded cells within the scaffold may require mechanical signals to achieve the desired cell behavior, which the scaffold must successfully endure at all times during its time in the bioreactor. If the scaffold is permanently deformed under its operational loading environment, it is considered to have failed. Likewise, a scaffold experiencing unacceptable magnitudes of deformation or possibly fracture/breakage during the treatment period must be redesigned to eliminate this unacceptable performance. It is also known that the mechanical stimulation given by a cell's surroundings will have an effect on the behavior of those cells, so the mechanical properties of a scaffold will strongly influence the local mechanical environment experienced by the cells, which will influence their metabolic and differentiation behavior. All of the above issues highlight the necessity to design scaffolds with controllable and known mechanical properties and time dependent behavior.

While the design of scaffolds can theoretically be achieved by an unguided random approach consisting of a vast number of experiments both *in vivo* and *in vitro* to determine the influence of the vast number of existing scaffold design parameters on the scaffold's ultimate success at inducing tissue and organ regeneration, such a process would involve such a vast amount of direct experimentation that it is for all intents and purposes an impractical proposition. The

performance of the scaffold must be quantified in the form of validated mathematical models and these models used to guide the design process and identify promising candidate designs from the enormous number of possibilities.

There are two broad research issues of significance that can be readily identified. The first is the creation of an acceptable mathematical model of scaffold behavior at both a single specific instant in time and as a function of time within the body. The mechanical properties that are of interest must be identified and then a time independent model of the scaffold must be created. This model's time dependent parameters must then themselves be represented as time dependent mathematical models to consider the growth of new tissue and the degradation of the scaffold. Once this mathematical model is created, its parameters must be determined from experimental evidence, which raises an interesting problem. The behavior of the scaffold within the body does not conform to the behavior of the scaffold under simple tabletop degradation environments. This means that *in vivo* experimentation will be necessary to fully capture and model the true behavior of the scaffold in its full design environment. This leads to the question of how to obtain appropriate experimental *in vivo* evidence to estimate the parameters in the model of scaffold performance.

The research objectives of this thesis were twofold; 1) to thoroughly model the time independent and dependent elastic property of a tissue scaffold for bone tissue engineering, with an emphasis on the composite nature of this scaffold, and 2) following this, to consider and validate various methods for collecting experimental data *in vivo* for parameter estimation. For a rapid prototyping manufactured Hydroxyapatite/Polycaprolactone tissue scaffold suitable for bone tissue engineering applications, absent any regenerating tissue, the parameter controlling hydrolysis based degradation was estimated to be k_1 =0.00019 $h^{-1}$from experimental stress-strain test measurements of scaffold stiffness with time. The parameter controlling self-catalyzing hydrolysis was found to be k_2 = 0.0011 h^{-1} mm^3 /mole. With these identified parameters the mathematical model of degradation was able to accurately predict the time dependent stiffness parameter of the scaffold when the scaffold geometry was changed. Specifically, an independent set of scaffolds with unique geometry parameters were degraded over time, and the time dependent measurements of their modulus were employed to estimate the parameters in a model

of scaffold degradation. This model with now estimated known parameters was then validated by employing it to model the degradation of a scaffold with a different strand spacing and diameter. The coefficient of determination R^2 was calculated to evaluate the model's agreement with experimental evidence. The calculated value of R^2=0.77 between model and experiment indicates that the model is able to predict the modulus of the scaffold with time with acceptable accuracy. The success of the model in simulating the behavior of this new set of scaffolds indicates that the model is valid for any rapid prototyping scaffold composed of the same material in the same degradation environment that has individual layers oriented 90 ° to each other. The model is able to consider the changes to degradation rate induced by different strand spacing and strand diameter. This research demonstrates that if the scaffold stiffness is experimentally known with time for a single geometry, this data can be used to estimate the parameters in a degradation model and be used to predict scaffold behavior for different model geometry parameters. It is strongly inferred from this work that if an *in vivo* method can be employed to measure the scaffold properties with time, a model can be created that will be a useful design tool and allow the degradation of other scaffold geometries to be accurately modelled.

In order to model the actual *in vivo* behavior of scaffolds in the human living environment, the scaffold will need to be monitored with time. Conventional methods for this characterization that involve the use of potentially dangerous radioactive tracers or fluorescing dyes that can possibly change the nature of the scaffold are not ideal, and the current practice of removing the scaffold at various time points surgically is not possible in a clinical setting with human patients. When the scaffold is outside of the body before transplantation, it is possible to fully characterize the linear and nonlinear scaffold stress-strain behavior and relate it to scaffold geometry parameters and the chemical parameters of the tissue scaffold material like its molecular weight. With the relationship of these parameters to scaffold mechanical performance well known, the ability to measure just a single property like geometry and elastic modulus *in vivo* allows, through a mathematical model, the prediction of a wide range of scaffold properties such as its molecular weight, and nonlinear stress-strain behavior. With this understanding, a method was then sought to remotely characterize the tissue scaffold with time inside the body.

The idea of ultrasound based remote deformation of the scaffold by ultrasonic radiation forces and deflection characterization by x-ray imaging was explored as a possible way to measure the elastic property of the scaffold, predict its molecular weight with time, and estimate its nonlinear behavior from this chemical parameter. In this proposed approach to scaffold characterization within the body, a source of acoustical energy results in a steady state force on the scaffold, causing its deformation. These deflections, in turn, are identified and their magnitudes characterized by comparing x-ray images of the scaffold in both the initial and deformed configuration. From these deflections and an understanding of the load being exerted on the scaffold, the material properties can be determined. To the author's best knowledge this is the first example of deflection measurement by diffraction enhanced x-ray imaging or propagation based phase contrast imaging being combined with ultrasonic remote palpitation to determine the moduli and Poisson ratios of a tissue scaffold. The scaffold moduli were determined to be 412 ± 97 KPa in the transverse direction and 310 ± 65 KPa in the longitudinal direction, which were within 12% of the values measured by compressive testing of the scaffold.

The allowable intensity of ultrasound within the body is limited by tissue heating constraints, which limit the magnitude of ultrasonic force that can be safely applied to the scaffold *in vivo*. The deflection of scaffolds exceeding certain stiffness will become very difficult to detect using conventional image analysis techniques like square sum of errors. The use of periodic structural components of the scaffold and Fourier analysis of transverse samples of images before and after deformation shows promise as a way to detect sub-pixel sized scaffold deflections. This method was successfully demonstrated, and accurately measured the known moduli of the scaffold from deflection under a steady state ultrasonic radiation force. Furthermore, it was determined that only a single unique loading condition is required to find a unique and stable estimate for the properties of a transversely isotropic scaffold, and that three unique loading conditions are able to estimate the properties of a fully orthotropic scaffold. It now should be possible to utilize this method in the study of scaffold degradation *in vivo*.

While it is possible that stiffness measurements of the scaffold can be related to molecular weight decline and therefore mass loss, there is a more direct way to evaluate mass loss *in vivo* if the scaffold is displaying primarily surface erosion degradation behavior. The outward geometry

of scaffolds and implants that display surface degradation can be visualized within the body without implant/scaffold removal. This suggests that imaging data can be employed to estimate the parameters in surface degradation models so that they can represent the behavior of the scaffold *in vivo*. To demonstrate this *in vivo* monitoring method, tissue scaffolds were subjected to surface degradation and their geometries imaged with time during the degradation process. Scaffold mass and stiffness were inferred from imaged geometry and models, and these inferences were then validated by directly measuring the weight and load displacement behavior of the scaffolds with time. A proof of concept experiment also demonstrated the inference of the nonlinear stress-strain behavior of the scaffold from imaging based geometry characterization. Taking a representative sample of scaffold locations and imaging strand diameter to find an average value for the whole scaffold allowed mass and modulus to be estimated within 20% of the actual values. Full reconstruction of the stress-strain curve of a scaffold from imaging data was accomplished, with the experimentally characterized behavior within 25% of the Finite Element model with imaging acquired geometry data. Full three dimensional computed tomography reconstruction would allow both estimates of mass loss and mechanical characteristics to be improved in the future. The model of surface degradation had one unknown parameter k_1, which was estimated from imaging data to be 3.74 hr^{-1} for a Polylactic Glycolic Acid cylinder, and 0.28 $hr^{-1}$for a rapid prototyping method manufactured tissue scaffold composed of Polycaprolactone.

CHAPTER 8

CONCLUSIONS AND FUTURE WORK

Many illnesses and injuries will remain untreatable unless a way is discovered to either regenerate lost tissues and organs or replace them with manmade equivalents. The seeding of cells onto biocompatible biodegradable extracellular matrix analogs is a promising method for achieving this end. Modelling, in as much detail as is required, the scaffold behavior and its degradation would help in the design of improved scaffolds. Of special importance are the complexities associated with degradation with a complex environment like the body as opposed to what is generally seen in basic salt water pH controlled surroundings or even cell culture medium.

The research in this thesis can be broadly separated into two categories; 1) modelling of tissue scaffolds, and 2) the design of *in vivo* experiments. In the modelling component of this research, models for the degradation of tissue scaffolds experiencing bulk degradation and surface erosion were created encompassing specific degradation environments and scaffold materials. In the case of bulk degradation, the model developed is unique in that it includes most of the structural levels of the tissue scaffold in question as well as the influence of manufacturing such as the plasticization of the scaffold caused by solvent residue. In the case of surface erosion, the model is unique since it considers an accelerated degradation environment that can be related to the actual degradation of a realistic scaffold in future work. In the second part of this research, the design of *in vivo* monitoring techniques was considered in an attempt to find creative ways to possibly follow degradation in the body with *in vivo* imaging and characterization techniques. A novel method was developed which utilizes x-ray deflection characterization along with ultrasonic remote palpitation and finite element modelling with regularization to characterize the transversely isotropic linear elastic properties of a scaffold remotely in a challenging imaging environment where the scaffold and the surrounding medium had almost identical absorption contrast. In addition, the morphology of a scaffold characterized in a simulation of the *in vivo* environment was successfully able to predict the linear and nonlinear stress-strain behavior of an anisotropic scaffold and its mass loss. This information was then successfully employed to

estimate the parameters of surface degradation models, which then were able to with reasonable accuracy predict the mass loss and stress-strain behavior of the scaffold with time.

Future work can be divided into two broad categories; 1) the modelling of more complex scaffold geometries and materials with the inclusion of the tissue in the mechanical model and the consideration of large deflections and nonlinear and strain rate dependent material properties, and 2) the consideration of other signals that may be present in degrading tissue scaffolds that can be detected *in vivo* and utilized to estimate the parameters of mathematical degradation models.

Polymeric biomaterials consist of multiple benign biocompatible monomers bound together into large long chain molecules. These molecules interact with each other in polymer chain networks to give the large scale mechanical properties of polymeric biomaterials. In the case of semi-crystalline materials these polymer chains form into amorphous disordered and ordered crystalline regions, which then form into the well-known spherulite microstructure. The reinforcement of biocompatible polymers with material property enhancing composite particle phases should consider the interaction of the inclusions with the matrix and also model the influence of reinforcing particle size distribution and shape on the properties of the scaffold composite biomaterial. In addition, future work should consider the dynamic properties of the tissue scaffold as well with the aim of matching those found in the natural tissue being replaced or repaired. These intricacies were not considered in the current work, but will need to be considered for more complex and detailed future scaffold design.

As to signals that may be of interest as possible ways to characterize scaffolds *in vivo*, the formation of internal voids due to trapped acidic degradation by-products in bulk degrading scaffolds should be visible via synchrotron imaging, and the onset of this stage of degradation would allow the estimation of the parameters in a finite element model of scaffold to be tuned until the models displayed behavior like that observed in experiment. In addition, the wave speed of ultrasound through tissue is directly related to the speed of sound in the scaffold. An imaging system capable of collecting data at a frame-rate sufficient to capture the motion of the sound

wave through the scaffold could characterize the speed of sound in the scaffold, and from this measure its modulus.

In addition, the above mentioned methods of diffraction enhanced imaging and the Fourier analysis of moving periodic structures to detect deflection have as a weakness the fact that the noise produced in the living environment by blood circulation, heart rate and respiration will overwhelm any *in vivo* signal. Motion detecting methodologies will need to be employed pixel by pixel, to detect movement and move pixels back to their original locations in the image, in order to filter out the effect of target motion from ordinary everyday biological processes. Alternatively, the possibility exists of employing new techniques in the field of suspended animation, where the test animal would be cooled and its blood temporarily replaced with cryogenic saline. In this state, there would be a window of opportunity of a few hours in which to image the animal and palpitate the scaffold remotely with ultrasound and detect faint deflections without any interference from blood flow, diaphragm movement, or a heartbeat.